To the Graduate Council:

I am submitting herewith a thesis written by Cathy J. Lewis entitled "Measurement of the Neutron Dose Near An Accelerator Used for Radiation Therapy." I have examined the final copy of this thesis for form and content and recommend that it be accepted in partial fulfillment of the requirements for the degree of Master of Science, with a major in Nuclear Engineering.

Laurence F Miller

Dr. Laurence F. Miller, Major Professor

We have read this thesis
and recommend its acceptance:

E. Marcia Katz

Dr. E. Marcia Katz, Nuclear Engineering

Lawrence W. Townsend

Dr. Lawrence W. Townsend, Nuclear Engineering

Accepted for the Council:

Lawminkel

Associate Vice Chancellor and Dean of the
Graduate School

# MEASUREMENT OF THE NEUTRON DOSE NEAR AN ACCELERATOR USED FOR RADIATION THERAPY

A Thesis

Presented for the

Master of Science

Degree

The University of Tennessee, Knoxville

**Cathy Jo Lewis**

**May 1996**

## *Dedication*

This thesis is dedicated to my parents, Mr. Robert F. and Mrs. Wilma J. Lewis, for their continuous love, encouragement, and support throughout my life. Their willingness and diligence to provide me educational opportunities will be forever appreciated. The support, understanding, and strength of my sister, Mrs. Robyn Rogers, has been an essential contribution for which I will always be grateful. This thesis is also dedicated to the loving memory of my grandmother, Mrs. Sarah Frances Cyrus.

## *Acknowledgments*

I would like to acknowledge the East Tennessee Baptist Hospital for the use of their Varian Clinac® 2100C linear accelerator for the duration of this study. I would also like to thank my major professor, Dr. Laurence F. Miller, for his guidance, patience, and willingness to listen. I would also like to recognize my other committee members: Dr. E. Marcia Katz and Dr. Lawrence W. Townsend. Their comments and suggestions made the end result well worth the effort. I would like to express my gratitude to Oak Ridge National Laboratory's Health Sciences Research Division for allowing me to use the RADCAL facility. In particular, I would like to thank Bill Robbins and Genia Lee-McDuffee for their assistance with the RADCAL exposures and equipment. I would also like to express my gratitude to Jana Hammonds for the continuous friendship and encouragement over the past eight years. My Masters degree would have never been a reality without the constant support and encouragement of my mother, father, and sister. They believed in my abilities, even when I doubted myself. I would like to acknowledge my grandparents, Everett Franklin Lewis, Nellie Marie Lewis, and Herman Odell Cyrus for always listening. And finally, I would like to express my sincere appreciation to Tim Ward for being patient, understanding, and encouraging throughout this ordeal. Your love and support will never be forgotten.

*Abstract*

Neutron dosimetry is especially difficult due to spectral effects, the unavoidable presence of gamma rays, and the fact that most detection systems respond to both gamma rays and neutrons. Thermoluminescent dosimetry is a convenient method with which to measure gamma exposures in a medical facility. However, in medical facilities, neutrons are also a component of the dose received by personnel and patients. Therefore, a study was undertaken to determine the neutron dose using thermoluminescent materials and a relatively new detector, the bubble detector. Three methods are presented for estimating the radiation dose to be expected at various locations within the treatment room maze, where neutrons are present.

Three types of detectors were used to determine the neutron dose expected in the maze of a linear accelerator: Panasonic $Li_2B_4O_7$ TLDs, Harshaw LiF TLDs, and Apfel Neutrometer™ bubble detectors. In all comparisons, the TLDs primarily responded in a similar manner. The bubble detectors' responses were not consistent with either of the TLDs used. The TLD dose responses were within a factor of two for each location within the maze. The TLDs were within a factor of three of the dose response predicted by an analytical method, while the bubble dosimeters' dose response varied significantly (a factor of 85 times) from the expected dose.

The advantage of using the TLDs was that a dose estimate could be obtained at the outer end of the maze, where the Neutrometer™ did not respond. An analytical method was used to determine the neutron dose at the inner and outer end of the maze. This method

included the use of the inverse square relationship to determine the dose at the inner end of the maze and using the tenth value distance (TVD) to determine the neutron dose at the outer end of the maze. Using the inverse square relationship and the TVD to estimate the dose at the inner and outer end of the maze, the LiF detector produced the best result for the inner end of the maze, while none of the detectors gave an adequate response for the outer end of the maze.

The $Li_2B_4O_7$ and the LiF thermoluminescent dosimeters and the Neutrometer™ dosimeter are acceptable devices for measuring neutron doses in medical accelerator facilities. These devices could be used in combination to utilize each detector's strong qualities. The TLDs could be used to determine the dose at the outer end of the maze, with the Neutrometer™ being used at the inner end of the maze. Regardless of the detector type chosen, maze design and shielding will influence how the detectors respond to neutrons and to gammas if the detector is sensitive to these rays.

*Table of Contents*

## *List of Tables*

## *List of Figures*

## 1.0 *Introduction*

High-energy electron accelerators such as the Varian Clinac® 2100C are used routinely to generate beams of photons for various types of cancer therapy. However, a problem that must be considered when using these devices is that the radiation produced from this device is contaminated with neutrons, the products of photon and electron interactions in the accelerator target, shield, collimator, and flattening filter (McGinley, et al., 1976). Because photons and neutrons are produced, the dose deposited in patients undergoing radiation therapy and operating personnel is of concern to therapists and medical health physicists (McGinley and Butker, 1991). To protect against overexposure, radiation exposure limits or standards were introduced as early as the start of the twentieth century when the potential hazards of radiation were realized (Khan, 1984). One of the initial standardizing organizations was the International Commission on Radiological Protection (ICRP), which continues to function through a series of publications. The documents prepared by this organization serve as the basis for many national protection guidelines and limits. The National Council on Radiation Protection and Measurements (NCRP) has functioned as the primary standard-setting organization in the United States. This body also prepares guidelines and standards, separate from the ICRP. The Nuclear Regulatory Commission (NRC), the regulating power in the United States, has control over all reactor-produced materials. However, this organization does not have regulatory control over naturally occurring radioactive material or x-ray machinery. These two areas are under individual State's jurisdiction (Taylor, 1995).

Radiation protection guidelines for the design of structural shielding for therapy units have been reported in NCRP Report No. 51. According to this document, "protective barriers are designed to ensure that the dose equivalent received by any individual does not exceed the applicable maximum permissible value" (NCRP, 1977). Protective barriers are used in areas that surround the accelerator room, and these areas are designated as either controlled or uncontrolled, depending on the use of the adjacent areas. A controlled area is under the supervision of the Radiation Protection Supervisor or Medical Physicist. For protection calculations, the maximum permissible dose equivalent (MPDE) is assumed to be 0.1 rem per week for controlled areas and 0.01 rem per week for uncontrolled areas (NCRP, 1977). These limits are approximately equivalent to the annual limits of 5 rem per year and 0.5 rem per year, respectively, which are recommended guidelines for radiation exposure to workers and the public, respectively (NCRP, 1977).

In order to maintain exposures to workers and to the public below these limits, the medical physicist designs protection barriers against three types of radiation: primary radiation, scattered radiation, and leakage radiation. Primary radiation is the useful radiation produced directly from the beam. Scattered radiation is radiation that has struck an object outside the accelerator and is attenuated. Leakage radiation can be classified as any radiation coming from within the accelerator components that is not part of the useful beam. The barrier made of materials sufficient to attenuate the useful beam to the required degree is known as the primary barrier. The barrier made of sufficient materials to block stray radiation (leakage and scatter) is known as the secondary barrier. These barriers generally consist of concrete, metal, earth, or a combination. When the accelerator beam

encounters these materials, photoneutrons result, thus increasing the dose to the patient and personnel operating the accelerator.

## 1.1 *Problem Statement*

Neutron production in accelerators used for therapy can result in doses to patients and to operating personnel from direct exposure to both neutrons and the resulting residual radioactivity (NCRP, 1984). The potential sources of neutron contamination are any materials in which the electron beam or x-ray beam is incident. These materials include, but are not limited to the waveguide, the collimators, the air path of the beam, the walls, and the patient. The potential sources of residual radioactivity include any location where neutrons are produced or absorbed (NCRP, 1984). Since accelerator beams produce neutrons, and because the primary barriers used to protect patients and operating personnel also contribute to the number of neutrons present, a study was initiated to estimate the dose attributed solely to neutrons. The purpose of the study was to estimate the neutron dose to an individual located at different positions in the maze of an 18 mega electronvolt (MeV) linear accelerator used in radiation therapy at East Tennessee Baptist Hospital using personnel dosimeters.

This study was conducted using an intercomparison methodology. The responses of three different personnel monitoring devices were obtained at the same locations in the maze, which is the corridor separating the accelerator and the door to the patient waiting area. The devices included Panasonic lithium tetraborate ($Li_2B_4O_7$) TLDs mounted on a polymethyl methacrylate (PMMA) phantom, Harshaw lithium fluoride (LiF) TLDs mounted on a

polyethylene sphere (Piesch Sphere), and Apfel bubble detectors suspended in air. All measurements were made using the Varian Clinac® 2100C as the source of radiation. The TLDs were calibrated with a $^{137}Cs$ source and a deuterium ($D_2O$) moderated $^{252}Cf$ source at the Radiation Calibration Laboratory (RADCAL) facility, at Oak Ridge National Laboratory (ORNL), prior to use at East Tennessee Baptist Hospital.

### 1.2 *Thesis Structure*

Chapter II briefly describes the manner in which neutrons are produced, illustrates the theory of linear accelerators, and diagrams the facility's structural design. This section also identifies the regulations involved in shielding linear accelerator facilities. The following chapter describes the thermoluminescent dosimeter (TLD) and the bubble detector. Separate sections for the Panasonic and the Harshaw TLD are provided. In addition, the characteristics and differences of the two phantom materials are provided in this section. The methodology for the measurements and calibrations is described in Chapter IV. Chapter V provides the results of the study, the comparison of the observed dose with estimates previously made by R.W. Kersey (Kersey, 1980), and the inverse square relation. The final chapter outlines the conclusions made from this study and provides recommendations for future work in the area of neutron dosimetry around medical accelerator facilities.

## 2.0 *Background Information on Neutron Production, Accelerators, and Radiation Protection*

The radiation beams generated by high energy medical accelerators are usually contaminated with neutrons as a result of ($\gamma$, n) and (e; e', n) interactions in machine components such as the target, the beam flattening filter, and collimators (McGinley et al, 1979). The production of these neutrons via photonuclear reactions results in a mixed radiation field in the beam and peripheral areas (Palta et al., 1984). These reactions lead to a non-negligible neutron field inside the treatment room (Tosi et al., 1991). The photonuclear cross-sections for most materials used in the treatment head of linear accelerators have a threshold between 7 and 8 MeV; however, the photonuclear cross-sections for lead and tungsten peak in the range of 12-14 MeV (Palta et al., 1984). Therefore, a significant number of neutrons can be produced in accelerators with photon energies greater than 10 MeV (Palta et al., 1984).

### 2.1 *Neutron Production*

Neutrons can be produced by several processes which include, bremsstrahlung, photodisintegration, neutron capture, pair production, and annihilation. The various possible processes are shown schematically in Figure 1 (NCRP, 1964). A brief description of each process is provided in the following text.

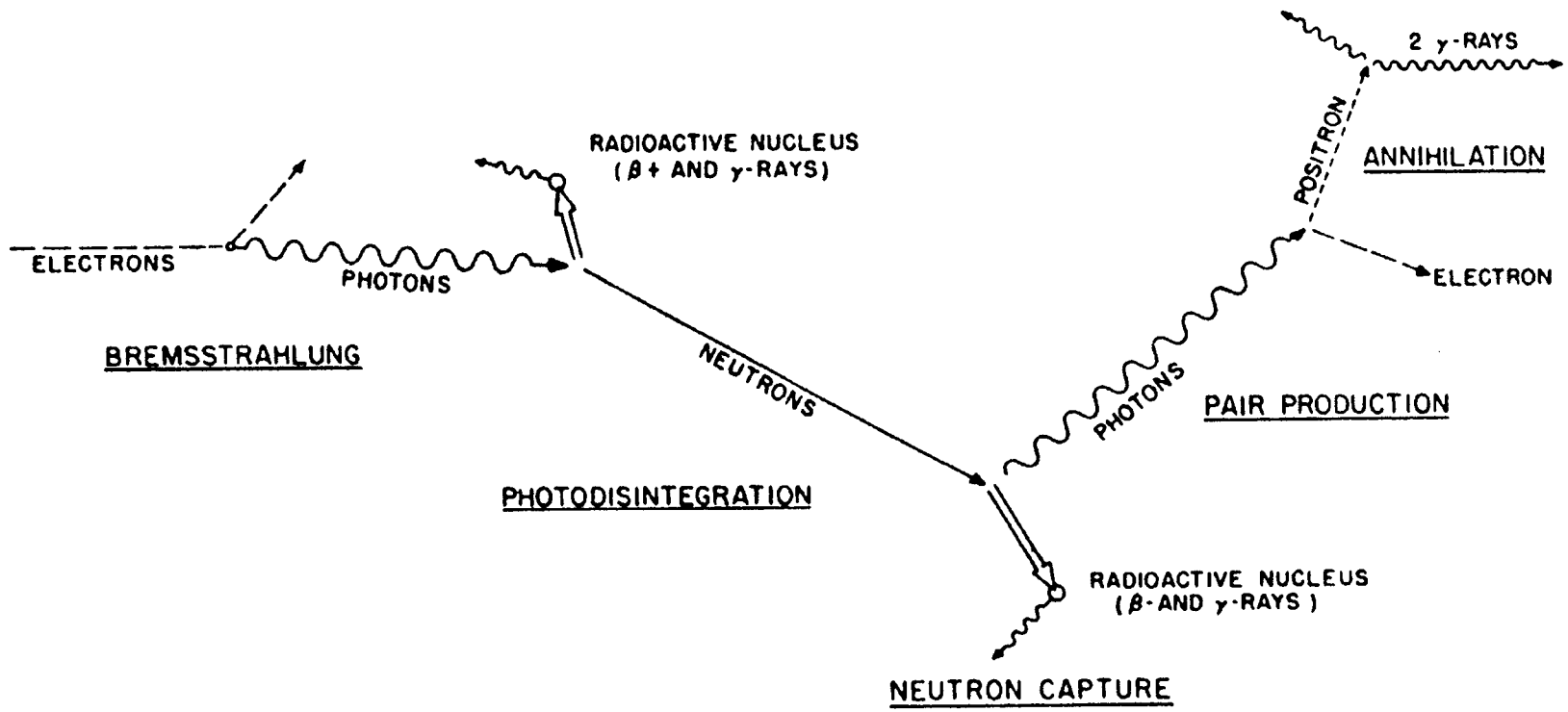


Figure 1. Interaction of radiation with matter (NCRP, 1964).

### 2.1.1 *Bremsstrahlung Radiation*

Bremsstrahlung radiation or braking radiation is the result of radiative interaction between a high speed electron and a nucleus. When the electron passes near a nucleus, the electron can be deflected from its path by Coulombic forces of attraction and can lose energy as bremsstrahlung (Khan, 1984). All or part of the electron's energy is dissociated and propagated into space as electromagnetic radiation. The mechanism of bremsstrahlung production is illustrated in Figure 2. The electron can undergo one or more bremsstrahlung interactions in the target material. This interaction may result in complete or partial loss of energy. The resulting bremsstrahlung photon can have any energy, with a maximum of the electron's initial energy (Khan, 1984). The emission direction of the bremsstrahlung photon depends on the incident electron's energy. At energies below 100 keV, photons are emitted approximately equally in all directions (Khan, 1984). As the kinetic energy of the electrons increases, the direction of photon emission becomes increasingly forward.

### 2.1.2 *Photodisintegration*

An interaction of a high energy photon with an atomic nucleus can lead to a nuclear reaction and to the emission of one or more nucleons (i.e., protons and neutrons) (Khan, 1984). However, in most instances, the process of photodisintegration results in the emission of neutrons by the nuclei. The photon must have enough energy to overcome the binding energy of the ejected nucleon; this can occur only if the photon exceeds a threshold value, which varies for each nucleus (Turner, 1986). Since the energy requirements are so

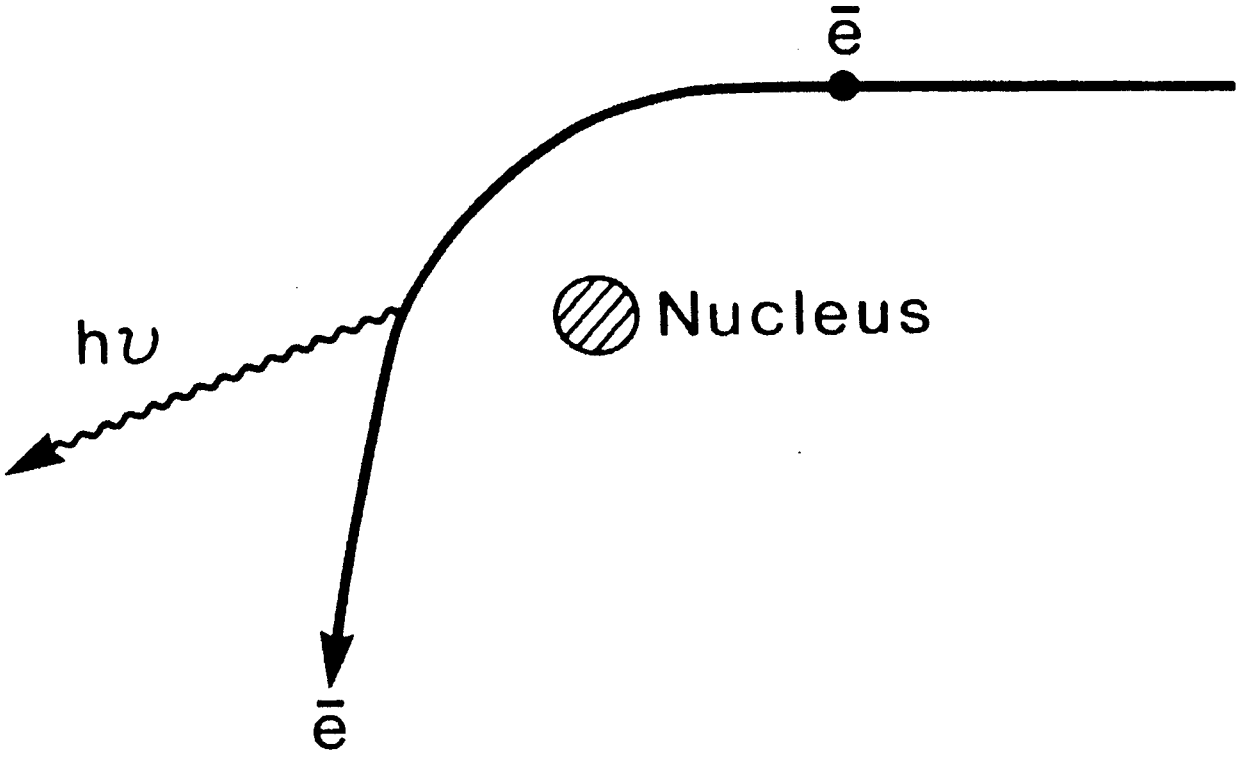


Figure 2. Bremsstrahlung radiation production (Khan, 1984).

great for this process, the probability of the process occurring is orders of magnitude smaller than for the other processes (Turner, 1986).

### 2.1.3 *Neutron Capture*

Neutron capture occurs when the target nucleus absorbs a neutron. Sometimes, the new isotope drops to ground state by the emission of a gamma ray (Foster and Wright, 1968). The most common process of neutron capture is the (n, $\gamma$) reaction (Khan, 1984). In this reaction, the target nucleus is raised to an excited state and then immediately returns to its normal state with the emission of a gamma ray photon. These gamma rays are known as capture gamma rays and can be observed coming from hydrogenous materials such as paraffin and polyethylene (Khan, 1984).

### 2.1.4 *Pair Production*

If the energy of the photon is greater than 1.02 MeV, the photon can interact with the target material through the mechanism of pair production (Khan, 1984). In the process of pair production, the photon interacts with the electromagnetic field of an atomic nucleus and releases all its energy in the process of creating a positron and electron pair. The electron has a negative charge, while the positron has a positive charge. A diagram illustrating pair production is shown in Figure 3.

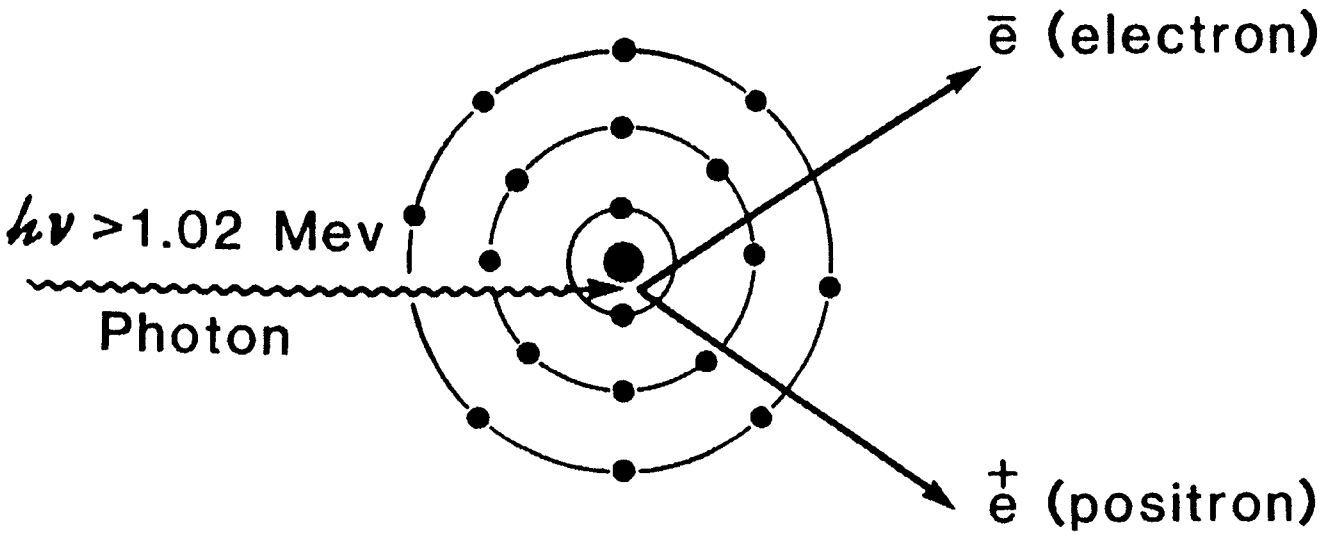


Figure 3. Pair production process (Khan, 1984).

### 2.1.5 *Annihilation*

The positron created as a result of pair production loses its energy as it traverses matter (Khan, 1984). As the positron loses energy, the slowly moving positron combines with one of the free electrons in the vicinity. This combination produces two annihilation photons of equal energy, 0.51 MeV. These two photons are ejected in opposite directions to conserve momentum (Turner, 1986). Figure 4 illustrates the production of annihilation radiation.

## 2.2 *Accelerators*

The betatron was the first accelerator to produce particles with energies greater than 10 MeV to be developed. This accelerator was used for electron therapy and photon (x-ray) therapy. The betatron produced radiations with energies sufficient to produce neutrons (NCRP, 1984). Linear accelerators were later developed and used in hospitals for radiation therapy. This section describes the linear accelerator and the radiation protection guidelines used in hospitals presently.

### 2.2.1 *Linear Accelerators*

The linear accelerator or linac is a device which uses high-frequency electromagnetic waves to accelerate charged particles, such as electrons, to high energies through a linear tube. The high energy electron beam can be used for treating superficial tumors or it can be directed toward a target to produce x-rays. Electrons are used in the treatment of skin

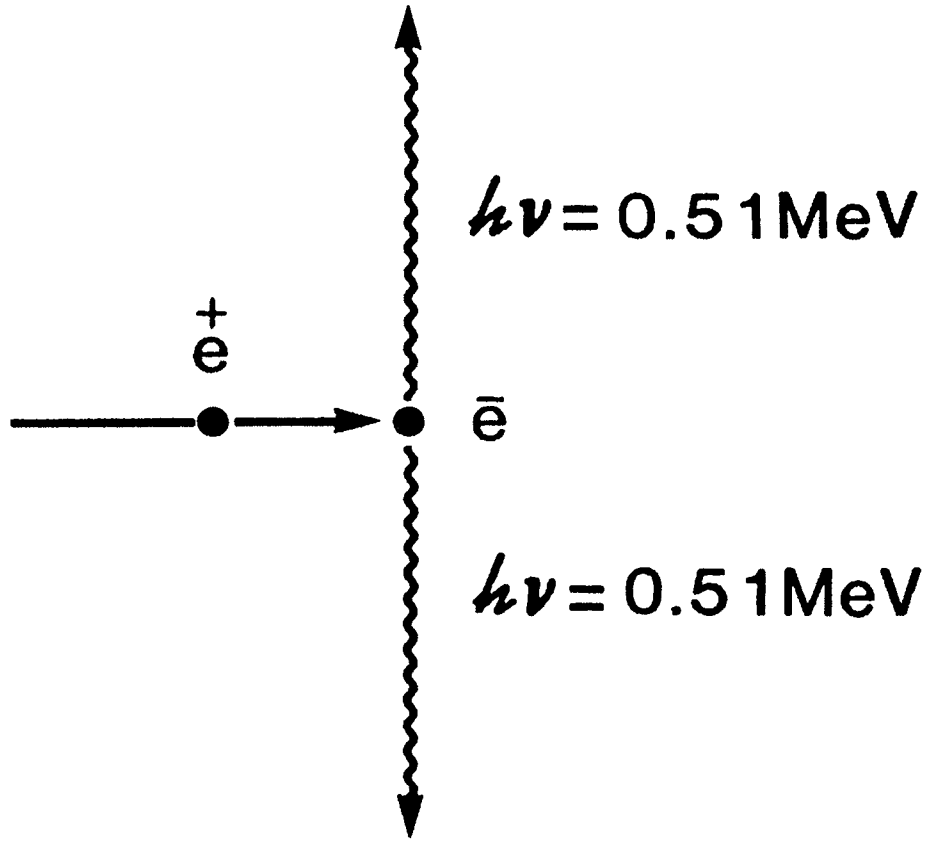


Figure 4. Production of annihilation radiation (Khan, 1984).

cancer and other types of superficial skin lesions. Electrons are also used to reduce scar tissue (most often in women who have undergone a lumpectomy), to irradiate lymph nodes, and to treat head and neck tumors that lie very near the spinal cord (Zartman, 1995). Photons or x-rays are used for the treatment of "deep" tumors, such as those in the lung, breast, prostate, or pelvis (Zartman, 1995).

There are several types of linear accelerators, but the ones used in radiation therapy accelerate electrons either by traveling or stationary electromagnetic waves. Both waves are disturbances or variations in the electromagnetic spectrum that transfers energy progressively from point to point in a medium (Woolf, 1973). The waves generated are within the microwave region of the energy spectrum (approximately 3000 MHz) (Khan, 1984).

The traveling wave accelerators require a terminating load, such as a bend magnet, in order to absorb the residual power at the end of the accelerator. Absorption is required to prevent the wave from reflecting back into the accelerator. On the other hand, the standing wave accelerator provides maximum reflection of the wave at both ends of the structure. The result of the forward and reverse traveling waves is a stationary wave. The stationary wave design is more efficient in delivering the radiation, but requires more equipment to optimize production. Therefore, the added expense often outweighs the benefits of efficiency.

Both types of accelerators use a copper tube with interior copper discs, spaced at various intervals. This area is evacuated to generate a vacuum. The electrons are initially

introduced into the copper tube at a potential energy of 50 kilovolts (keV). As the electrons are injected into the accelerator, they interact with the electromagnetic field of the microwaves and gain energy from the sinusoidal electric field. As the high energy electrons exit the accelerator, they proceed in straight lines and strike a target made of an element with a high atomic number (high Z material), such as lead, tungsten, or lead-tungsten alloy, to produce x-rays. Bremsstrahlung x-rays are produced when the incident electrons strike the target. The Bremsstrahlung x-rays are a desired product when electrons encounter matter. These x-rays are beneficial in the treatment of nonsuperficial tumors such as those of the lung, brain, and breast. The target is water-cooled and is thick enough to absorb most of the electrons produced. Bremsstrahlung interactions produce a spectrum of electron energies, with the maximum energy equal to the incident electron energy. Again, this is a desired byproduct of electron/matter interactions because these x-rays can be used in the treatment of "deep" tumors. The average photon energy is approximately one-third of the maximum energy (Khan, 1984).

Since both superficial and internal tumors are treated at cancer treatment centers today, a device that can produce both electrons and x-rays is a vital part of the battle against cancer (Sofield, 1993). Linear accelerators that have both electron and x-ray treatment capabilities are manufactured by Varian Associates, Incorporated. The Varian Clinac® 2100C produces five different energy electron beams and two different x-ray beams. Figure 5 provides a schematic of the Varian Clinac® 2100C. Low x-ray energies are typically 6 or 8 MeV and high energy x-rays are 10, 15, or 18 MeV. The electron energies range from 4 to 20 MeV (Varian, 1991).

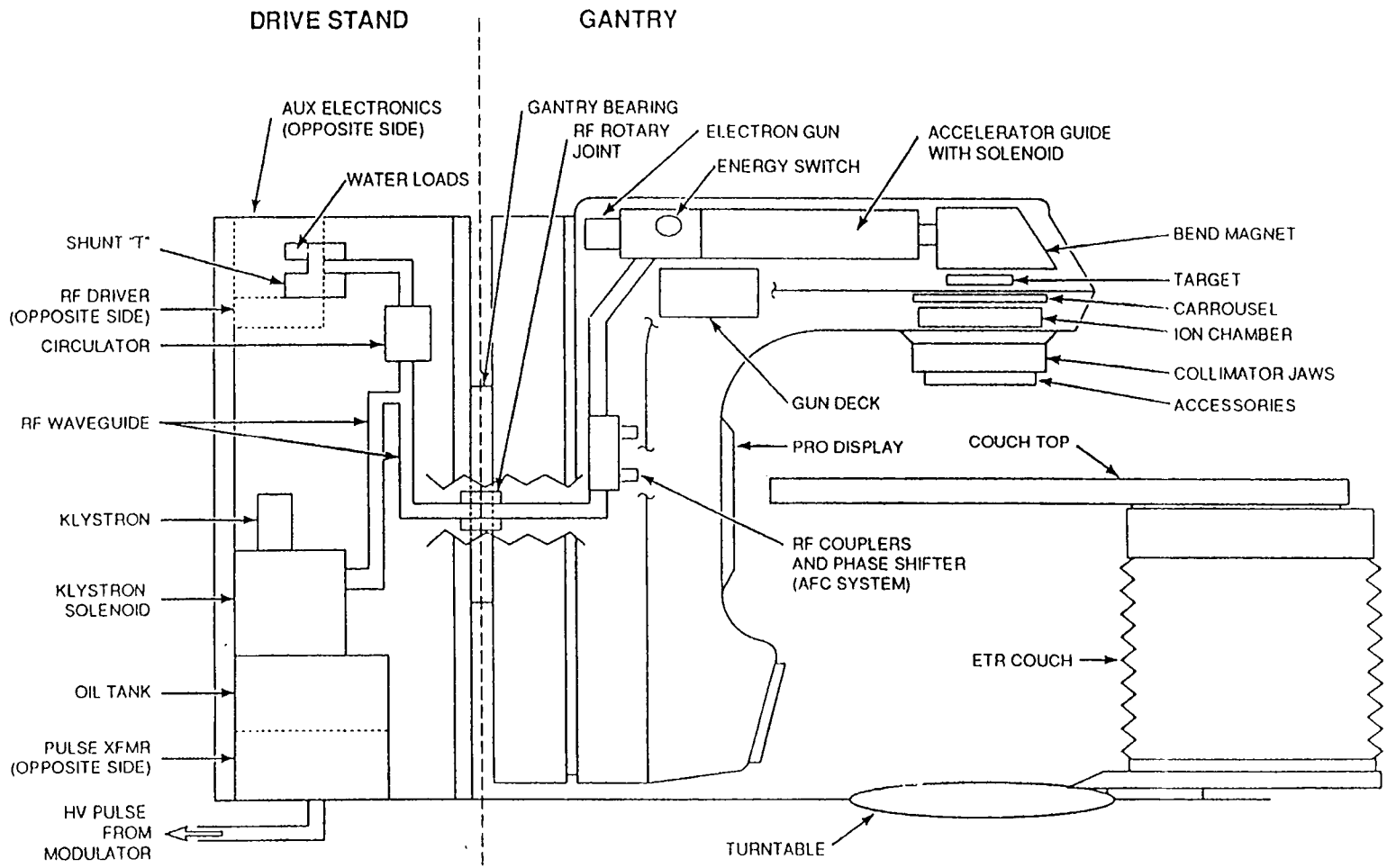


Figure 5. Schematic of the Varian Clinac® 2100C (Varian, 1991).

The electron beam exits the window of the accelerator tube as a narrow pencil beam, approximately 3 millimeters (mm) in diameter. In the electron mode, this beam does not strike a target. Instead, the beam strikes a scattering foil in order to spread the beam, in addition to producing a uniform electron fluence across the treatment field. The scattering foil consists of a thin metallic foil, usually lead. The thickness of the foil is determined to optimize the scattering of the electrons and minimize bremsstrahlung. However, a small portion of the total energy is converted into bremsstrahlung, thus contaminating the electron beam with x-rays (Khan, 1984). X-rays are also produced by the electron beam striking the collimator and other high Z materials in the collimating system. The components of the treatment head for both x-ray and electron therapy are shown in Figure 6. For the Clinac® 2100C, the beam is directed along a series of electromagnetic steering coils, which ensure proper alignment of the electron beam axis along the accelerator and bend magnet. The bend magnet consists of an evacuated chamber within an electromagnet. This magnet is programmed to select only electrons which possess a desired energy (Varian, 1991) and to focus the beam on a metal (tungsten) target, which produces x-rays for photon exposures. When an electron beam exposure is desired, the tungsten target is retracted and a scattering foil inserted.

The following assemblies shape and define the treatment field: the primary collimator, flattening filters, scattering foils, ion chambers, and variable collimators. The primary

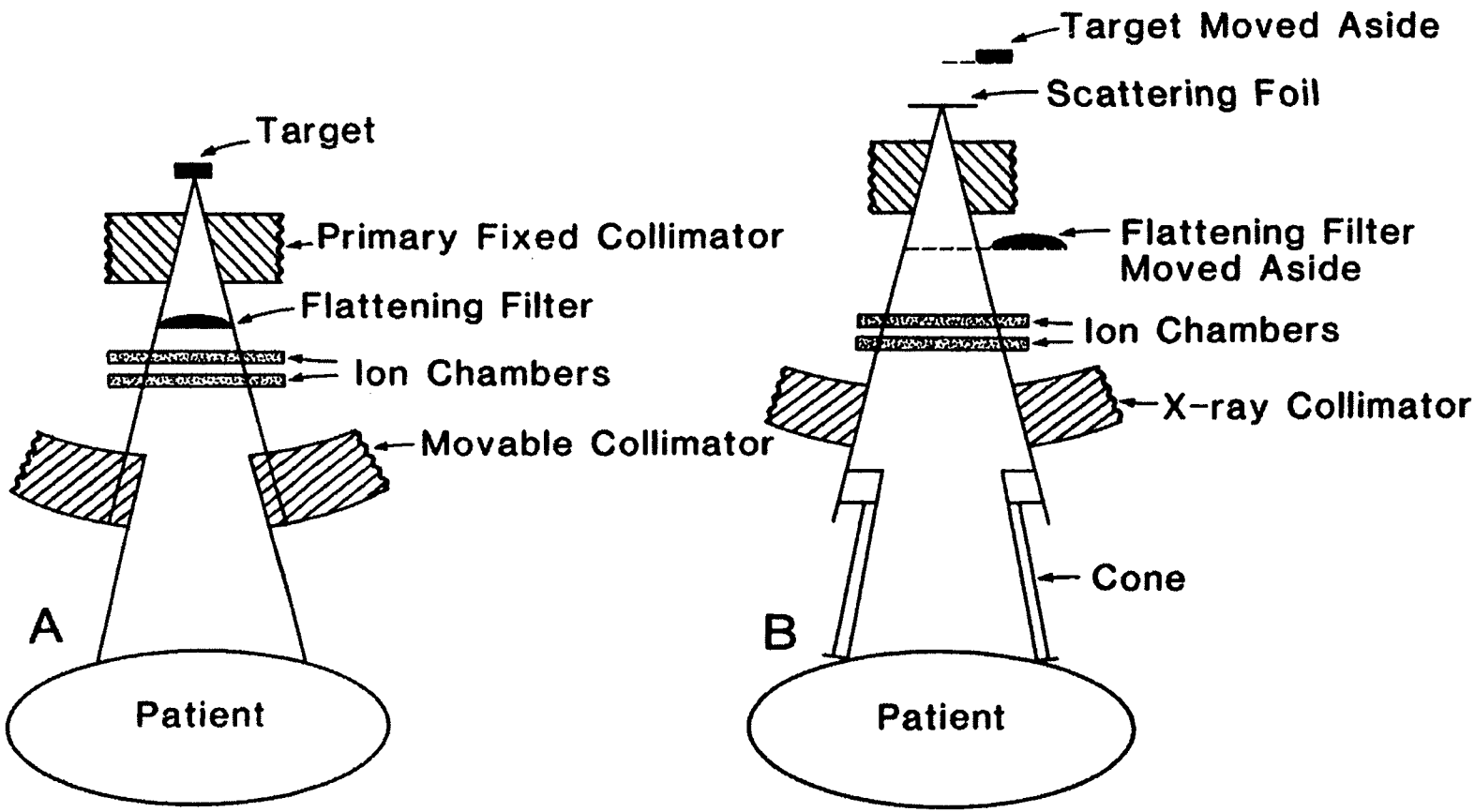


Figure 6. Components of the treatment head. (A) X-ray therapy mode; (B) electron therapy mode (Khan, 1984).

collimator confines the radiation from the target to the maximum field size for x-ray therapy. This collimator is not adjustable. A rotating carrousel below the primary collimator contains flattening filters and scattering foils to improve the uniformity of the beam. Flattening filters are used in photon modes, and scattering foils are used for electron modes. Since linear accelerators produce electrons in the megavolt range, the x-ray intensity is peaked in the forward direction. In order to make the beam intensity uniform across the treatment field, the flattening filter is inserted into the beam. The flattening filter is usually constructed of lead. However, tungsten, uranium, steel, and aluminum or a combination of these materials has also been suggested (Khan, 1984). Between the carrousel and the secondary collimator, two ion chambers, radial and transverse, produce current signals, which are used to monitor the radiation output and dose-rates. The variable collimators or jaws are used to provide further field definition. If prescribed by the physician, wedge filters, shadow block trays, compensating filters, electron applicators, cones, and other accessories can be attached to the treatment head to further modify the size or shape of the treatment field.

Most of the linear accelerators currently produced are manufactured so the radiation source can rotate about a horizontal axis. Figure 7 indicates the gantry, which is the rotating unit of the Clinac® that emits the treatment beam, slightly rotated about the horizontal axis of the patient. As the gantry rotates, the collimator axis moves in a vertical plane. The point of intersection of the collimator axis and the axis of rotation is known as the isocenter. Isocentric rotation allows the radiation beam to be directed from different angles, yet intersect at the same point or isocenter of the patient. The Clinac® 2100C utilizes the isocentric treatment technique. The isocentric treatment technique aids in

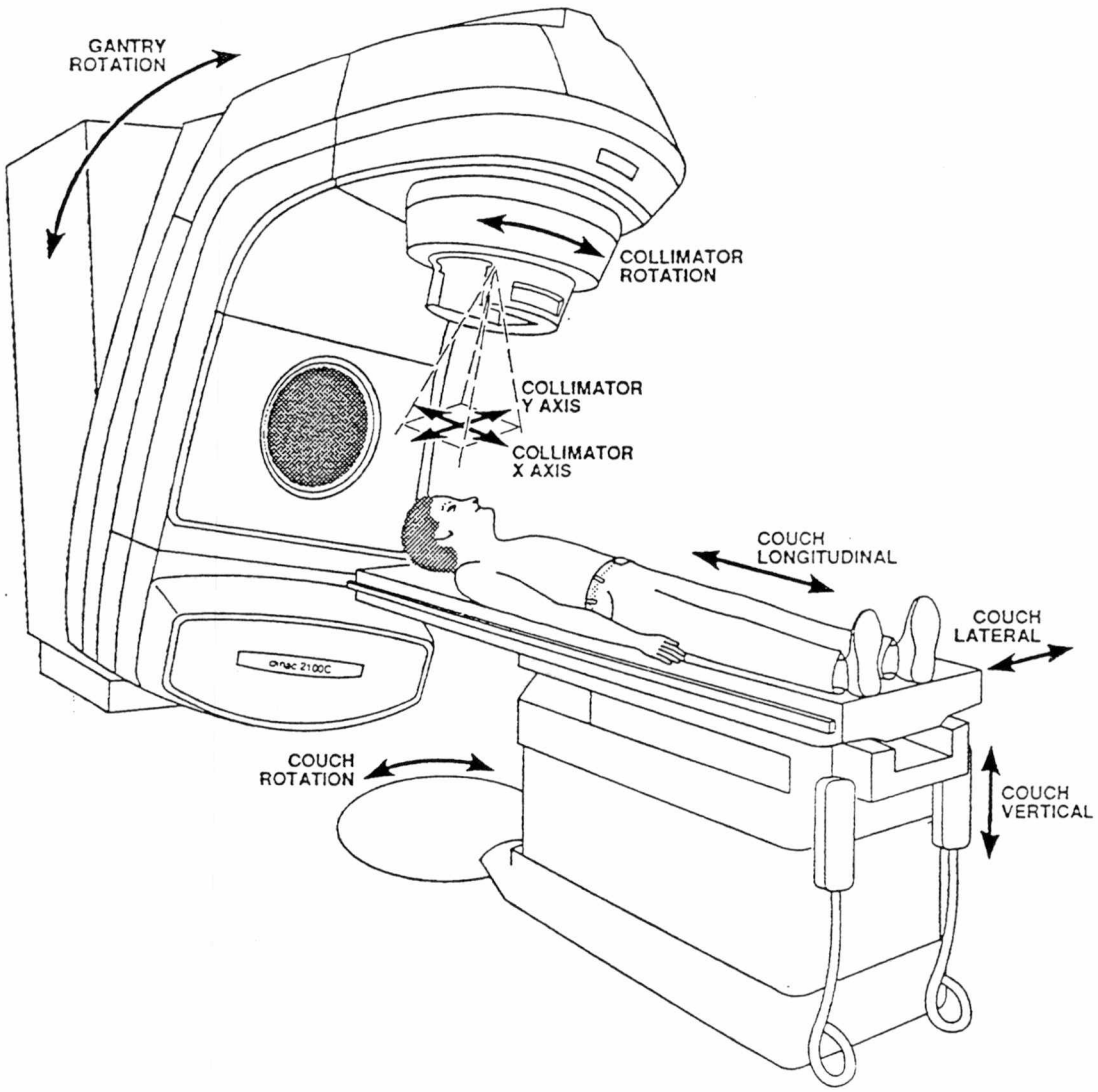


Figure 7. Diagram of the Varian Clinac® 2100C gantry rotation (Varian, 1991).

treating the entire tumor volume from various angles, thus possibly decreasing the number of treatments and damage to healthy tissues (Sofield, 1993).

The Clinac® 2100C contains a beam generation system capable of producing a series of beam pulses at a rate of 30 to 300 pulses per second (Varian, 1991). The pulses are produced when electrons are injected into the linear accelerator by an electron gun and accelerated to near light speed to yield the high energy required for therapeutic use. High power radio frequency (*rf*) pulses accelerate the electrons. The *rf* pulses are generated by the klystron, which forms standing waves in the accelerator. The klystron is an electron tube used as an oscillator or amplifier at microwave frequencies (Varian, 1991). The high energy electrons may be used directly for electron therapy or they may be directed toward a tungsten/copper target to produce x-rays for use in x-ray therapy.

When the electron beam strikes the target, the electrons slow as they pass near the positively charged atomic nuclei in the target. The positively charged nuclei cause the electrons to release energy in the form of x-rays. Due to the high energy of the incident electrons, x-ray radiation is emitted from the target on the opposite side from which the beam strikes. The photons produced by the slowing or braking of the electrons is bremsstrahlung radiation. Bremsstrahlung has a continuous energy spectrum and the maximum energy is a function of the energy of the accelerated electrons incident on the tungsten/copper target (Varian, 1991). When the accelerator unit is in the electron therapy mode, the target is fully retracted from the beam's path. In low energy x-ray modes, 6, 8, and 10 MeV, the thin area of the target is inserted directly into the beam's path. In high energy x-ray mode, the thick area of the target is inserted into the beam.

Regardless of the therapy mode used, the direction of the radiation beam is crucial to the protection of workers and the patient. If the primary beam is not being concentrated within the desired treatment field, the patient is in danger of an overexposure or damage to healthy tissues. If the scattered radiation is not being attenuated by the primary barrier, workers, other patients, and members of the public could be receiving a dose. Therefore, the direction of the radiation beam is a vital component of the design of the treatment facility.

### 2.2.2. *Accelerator Facility Design*

Most radiotherapy units are installed in concrete rooms to shield the outside structures and individuals from exposure to radiation produced by the accelerator (NCRP, 1984). The Varian Clinac® 2100C located at East Tennessee Baptist Hospital is no exception. This machine is surrounded by at least one foot of solid concrete on all sides, even the roof, which is also under several feet of dirt. Concrete was used because it is an effective attenuating material and is the most inexpensive shielding material available (Khan, 1984). The right and left sides of the facility shielding are a combination of concrete and steel, which has been layered to provide radiation protection and additional structural support for the concrete. Steel was used because space surrounding the accelerator facility was at a premium and it provides additional attenuation of neutrons (Sofield, 1995). Figure 8 provides a diagram of the concrete and steel shielding around the accelerator.

Concrete may be the most inexpensive shielding material available, but this material contributes significantly to the number of low-energy neutrons present in the accelerator therapy room (Khan, 1984). A "cookbook" method was developed by R.C. McCall and

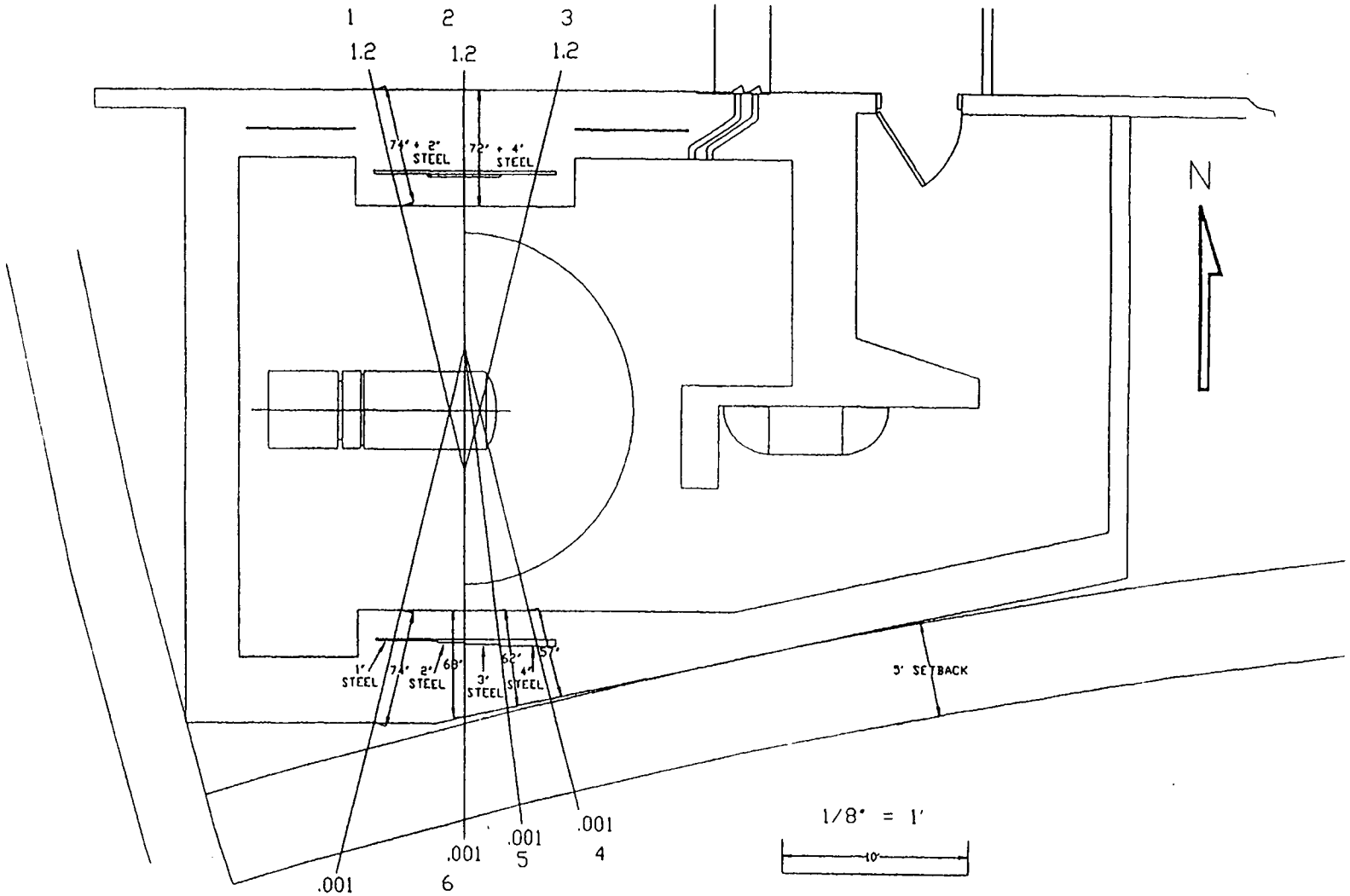


Figure 8. Diagram of the East Tennessee Baptist Hospital Radiotherapy Facility (Sofield, 1993).

C.M. Eisenhauer, who showed that spatial distribution of the neutron flux, originating in accelerator therapy rooms when energies above the ($\gamma$, n) threshold reaction are employed, can be divided into two components: a direct component coming from the accelerator head and a diffused component generated by wall scattering (Agosteo et al., 1992). Employed to determine the neutron scattering in a concrete room, their method was based on empirical relationships obtained from Monte Carlo simulations (Khan, 1984). Initially, the neutron field is described as the sum of neutrons coming directly from the source and from wall scattering interactions. The direct component is usually described by the inverse square law.

The treatment head, usually made of tungsten and/or lead and approximately 0.1 m thick, attenuates the direct component by 15-25% and reduces the mean energy of the neutron spectrum from 1-2 MeV to approximately 0.5 MeV (Agosteo et al., 1992). The diffused component of the neutron flux is usually assumed to be uniform and inversely proportional to the surface area of the treatment room, for walls constructed of a uniform composition.

The surface area for a parallelepiped radiotherapy room, where length, width, and height, are nearly similar is defined as

$$S = 2\left[(a \times b) + (b \times c) + (a \times c)\right] \quad (1)$$

where

S = surface area of the treatment room ($cm^2$),

a = length of the treatment room (cm),

b = width of the treatment room (cm),

and c = height of the treatment room (cm) (Agosteo et al., 1992).

However, this assumption is not valid near walls and in corners, where scattering interactions increase. Using the information above, C.M. Eisenhauer and R.C. McCall deduced that the typical neutron makes approximately 2.4 traversals of the room before it is captured or its energy falls below the cadmium cutoff energy, which is 0.41 eV (NCRP, 1984).

Most therapy accelerator rooms are designed with a maze or labyrinth, which eliminates the use of massive hydraulic doors (NCRP, 1984). The maze is designed to decrease the number of photons or neutrons from reaching the door of the treatment room by attenuating them along the walls. Most labyrinths are designed to cause energetic photons and/or neutrons to traverse the width of the maze at least two times (Sofield, 1995). If the maze provides sufficient attenuation, the door alone can be used to provide access security. Often, however, the design of the therapy facility does not allow for an adequate labyrinth or consider neutron shielding. In addition, old accelerators are often replaced with higher energy machines, but no shielding or room modifications are incorporated. Both of these situations contribute to patient and operating personnel exposure. Figure 9 represents two designs employed in radiotherapy facilities. Maze (a) is a poor design because large areas, which are directly illuminated by neutrons from the accelerator, are visible at the end of the maze (NCRP, 1984). In this maze, neutrons can reach the door in a single scattering event and are minimally attenuated. The other maze (b) is well designed. In this configuration,

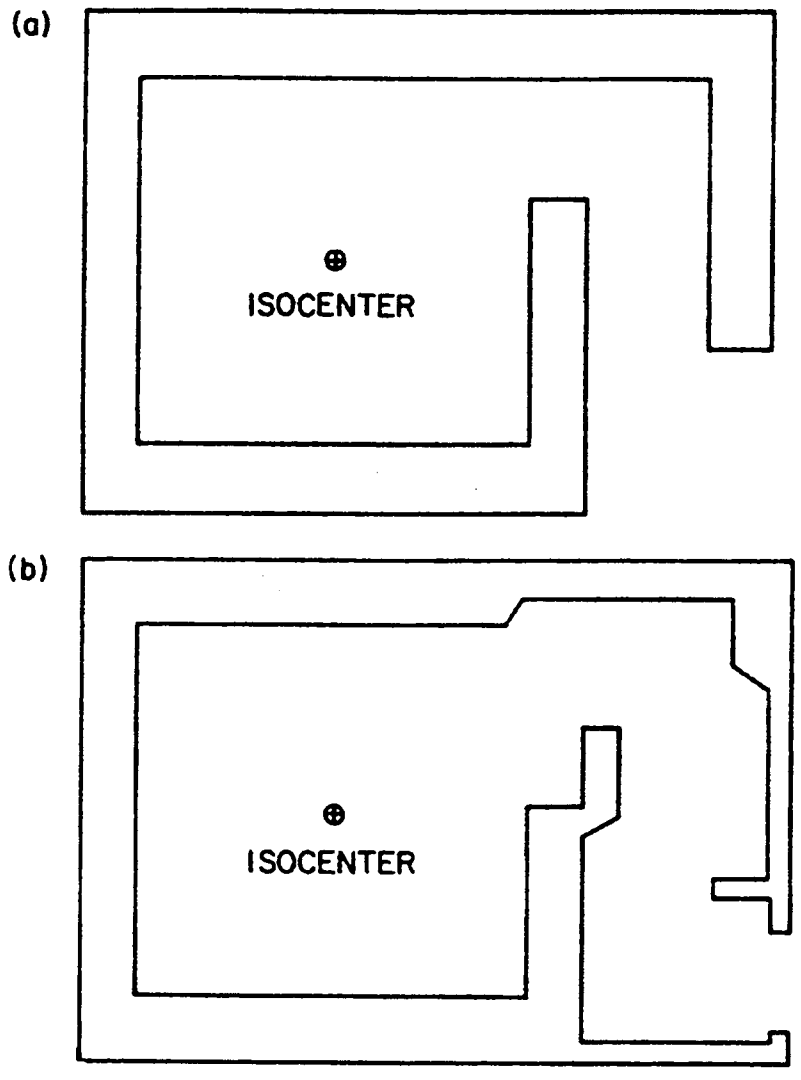


Figure 9. Maze configurations: (a) poor maze design and (b) a good maze design (NCRP, 1984).

the neutrons must scatter at least twice to reach the end of the maze. This is similar to the maze construction at East Tennessee Baptist Hospital.

The door of the radiotherapy facility can also be important in the reduction of radiation outside the treatment room, if the maze does not sufficiently attenuate charged particles. The amount of shielding necessary at the door is closely related to the maze design (NCRP, 1984). For accelerators with a nominal energy of 15 MeV and a workload of 80,000 rad $week^{-1}$ at the isocenter, dose equivalents of 2-10 rem $yr^{-1}$ have been found at the door (McCall, 1979). The dose equivalent reported by McCall (1979) was for both photons and neutrons. There is often a high occupancy factor just outside the treatment room door, due to operating staff, support staff, patient, and visitor activities. Therefore, the necessity exists to reduce these radiation levels by a factor of 4 to 20 (NCRP, 1984). A solid-core wooden door, rather than a metal door, should be chosen if polyethylene or borated materials are not employed. An industrial wooden door, one and three-quarter inches thick, would be expected to attenuate the fast neutrons at the door by a factor of approximately 0.75 (NCRP, 1984). Four centimeters of wood provides approximately the same neutron shielding as 1 cm of polyethylene (NCRP, 1984). East Tennessee Baptist Hospital has incorporated a 4 cm wooden door into the design of their radiotherapy room.

There are only two methods of reducing neutron emissions from accelerators: 1) reduce the number of neutrons produced per useful photon or 2) incorporate shielding around the accelerator to absorb the neutrons. R.C. McCall and W.P. Swanson (1979) analyzed the neutron production in a typical accelerator head and discovered that the neutron production could be reduced by absorbing the unwanted neutrons in a material of medium Z material,

such as iron. However, they also discovered that a larger quantity of iron was required to produce the necessary shielding provided by a smaller amount of lead or tungsten (NCRP, 1984). Therefore, lead and tungsten have remained popular shielding materials.

### *2.3 Radiation Protection Guidelines*

Radiation protection standards have evolved over the years and have been undergoing changes, additions, and revisions (Turner, 1986). Both advisory bodies, ICRP and NCRP, recognize the need to continually review the basic principles and upgrade the scientific information on which their recommendations are based. NCRP Report No. 39 (1971) defines occupational exposures as exposures that exclude contributions from natural background, man-made devices outside the work environment, and exposures in the healing arts. This report indicates, "the maximum permissible prospective dose equivalent for whole body irradiation from all occupational sources shall be 5 rem in any one year (NCRP, 1971)." The dose equivalent (H) is defined as the product of the absorbed dose times the quality factor for the radiation of interest (Khan, 1984). For neutrons, the quality factor varies from 3 to 10, depending on the energy of the neutron (NCRP, 1971). Absorbed dose is defined as the quotient of the mean energy imparted by the ionizing radiation per unit mass.

Maximum limits on dose equivalent have been proposed by the NCRP for persons whose occupation centers around radiation as well as for the general population. These standards have been established with the belief that at these dose levels, there is negligible probability of any demonstrable bodily injury to the individual (Khan, 1984). The maximum

permissible dose equivalents for radiation workers are set higher than those for the general public by a factor of 10. The recommended dose equivalent for occupational workers is 5 rem $yr^{-1}$, compared to the 0.5 rem $yr^{-1}$ for the public (NCRP, 1993). These values correspond to weekly limits of 0.1 rem for occupational exposures and 0.01 rem for public exposures, respectively.

## 3.0 *Theory of Radiation Detection Devices*

High-energy electron accelerators such as the electron linear accelerator are used routinely to produce beams of photons for cancer therapy. The beams generated by this device are usually contaminated with neutrons resulting from photon and electron interactions in the accelerator target, shield, collimator, and flattening filter. The dose deposited by these neutrons in patients undergoing therapy and personnel operating the accelerator is of concern to the therapist and medical health physicist. Personnel dosimeters have been aiding in the determination of neutron dose to the individuals exposed. Thermoluminescent dosimeters (TLDs) and bubble or superheated drop detectors are two of the dosimeters currently used at radiotherapy facilities. This section describes the theory on which these devices are based.

### 3.1 *Thermoluminescent Dosimetry*

Thermoluminescent dosimeters (TLDs) are solid state radiation detection devices which are commonly used by nuclear scientists, medical doctors, geologists, and archeologists (Lancaster, 1969). Nuclear scientists and doctors use these devices to determine "how much radiation has been absorbed in a given time," while the geologist and the archeologist use these devices in geological age determinations and archeological dating (Lancaster, 1969). TLDs operate by a process known as thermoluminescence, which is different from luminescence and incandescence. Luminescence is the emission of light that occurs at low temperatures and is produced by electrical action, friction, physiological processes, or chemical action (Woolf, 1973). Incandescence is defined as the emission of visible

radiation by a hot body (Woolf, 1973). On the other hand, thermoluminescence is the release of light by a crystalline material as it is heated at a constant rate.

The mechanism of thermoluminescence is dependent on the release of trapped radiation in the dosimeter chip. When the chip is heated, the trapped energy is released in the form of light. The emission of light from the heated chips is the process known as thermoluminescence. The light emitted is proportional to the amount of energy absorbed by the chips. Although many materials possess the thermoluminescent property, the most common materials or TL phosphors used as dosimetry chips are lithium fluoride (LiF), lithium borate ($Li_2B_4O_7$), calcium fluoride ($CaF_2$), and calcium sulfate ($CaSO_4$) (Lee, 1994). Table 1 provides some of the characteristics of these phosphors. Of these phosphors, LiF is most extensively studied and most frequently used for clinical dosimetry (Khan, 1984).

The crystal lattice and the energy bands play a vital role in the process of thermoluminescence. In crystalline substances, an arrangement or lattice of ions and impurities exists. Strong forces called valence bonds hold the ions and impurities in this alignment. The lattice remains unchanged until a high energy particle displaces an ion and ejects one of its electrons into orbit. In the process, the electron moves into another energy level. This level is inaccessible to the ion losing the electron, so this electron cannot be recaptured. As more and more high energy particles strike the lattice, more electrons are ejected into orbit, forming an electron cloud (Lancaster, 1969). The greater the radiation or

Table 1. Characteristics of various phosphors (Khan, 1984).

| **Characteristic** | **LiF** | **$Li_2B_4O_7$:Mn** | **$CaF_2$:Mn** |
|---|---|---|---|
| **Density** (g $cc^{-1}$) | 2.64 | 2.3 | 3.18 |
| **Effective atomic number** | 8.2 | 7.4 | 16.3 |
| **TL emission spectra range** (A) | 3500-6000 | 5300-6300 | 4400-6000 |
| **Temperature of main glow peak** (°C) | 195 | 200 | 260 |
| **Energy response** (eV) | 1.25 | 0.9 | 13 |
| **Useful range** | mrem-1x$10^5$ rem | mrem-1x$10^6$ rem | mrem-3x$10^5$ rem |
| **Fading** (%) | < 5% per 12 week period | 10% in first month | 10% in first month |
| **Light sensitivity** | Essentially none | Essentially none | Essentially none |

the longer the radiation dose occurs, the larger the electron cloud. Some impurities however, can capture the free electrons and are called traps. The more electrons in the electron cloud, the greater the possibility of a trap becoming filled.

In an individual atom, electrons occupy discrete energy levels. However, in a crystal lattice, electronic energy levels give rise to energy bands: "allowed" energy bands and "forbidden" energy bands (Khan, 1984). The "forbidden" energy band is where the impurities create the electron traps previously mentioned. These traps create metastable states for the electrons. When the material is irradiated, some of the electrons in the valence band or ground state receive sufficient energy to be raised to the conduction band. The conduction band is the highest band of energy available for electrons. However, the valence band is the band most often occupied by electrons and the band utilized in thermoluminescence. The energy difference between these bands is known as the band gap. If a thermoluminescent material is pure, an electron will not be found in the band gap. However, most thermoluminescent materials contain impurities. These impurities can be either man-made or naturally occurring. Man-made impurities are used to activate or "dope" the thermoluminescent material and can cause electrons to be trapped in the band gap. Doping is used to increase the number of traps in the material. Increasing the number of traps causes the material to thermoluminesce more brightly.

When the impurities are present in the thermoluminescent material, electron traps and holes are created. There is a vacancy formed in the valence band when the electron is promoted. The vacancy is called a hole (Knoll, 1989). If an electron from the valence band is promoted to the conduction band, the electron is free and can be caught in an electron trap.

The excess electrons are loosely bound in the crystal lattice; therefore, the holes lie just above the valence band. Since impurities create both traps and holes, both are found in thermoluminescent materials.

When radiation is absorbed by the thermoluminescent material, electrons in the valence band can be promoted into the conduction band. Once the electrons are in the conduction band, they are capable of moving into the electron traps. The holes created in the valence band can then migrate to the traps. This movement results in both a filled electron trap and electron hole. When thermoluminescent material is heated, recombination occurs. Recombination is the process by which electrons are removed from the electron holes and electron traps. Recombination results in the emission of light from the thermoluminescent material. Recombination can occur by either of two methods. The first method involves the electrons in the traps. These electrons gain enough energy to be displaced back into the conduction band. The displaced electrons can then migrate to fill a hole in the valence band, where recombination occurs with the emission of a photon. The second method of recombination involves the hole in a filled trap gaining enough energy to migrate to an electron trap. Again, recombination results in the emission of a photon. The photon emitted can then be measured and related to the energy initially absorbed in the thermoluminescent material (Knoll, 1989). A simplified energy-level diagram is provided in Figure 10.

Glow curves depict thermoluminescence versus temperature. As the temperature of the thermoluminescent material exposed to radiation is increased, the probability of releasing

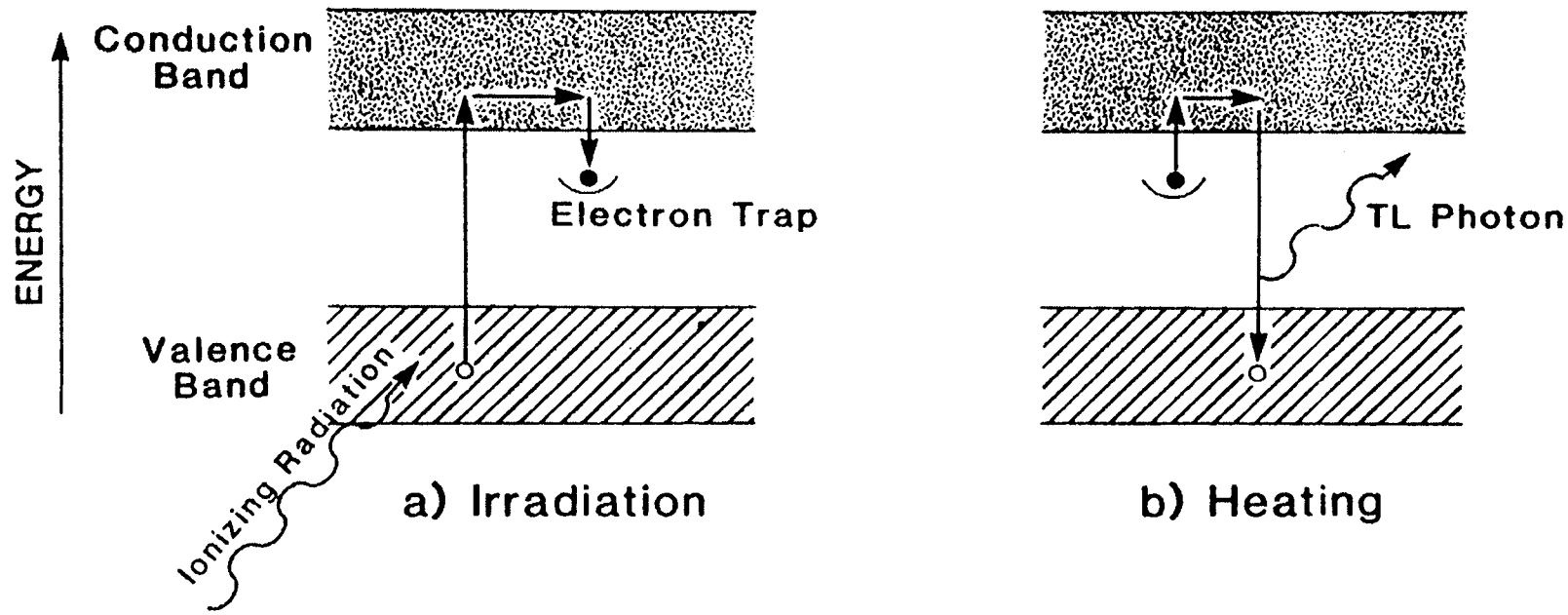


Figure 10. Energy-level diagram to illustrate thermoluminescent process (Khan, 1984).

trapped electrons increases (Khan, 1984). The light emitted increases, reaches a maximum, and then returns to zero. Since most phosphors contain a number of electron traps at various energy levels in the "forbidden" band, the glow curve can consist of a number of glow peaks. Figure 11 provides a glow curve, which represents this process. The different peaks correspond to different trapped energy levels. The total area under the glow curve, or the total light emitted, is proportional only to the received radiation (Lancaster, 1969). The heating of the phosphor will affect the height of the peak; however, heating does not affect the total amount of light output. By exposing the phosphor to a known radiation dose, an output light level can be obtained. This level can then be used to determine an unknown dose by simple proportion (Lancaster, 1969).

### 3.2 *Panasonic Thermoluminescent Dosimeter*

The Panasonic thermoluminescent dosimeter (UD-809AS) is used in personnel dosimetry and can measure neutrons (Lee, 1994). Figure 12 provides a schematic of the Panasonic TLD. As can be seen from this diagram, the dosimeter has four elements or chips constructed of lithium borate ($Li_2B_4O_7$) activated by copper ($Li_2B_4O_7$:Cu). One of the four chips is 7-lithium-11-borate ($^7Li_2{}^{11}B_4O_7$), while the other three chips are 6-lithium-10-borate ($^6Li_2{}^{10}B_4O_7$) (Lee, 1994). Filters cover these elements on both the front and back sides of the dosimeter. The front filters consist of 0.7 mm of cadmium, tin, cadmium, and cadmium, covering elements 1-4, respectively. The back filters are constructed of 0.7 mm of cadmium, cadmium, cadmium, and tin, respectively. Therefore, the fourth chip is sensitive to back-diffused thermal neutrons; the third chip is sensitive to epithermal neutrons; the second chip is sensitive to incoming thermal neutrons; and the initial chip is

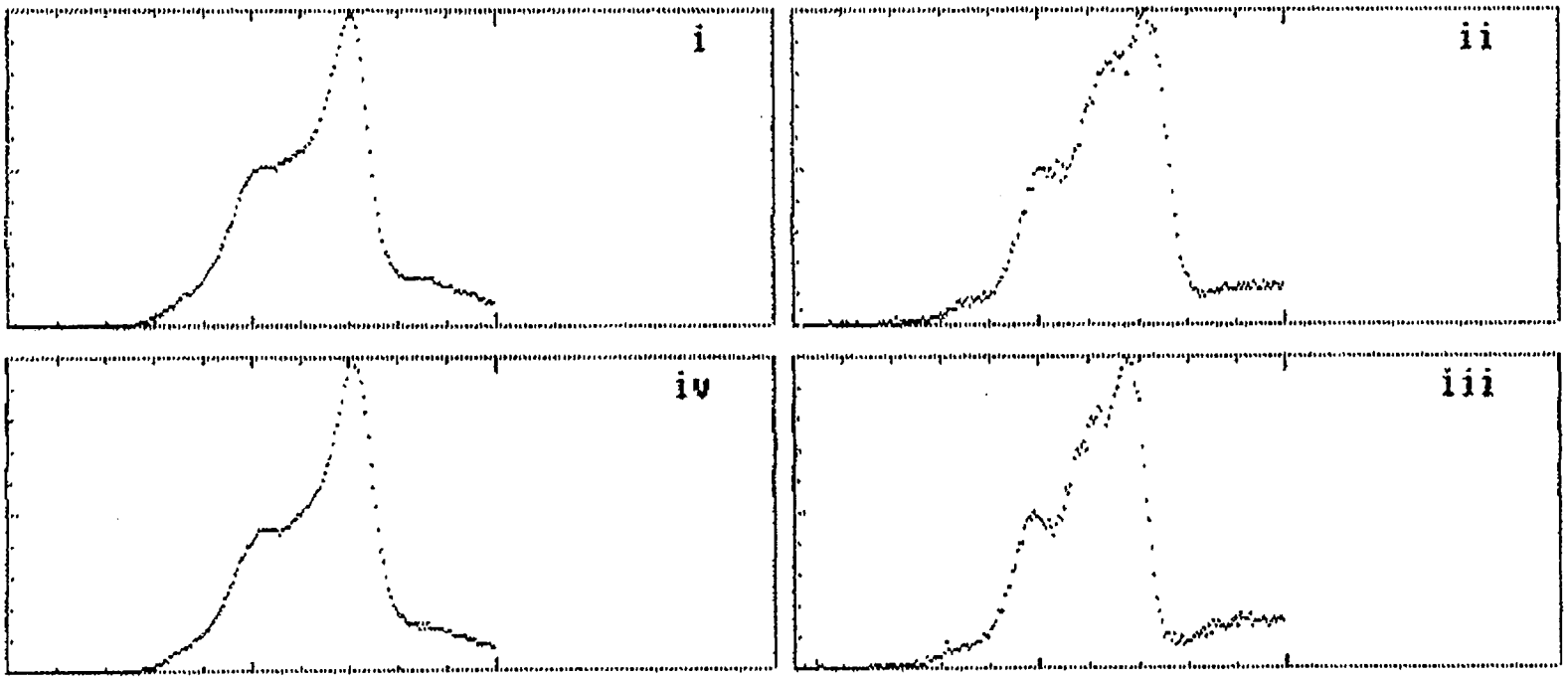


Figure 11. Glow curves (light output versus channel) for a TLD card containing four chips.

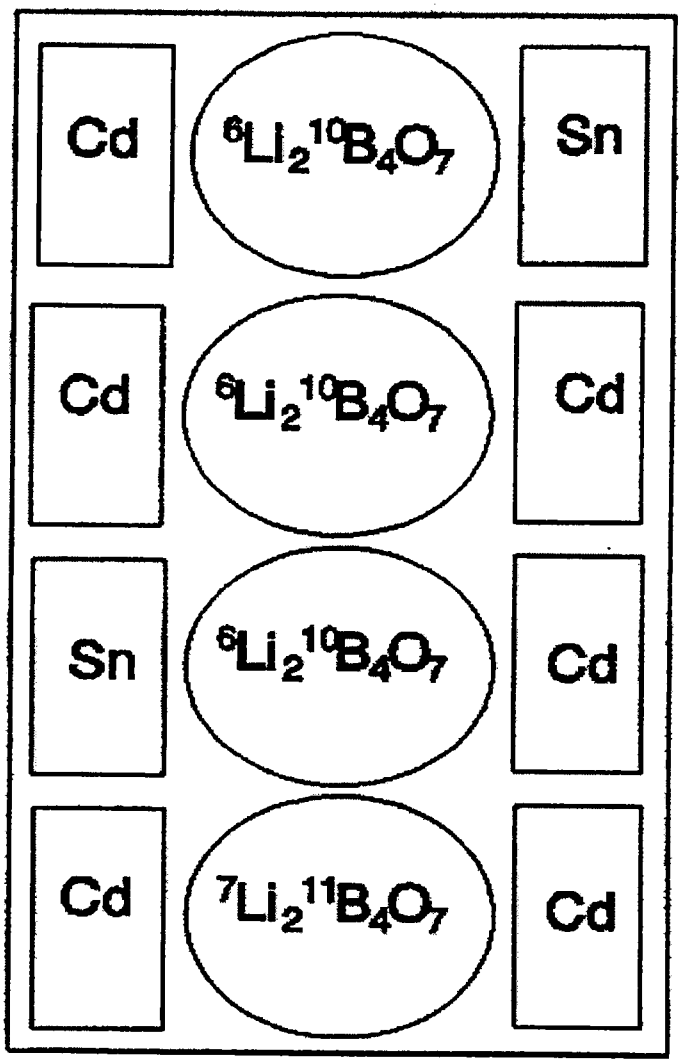


Figure 12. Panasonic UD-809AS TLD (Lee, 1994).

sensitive to gamma rays (Manfredotti and Zanini, 1993). Cadmium (Cd) is used as a thermal neutron shield because of its large absorption cross-section, 21,000 barns (b) (Turner, 1986). The absorption cross-section of $^{113}Cd$ for thermal neutrons is large for thermal energies up to approximately 0.5 eV; after that, the absorption decreases sharply (Turner, 1986).

The isotopes of lithium ($^{6}Li$) and boron ($^{10}B$) are commonly used to detect slow neutrons due to their large capture cross-sections, 953 b and 3840 b, respectively (Lee, 1994). However, the other isotopes of lithium ($^{7}Li$) and boron ($^{11}B$) are basically unresponsive to neutrons, due to their small neutron cross-sections. In order to get lithium borate to be more sensitive to thermal neutrons, the phosphor must be enriched with the isotopes of $^{6}Li$ and $^{10}B$. With the enrichment, $^{6}Li_2{}^{10}B_4O_7$ is extremely sensitive to slow neutrons. A small probability exists that epithermal and fast neutrons will be captured by the enriched lithium borate ($^{6}Li_2{}^{10}B_4O_7$) due to the Cd filter attenuating these neutrons as they pass through the filter. However, these neutrons generally interact in the individual's body and are reflected back toward the TLD (Lee, 1994). The result is that some of the epithermal and fast neutrons are moderated or slowed in the body, which allows the phosphor to capture them. These reflected, moderated neutrons are known as the albedo neutrons. The albedo effect forms the basis of the Panasonic UD-809AS (Panasonic, 1989). Although the enriched lithium borate is more sensitive to neutrons, both the unenriched and the enriched phosphors have approximately the same sensitivity to gamma ($\gamma$) radiation (Lee, 1994).

### 3.2.1 *Energy Deposition of $Li_2B_4O_7$*

The Panasonic dosimeter responds to both neutrons and gamma rays. In order to determine the response of the lithium borate to neutrons, it is essential to calculate the energy deposition in terms of kerma per unit fluence. Kerma is defined as the kinetic energy released per unit mass. Turner (1986) described kerma as the "initial kinetic energy of all charged particles liberated by the radiation per unit mass." Tanaka and Furuta (1972) calculated the response of lithium fluoride to neutrons using kerma. The kerma per unit fluence is calculated using the following equation:

$$K(E_n)_{i,j} = C\varepsilon_{i,j}(E_n + Q_{i,j})\sigma_{i,j}(E_n)D_j \qquad (2)$$

where

$K(E_n)_{i,j}$ = kerma per unit fluence for each *i*th reaction for the *j*th nucleus (erg $cm^2$ $g^{-1}$),

$E_n$ = neutron energy (MeV),

C = conversion factor from MeV to ergs ($1.6021 \times 10^{-6}$ ergs $MeV^{-1}$),

$Q_{i,j}$ = Q value of the *i*th reaction of the *j*th nucleus (unitless),

$\varepsilon_{i,j}$ = fractional energy transfer of the *i*th reaction for the *j*th nucleus for elastic scattering (unitless),

$\sigma_{i,j}$ = microscopic cross section of the *i*th reaction for the *j*th nucleus ($cm^2$),

and $D_j$ = atomic density for the *j*th nucleus (atoms $g^{-1}$) (Tanaka and Furuta, 1972).

The work performed by Lee (1994) determined the total kerma per unit fluence for lithium borate. This was accomplished by summing all *i* interactions for each nucleus (Li, B, and O) as shown in Equation 3.

$$K(E_n)_{total} = \sum_{i,j} K(E_n)_{i,j} \quad (3)$$

where

$K(E_n)_{total}$ = total kerma per unit fluence for all interaction for each nucleus (erg $cm^2$ $g^{-1}$),

and $K(E_n)_{i,j}$ = kerma per unit fluence for each *i*th reaction for the *j*th nucleus (erg $cm^2$ $g^{-1}$) (Lee, 1994).

Table 2 contains all the interactions used in the calculation of the energy deposited per unit fluence for $^6Li_2{}^{10}B_4O_7$ and for $^7Li_2{}^{10}B_4O_7$. The $^{10}B(n,\alpha)^7Li$ and $^6Li(n,\alpha)t$ are the primary reactions that contribute to the total kerma per unit fluence at the lower energies, while the elastic scattering of $^{10}B$, $^6Li$, and $^{16}O$ give the greatest contribution at higher energies (Lee, 1994). Figure 13 depicts the resulting curves for both isotopes of lithium and boron. This graph indicates that $^6Li_2{}^{10}B_4O_7$ responds better to neutrons than does $^7Li_2{}^{11}B_4O_7$.

### 3.2.2 *Integral Thermoluminescence*

Tanaka and Furuta (1977) determined that the integral thermoluminescence of a TLD could be estimated by the following equation:

Table 2. Interactions used in the calculation of energy deposited per unit fluence for $^{6}Li_2{}^{10}B_4O_7$ and for $^{7}Li_2{}^{11}B_4O_7$ (Lee, 1994).

| Isotope | $^{6}Li$ | $^{7}Li$ | $^{10}B$ | $^{11}B$ | $^{16}O$ |
|---|---|---|---|---|---|
| Interactions | $^{6}Li(n,\alpha)t$ | $^{7}Li(n,2n)^{6}Li$ | $^{10}B(n,\alpha)^{7}Li$ | $^{11}B(n,2n)^{10}B$ | $^{16}O(n,\gamma)^{17}O$ |
| | $^{6}Li(n,\gamma)^{7}Li$ | $^{7}Li(n,2n\alpha)^{2}H$ | $^{10}B(n,\gamma)\ ^{11}B$ | $^{11}B(n,n\alpha)^{7}Li$ | $^{16}O(n,d)^{15}N$ |
| | $^{6}Li(n,p)^{6}He$ | $^{7}Li(n,3n\alpha)^{1}H$ | $^{10}B(n,p)^{10}Be$ | $^{11}B(n,np)^{10}Be$ | $^{16}O(n,p)^{16}N$ |
| | $^{6}Li(n,2n\alpha)p$ | $^{7}Li(n,d)^{6}He$ | $^{10}B(n,t2\alpha)$ | $^{11}B(n,p)^{11}Be$ | $^{16}O(n,\alpha)^{13}C$ |
| | $^{6}Li(n,elastic)$ | $^{7}Li(n,\gamma)^{8}Li$ | $^{10}B(n,d)^{9}Be$ | $^{11}B(n,\gamma)^{12}B$ | $^{16}O(n,elastic)$ |
| | | $^{7}Li(n,elastic)$ | $^{10}B(n,elastic)$ | $^{11}B(n,t)^{9}Be$ | |
| | | | | $^{11}B(n,\alpha)^{8}Li$ | |
| | | | | $^{11}B(n,elastic)$ | |

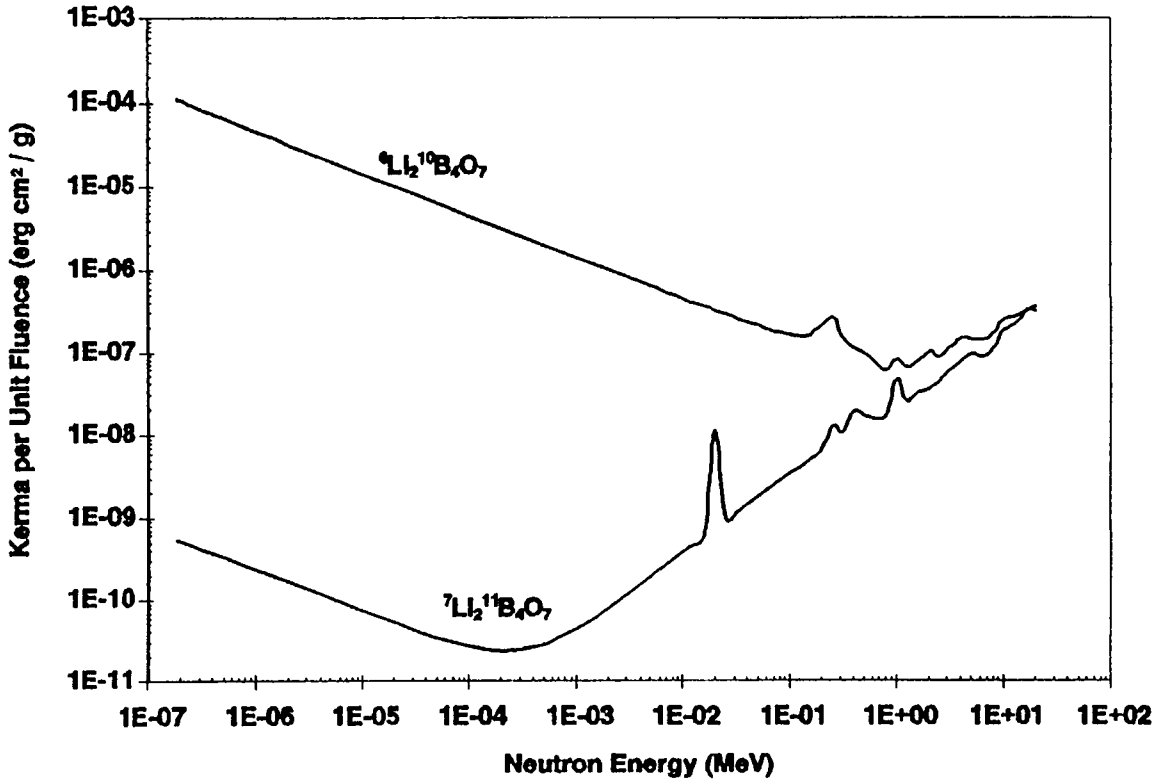


Figure 13. Energy deposition for $^6Li_2{}^{10}B_4O_7$ and $^7Li_2{}^{11}B_4O_7$ (Lee, 1994).

$$G(E_n,\lambda)_{Li_2B_4O_7} = a(\lambda)\ x\ g(\lambda)_{LiBO_{(i)}}\ x\ C_{LiBO_{(i)}}\ x\ K(E_n)_{total} \quad (4)$$

where

$G(E_n,,\lambda)_{Li_2B_4O_7}$ = Integral thermoluminescence of the TLD in a light wave band ($\lambda$),

$a(\lambda)$ = self-absorption factor of 6-lithium borate for luminescent light in wave band $\lambda$,

$g(\lambda)_{LiBO\ (I)}$ = conversion efficiency from kerma by *i*th reaction to 6-lithium borate integral thermoluminescence in wave band $\lambda$,

$C_{LiBO\ (I)}$ = correction factor for the imparted energy by the *i*th particle to 6-lithium borate TLD from the kerma value,

and $K(E_n)_{total}$ = kerma per unit fluence for all interactions of 6-lithium borate with neutron energy $E_n$.

Since the self-absorption fraction, the conversion efficiency, and the correction factor are unknown values, Tanaka and Furuta (1977) developed an overall conversion efficiency from kerma to integral thermoluminescence. The overall efficiency is determined by the following:

1. Obtain the dosimeter response to a deuterium ($D_2O$) moderated $^{252}Cf$ source that includes the summation of direct radiation and backscattered radiation from the phantom,

2. Expose the dosimeters to a known dose of $^{137}Cs$,
3. Expose the dosimeters to a known dose of $D_2O$-moderated $^{252}Cf$,
4. Obtain a ratio of $^{137}Cs$ dose to $D_2O$-moderated $^{252}Cf$ dose, and
5. Determine the overall conversion efficiency by dividing the result obtained from Step 4 by the result from Step 1 (Lee, 1994).

Using the overall conversion efficiency, the integral thermoluminescence can be determined by the following equation:

$$G(E_n,\lambda)_{Li_2B_4O_7} = \eta(\lambda)\ x\ K(E_n)_{total} \quad (5)$$

where

$G(E_n,\lambda)_{Li_2B_4O_7}$ = integral thermoluminescence of the TLD in a light wave band $\lambda$,

$\eta(\lambda)$ = overall conversion efficiency,

and $K(E_n)_{total}$ = kerma per unit fluence for all interactions of 6-lithium borate with neutron energy $E_n$.

### 3.3 *Harshaw Thermoluminescent Dosimeter*

Another popular TLD material is lithium fluoride (LiF), which is an alkali halide. According to Suntharalingam, "lithium fluoride continues to be the most commonly used phosphor for clinical dose measurements" (ICRU, 1984). However, very pure lithium fluoride does not thermoluminesce very well because there are not a significant number of traps to produce a visible light output (Lancaster, 1969). To increase the number of traps

in the material, impurities called activators are incorporated into the phosphor. Incorporation of these impurities into the phosphor is called doping. These activators are often trace quantities of magnesium, terbium, europium, or other rare-earth elements (Lancaster, 1969). The doped material thermoluminesces brightly, is chemically stable, reasonably nontoxic, and easy to form into a bar, rod, disc, or powder (Lancaster, 1969). The Harshaw Chemical Company produces lithium fluoride TLDs for use in both beta-gamma and neutron fields. (Harshaw, 1995). The TLD chips are small, portable, and nearly energy independent (Moscovitch, 1993). Since these TLDs are used in personnel dosimetry, the lithium fluoride must be able to detect albedo neutrons. Lithium fluoride has a fairly large thermal neutron absorption cross-section, approximately 940 b; therefore, it can be used as an albedo neutron TLD. The energy range of albedo neutrons is predominantly in the thermal range when exiting the body (Snapp, 1992). Albedo neutron TLDs must be worn close to the body so that the reflected neutrons can be detected upon exiting the body.

The Harshaw TLD is designed to house four individual LiF chips in an aluminum card with a thin mylar covering. A diagram of the Harshaw TLD is shown in Figure 14. Both isotopes of lithium, $^{6}$Li and $^{7}$Li, are incorporated into the Harshaw TLD, as well as in the Panasonic TLD. However, these two isotopes are paired in the Harshaw TLD design (i.e., one $^{6}$LiF chip and one $^{7}$LiF chip). One pair of chips is placed on the front plate of the plastic card and is covered by a 0.46 mm layer of cadmium (Cd). The other pair of chips is bare or uncovered. $^{6}$LiF is sensitive to thermal neutrons, beta, and gamma radiation, while $^{7}$LiF is sensitive only to beta and gamma. Since the beta/gamma response is almost

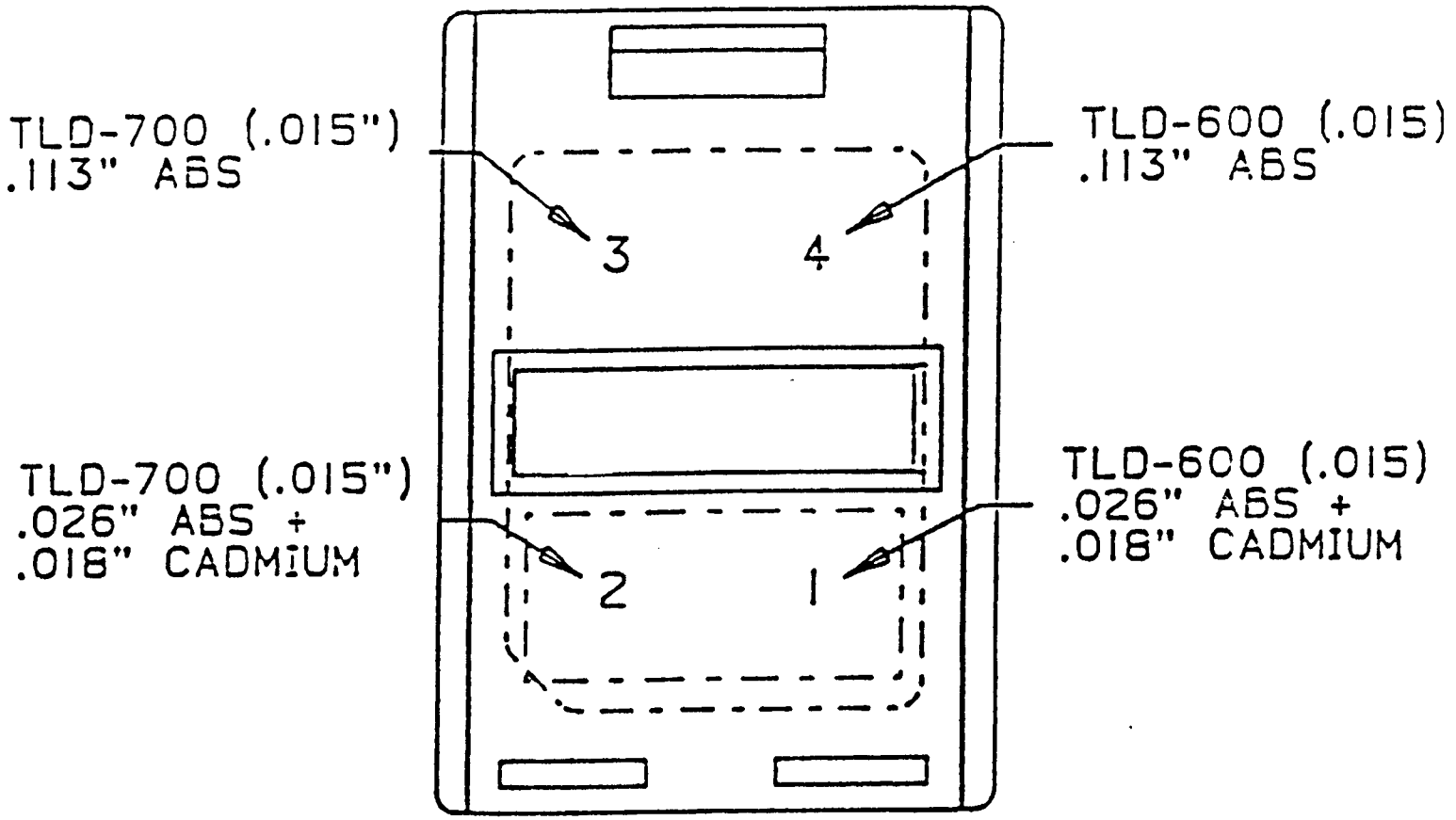


Figure 14. Diagram of the Harshaw neutron albedo TLD (Snapp, 1991).

identical for both isotopes of lithium fluoride, in mixed fields, the gamma component can be eliminated from the response (Snapp, 1992). The gamma response is eliminated by subtracting the response of $^{7}Li$ from the response of $^{6}Li$. As previously stated, Cd has a large thermal neutron absorption cross-section; therefore, the Cd-covered chips or elements detect primarily albedo neutrons, while the bare elements detect the total neutron flux (Snapp, 1992). In order to obtain only the thermal neutron component, the response of the Cd-covered elements is subtracted from the bare elements' response. The neutrons of interest in a medical facility and for radiation protection purposes are those which are above thermal energies. According to Budzanowski et al. (1993), thermal neutrons are absorbed mostly in the initial 0.3 mm of the LiF material, while absorption of 1 MeV photons is uniform throughout the detector thickness.

The Harshaw dosimeter responds to both neutrons and gamma rays. In order to determine the response and the integral thermoluminescence of the lithium fluoride to neutrons, the equations provided in the Section 3.1.1 and 3.1.2 can be used. For this dosimeter, Tanaka and Furuta (1972) determined that the main interactions between LiF and neutrons of energies below 14 MeV are $^{6}Li(n,\alpha)t$, while the elastic scattering of $^{6}Li$ and $^{19}F$ are the most contributing interactions at higher energies. A graph of the energy response for a bare LiF chip is provided in Figure 15.

### 3.4 *Auxiliary Equipment Used in Combination with TLDs*

Phantoms are used to cause dosimeters to be exposed to radiation fields similar to those appearing on the surface of the human body. Like the human body, the phantoms produce

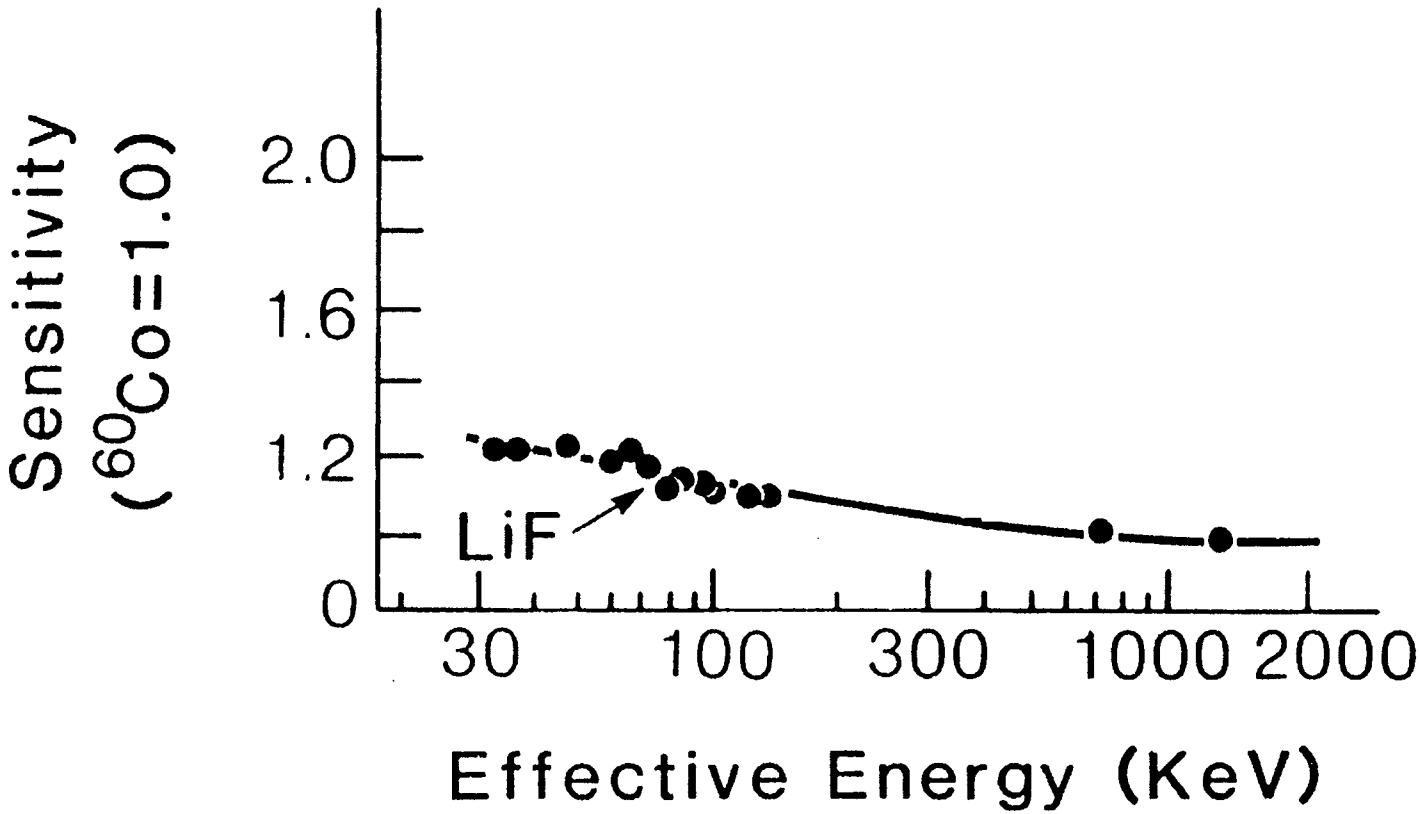


Figure 15. Energy response curve for LiF (Khan, 1984).

backscattering radiations with energy and angular distribution different from those of the incident radiations (Sims, 1993). Therefore, the phantom material should resemble human tissue so as to have the same or very similar neutron absorption and scattering properties (ICRU, 1989). According to ICRP Report 23 (ICRP, 1975), muscle, as well as other tissues such as the liver and kidney, have densities ranging between 1.03 and 1.05 g $cm^{-3}$. An ideal phantom material would be a muscle tissue-equivalent with a density of 1.04 g $cm^{-3}$ (ICRU, 1989).

### 3.4.1 *Polymethyl Methacrylate Phantoms*

The materials polymethyl methacrylate (PMMA) and Lucite are rugged solids, with a density of approximately 1.2 g $cm^{-3}$. Even though the density of PMMA is greater than the density of soft tissue, the chemical composition gives a reasonable approximation to tissue equivalence for photons (Sims, 1993). The major elemental ingredients for muscle are carbon, hydrogen, nitrogen, and oxygen, all of which are incorporated into PMMA (ICRU, 1989). For neutron radiation, the high mass density of PMMA is offset by its low hydrogen content to produce neutron scattering and dose distributions similar to that of human tissue (Sims, 1993). The rectangular shape of the phantom was originally selected for practicality, but the shape has proven to be adequate for both photon and neutron exposures (Sims, 1993). A 30 x 30 x 15 cm phantom is used to produce nearly 100% of the backscattered radiation for photon exposures. The radiation field is sufficiently uniform over the 15 x 15 cm useful area in the center of the phantom so that multiple dosimeters can be irradiated simultaneously. For neutron radiations, the phantom size was increased to 40 x 40 x 15 cm. The increase was due to the need to irradiate dosimeters

simultaneously. This was not possible with a 30 x 30 x 15 cm size phantom and neutrons, because the albedo neutron dosimeters may produce lower readings if positioned within 10 cm of the phantom edges (Sims, 1993).

### 3.4.2 *Piesch Sphere*

A method for improving the performance of moderator-type monitors that allows the estimation of neutron fluence, absorbed dose, dose equivalent, and quality factor in various stray neutron fields to an uncertainty of about ±25% has been suggested by E. Piesch (Ing and Piesch, 1984). The "single sphere technique" or the Piesch Sphere utilizes four TLDs, one mounted in the center of a 30 cm sphere and three located on the surface of the sphere. Figure 16 provides a diagram of the sphere with three thermoluminescent dosimeters mounted on the front, right, and left sides. The three TLDs positioned on the outside of the sphere act as albedo neutron dosimeters. According to J.E. Hoy (1972), the albedo neutron detectors are only slightly influenced by the neutron energy distribution, but strongly influenced by the amount of scattering material near the source. For scattered spectra, the albedo detectors over-respond (Hoy, 1972).

Ernst Piesch had determined that multisphere spectrometry or Bonner Sphere spectrometry was too cumbersome for use in the determination of unknown spectra in the field and that the computer codes used to analyze the results were too complex (Snapp, 1992). Piesch decided to develop another technique for use in the field that was less arduous and more

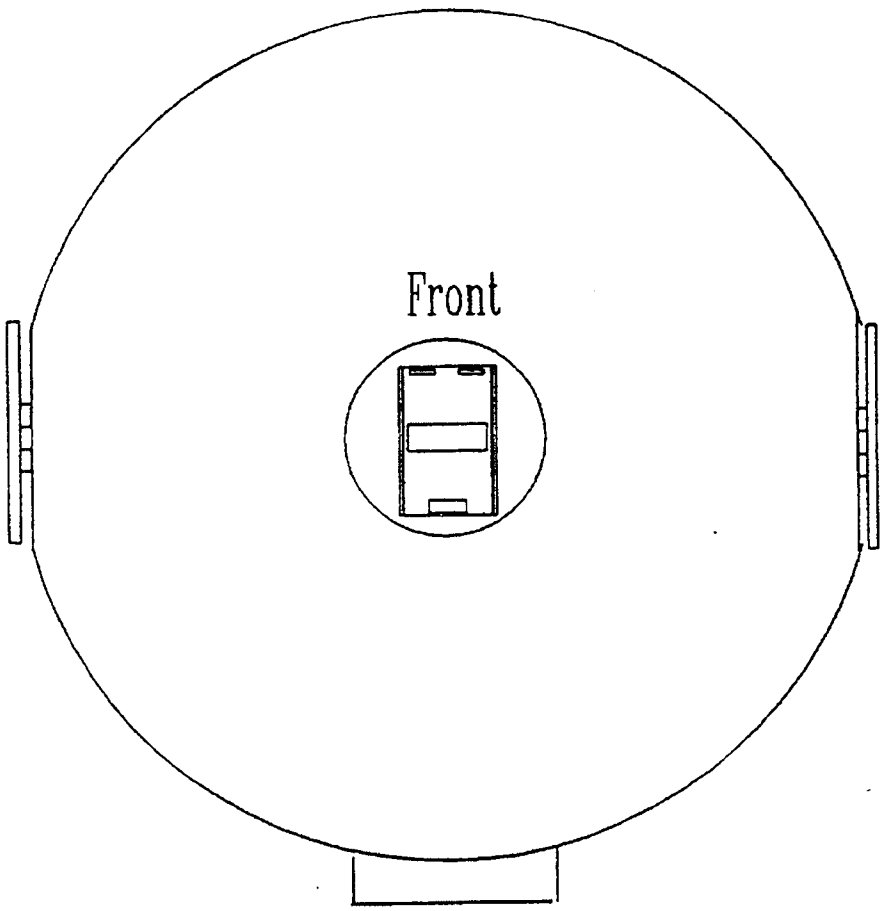


Figure 16. Piesch Sphere with TLDs mounted on the surface (Snapp, 1991).

straightforward. Piesch began his work by mounting an albedo dosimeter onto a polyethylene sphere and placing a thermal neutron detector inside the sphere. Thus, the sphere would serve as a moderator for fast neutrons and as a phantom for thermal neutrons. The detectors employed on the sphere were initially placed in boron loaded plastic holders. This setup was used to determine the incident thermal neutrons and the albedo neutrons reflecting from the sphere. Work conducted by Jonathan Snapp followed this methodology. However, the boron loaded encapsulated thermoluminescent materials were replaced with Harshaw neutron albedo thermoluminescent dosimeters placed in polyacrylonitrilebutadienestylene (ABS) plastic holders. The Harshaw detectors employ two isotopes of lithium in combination with fluoride as the thermoluminescent material.

Two isotopes of lithium fluoride ($^{6}Li$ and $^{7}Li$) were used with the "single sphere" for this work. Since $^{7}Li$ has a much lower response to neutrons than does $^{6}Li$, this isotopic material is assumed to respond only to gamma rays. $^{6}Li$ responds to both gammas and neutrons. The difference between the two can be used to measure mainly thermal neutrons (Ing and Piesch, 1985). This dosimeter consists of two TLD-600 Harshaw LiF chips and two TLD-700 Harshaw LiF chips. One of the TLD-600 chips is covered by 0.113 inches of ABS plastic only, while the other TLD-600 element is covered with both ABS plastic (0.026 in.) and 0.018 in. of cadmium. The cadmium shields the chip from thermal neutrons (Blackstock et al., 1978). The TLD-700 chips are arranged in the same manner. According to Blackstock et al. (1978), a primary advantage of using this type of albedo dosimeter is "its ability to record neutrons down to the cadmium cutoff."

### 3.5 *Apfel Bubble Detector*

Some liquids, in a superheated or metastable state, become radiosensitive (Glaser, 1952). This superheated state can be reached by decreasing the pressure of a vial containing the material to below the liquid's vapor pressure. When the vial is exposed to radiation, the incident radiation produces bubbles (Glaser, 1952). If adequate pressure is applied to the vial, the gas can be recompressed into the liquid phase, recreating equilibrium within the vial and permitting a reusable detector. Reducing the pressure in the vial by recompression would again superheat the liquid, enabling the liquid to detect other radiations. However, sustaining the liquid in the superheated state was difficult due to live time restraints (Buckner, 1991). Another problem associated with this technology was that the vial was capable of tracking only single ions. This lessened the practicality of using bubble detectors for neutron dosimetry (Buckner, 1991).

Apfel Enterprises discovered that the superheated state of a liquid could be maintained by isolating the liquid into droplets (Apfel, 1979). This discovery led to the production of the superheated drop detector (SDD™), a trademark of Apfel Enterprises Incorporated. The SDD™ isolates thousands of individual microscopic droplets of freon-based superheated liquid by dispersing them through few cubic centimeters of an inert medium (gel) contained within a vial (Riel, 1993). The isolation of the bubbles in this vial removes the difficulties associated with Glaser's bubble chambers because the droplets are maintained in a superheated state indefinitely, and the SDD™ is capable of detecting multiple ions (Buckner, 1991).

The SDD™ suspends the microscopic drops of the superheated liquid in a viscous gel and detects neutron interaction by measuring the gas volume resulting from bubble formation (Apfel, 1979). The SDD™ is contained within a piece of thin glass tubing; the resulting detector is known as a Neutrometer™, also a trademark of Apfel Enterprises Incorporated. The Neutrometer™ is a small, versatile, direct-reading, reusable neutron dosimeter. The Neutrometer™ is shown in Figure 17. A white disc floats on the surface of the superheated liquid. The formation of bubbles and the evolution of gas within the superheated liquid forces the disc upward in the Neutrometer™. The dose equivalent can be evaluated by correlating the disc position and scale provided on the vial.

The Neutrometer™, if used properly, can provide the dose equivalent neutron exposure over the entire neutron energy range, thermal to fast. This device consists of two chambers, separated by a clear piston. The lower chamber contains the gel, which is composed of a large number of 50-150 μm diameter microdrops of superheated liquid (Harper and Nelson, 1993). The drops are too small to be seen individually but cause the gel to appear cloudy. The upper chamber houses the white disc. The two chambers are separated by a clear piston that is impervious to the gel and the gas. The piston moves upward when a bubble is formed. When a neutron interacts with a superheated liquid drop, the drop suddenly boils; thus producing a gas bubble, which is large enough to be detected with the naked eye. The inert matrix holds each microscopic drop in a metastable state until high linear energy transfer (LET) radiation initiates vaporization (Riel, 1993). The vaporization is accomplished by the neutron traversing the droplet and depositing sufficient energy to form a visible bubble within the gel matrix (Harper and Nelson, 1993). Energy

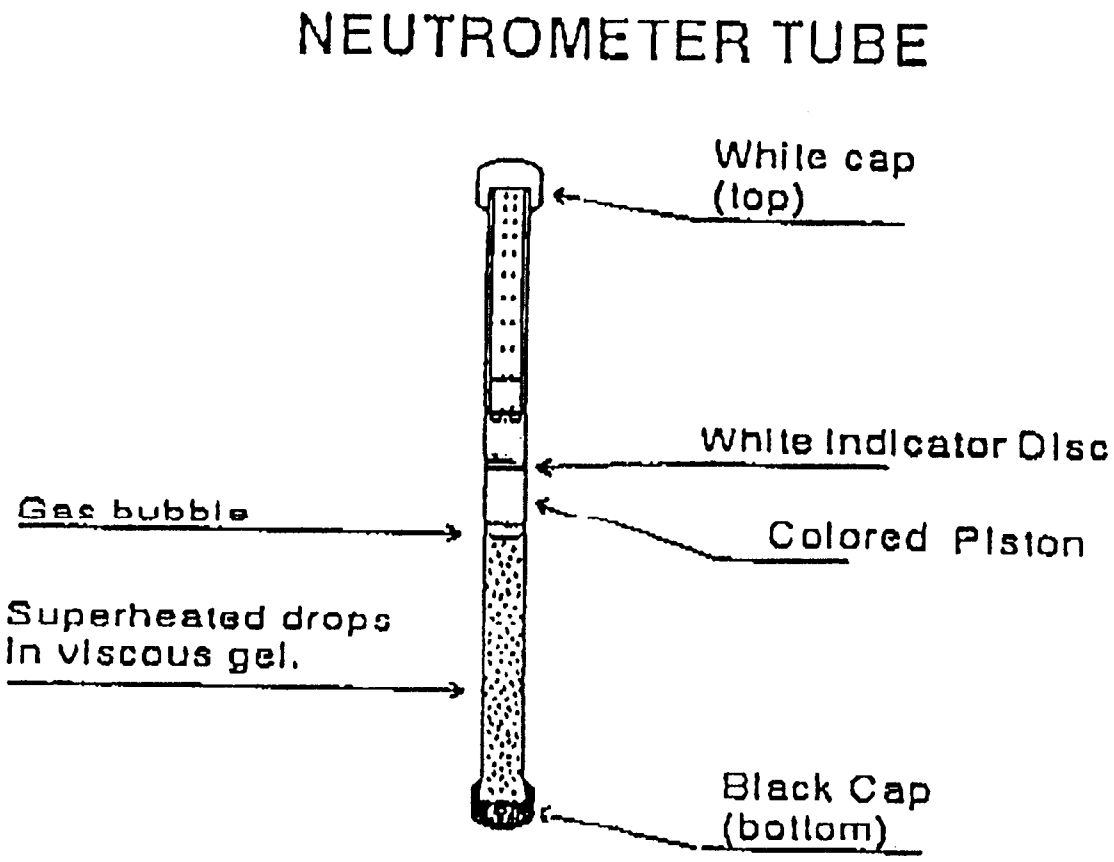


Figure 17. Diagram of an Apfel Neutrometer™ (Apfel, 1979).

stored in the drop or bubble expands the bubble from approximately $1x10^{-13}$ to $1x10^{-1}$ centimeters with no external power source (Riel, 1993).

Bubble formation is a complex process that involves the production of recoil ions, energy transfer, and sufficient bubble formation. The first phase of the process is the production of ions by a nonionizing neutron undergoing elastic scatter (Buckner, 1991). The ions produced by this scattering process are known as recoil ions. During collisions between different mass particles, energy and momentum are conserved. The conservation of energy and momentum in the center-of-mass system defines the relationship between the energy of the recoil ion and the kinetic energy of the incoming neutron in the laboratory coordinate system. The conservation of energy and momentum also defines the scattering angle of the recoil ion in the center-of-mass system, which is given by the following equation.

$$E_r = \frac{2A}{(1 + A)^2} (1 - \cos\theta_n) E_n \qquad (6)$$

where

$E_r$ = energy of the recoil ion in the laboratory system,

A = mass of the target nucleus,

$\theta_n$ = scattering angle of the recoil nucleus in the center-of-mass system,

and $E_n$ = kinetic energy of the incident nucleus in the center of mass system.

The scattering angle of the recoil ion in the center-of-mass system and the scattering angle of the recoil nucleus in the laboratory system can be related by Equation 7.

$$\cos\theta_r = \sqrt{\frac{(1 - \cos\theta_n)}{2}} \tag{7}$$

where

$\theta_r$ = scattering angle of the recoil neutron in the laboratory system

and $\theta_n$ = scattering angle of the recoil nucleus in the center-of-mass system.

Combining Equations 6 and 7 results in the relationship between the energy of the recoil ion in terms of its recoil angle in the laboratory system. The relationship is shown in the following equation:

$$E_r = \frac{4A}{(1 + A)^2}(\cos^2\theta_r)E_n \tag{8}$$

A distribution of the energy of the recoil ion from zero for grazing encounters ($\theta_r = 90°$) to a maximum energy for head-on collisions ($\theta_r = 0°$) is possible. After the energy has been

transferred to the recoil ion, the charged particle deposits its energy by interaction with the electrons and other nuclei within the gel. The interaction of the recoil ions and the gel results in ionization and excitation of the gelatinous matrix (Buckner, 1991). Ionization and excitation along the recoil ion's path induces heat, which causes the superheated liquid to vaporize or nucleate (Seitz, 1958). The basis of radiation-induced nucleation has been described by the thermal spike theory of Seitz (1958). However, fundamental questions still remain (Harper and Nelson, 1993). According to the thermal spike theory, the energy deposited by the moving recoil ion vaporizes a small amount of liquid directly along its path (the spike). This initial bubble begins to expand as it receives more thermal energy and as the spike's shock wave propagates outward into the surrounding liquid (Harper and Nelson, 1993). If the initial bubble expands to a critical size, it will become thermodynamically unstable and continue to expand by evaporating more of the liquid. The critical size of the bubble is determined by Equation 9.

$$r_c = \frac{2\sigma}{(P_b - P_l)} \tag{9}$$

where

| | | | |
|---|---|---|---|
| | $r_c$ | = | critical radius of the bubble, |
| | $\sigma$ | = | surface tension of the superheated liquid, |
| | $P_b$ | = | pressure on the inside of the bubble, |
| and | $P_l$ | = | pressure of the superheated liquid. |

This spontaneous process continues until all the host liquid has been vaporized and the resultant bubble is observable. However, if the amount of energy transferred from the recoil ion is less than the threshold required to generate a bubble of critical radius, then the

initial bubble will collapse and no vaporization will occur (Harper and Nelson, 1993). In summary, bubble formation takes place in three steps. Initially, an electrically neutral particle (neutron) interacts with the superheated liquid in the droplet, producing energetic recoil ions, which are charged particles. These charged particles deposit their energy over a given range of travel through the superheated liquid. If adequate energy is added to a small volume of liquid, a critical (small) bubble forms and continues to vaporize the entire droplet, thus forming a visible bubble (Harper and Nelson, 1993).

Neutrometers™ can be used for personnel dosimetry for doses in the range of 5 to 500 millirem. According to G. Riel (1993), bubble dosimeters are capable of measuring neutrons from the thermal range to 25 MeV, without a bulky moderator. The instrument provides high sensitivity to neutrons, while being insensitive to gamma rays. A scale is provided on the vial, but this is not used to determine the neutron dose. Instead of using the scale and the movement of the disc, which are based on the volume change, bubbles are counted. The number of bubbles can be directly correlated to the exposure, thus providing a portable, self-reading dosimeter, which is simple to use and relatively inexpensive (Harper and Nelson, 1993). The Neutrometer™ produces approximately three to five bubbles per millirem. The precise calibration is provided by the manufacturer. Bubbles of approximately one millimeter in diameter that form from the radiation interaction will rise to the top of the vial, where they can easily be counted. The sensitivity of these devices decreases in proportion to the dose, which depletes the superheated drops in the matrix (Riel, 1993).

However, this detector is temperature dependent. At room temperature, the Neutrometer™ is active. Therefore, to insure that no bubbles form due to background radiation, the detector requires refrigeration prior to use. The Neutrometer's™ sensitivity increases by about 5% per degree Celsius. Therefore, a temperature calibration factor must be multiplied by the number of bubbles detected in the superheated gel. The calibration factor of 1.0 assumes the detectors were exposed at 20 degrees Celsius. Table 3 provides the calibration factors for varying degrees in the control room. These devices also have an energy threshold of 0.025 eV (Apfel, 1995). However, the LET threshold can be changed by changing the degree of superheat, which depends on the matrix composition, pressure, and temperature (Riel, 1993).

Table 3. Temperature sensitivity correction factors (Apfel, 1992).

| Temperature (Degree Celsius) | Dose Correction Factor (unitless) |
|---|---|
| 18 | 1.10 |
| 19 | 1.05 |
| 20 | 1.0 |
| 21 | 0.95 |
| 22 | 0.91 |
| 23 | 0.86 |
| 24 | 0.82 |
| 25 | 0.78 |

## 4.0 *Methodology and Calibration*

This section details the manner in which the research was conducted, including the calibrations and correction factors used to obtain the neutron doses. For the calibrations, two sources were used with the thermoluminescent dosimeters: $^{137}Cs$ and $^{252}Cf(D_2O)$. The cesium source was used to determine the element correction factors for the Harshaw and Panasonic TLDs. The californium deuterium-moderated source was used for calculating the paired correction coefficients for the Harshaw TLDs and the neutron sensitivity factor for the Panasonic. The bubble dosimeters were not calibrated during this research because these detectors respond only to neutrons.

### 4.1 *Annealing Thermoluminescent Phosphors*

To empty a TL phosphor of all its previous radiation history, the material is annealed by heating (Lancaster, 1969). For effective annealing, the material is first heated to a very high temperature (400° C) for a relatively short time. Then the temperature is reduced to a moderate temperature for a long period of time. This two-step annealing process favors emptying both high-energy and low-energy traps. Annealing must be done every time the dosage history needs to be erased.

Annealing and reading of the Harshaw TLDs was accomplished using the Harshaw Model 4400 TLD measurement system. This system, which utilizes a sealed $^{14}C$ radioactive source contained as a Reference Light Assembly (Harshaw, 1988), is a precision, microprocessor-based, manually operated, hot gas thermoluminescent dosimetry system

used to evaluate thermoluminescent dosimeter cards, typically the 8800 Series TLD cards. The 4400 TLD Reader requires pre-purified, dry nitrogen for the heating medium.

Prior to annealing the TLDs, the cards were stored away from fluorescent light and natural sunlight, to prevent the thermoluminescent phosphor from absorbing energy. When the chips were ready to be annealed, the card was placed in the carrousel and exposed to the heating element. There are three temperatures required for each chip: preheat, maximum, and anneal. The preheat temperature establishes the temperature at which the chip will be held prior to data acquisition (Harshaw, 1988). The maximum temperature establishes the maximum temperature to be reached during the acquisition process. For this particular reader, the maximum temperature is 300 °C. The anneal temperature is the temperature level held at the end of the cycle to assure that all radiation effects are cleared from the chips (Harshaw, 1988). As each chip is individually read, the glow curve appears on the TLD reader screen. The glow curve is also read by the computer, along with the reading for each chip. The other chips are read in order, with the results displayed on the reader and the computer screen in nanocoulombs (nC). After the chips have been annealed, the previous radiation history has been erased and the chips are ready to be exposed.

The same method of annealing was conducted for the Panasonic TLDs, with the exception of the reader. For this series of dosimeters, the Panasonic UD-702E manual reader was used (Panasonic, 1989). This reader utilizes a tungsten lamp that is filtered by a silicon filter so that infrared radiation heats the thermoluminescent phosphor. After the phosphor is heated, the energy stored in the traps is released as photons, which are counted by a

photomultiplier tube (PMT). The photons emitted are displayed in units of mR*, which are Panasonic TLD reader output values (Panasonic, 1989).

### 4.2 *Calibration of Thermoluminescent Phosphors with Known Spectra*

The Harshaw TLDs and the Panasonic TLDs were irradiated with a $^{137}Cs$ source at a distance of 0.75 m on a PMMA phantom positioned 1 m above the floor at the Radiation Calibration Laboratory (RADCAL) facility. The distance of 0.75 m was chosen to be within the 0.5 m distance for standard neutron measurements and the 1.0 m distance for standard gamma measurements, according to the American National Standards Institute (ANSI) (ANSI, 1993).

A maximum of eight TLD cards were taped with masking tape to Lucite plates. The plates were then mounted to a PMMA phantom and irradiated to a dose of 500 mrem of $^{137}Cs$. After all cards were exposed, the annealing and reading process was conducted twenty-four hours after the calibration, as previously described. The cards were read twenty-four hours after irradiation to insure that most of the excited electrons have settled into traps. However, cards should be read within seventy-two hours to prevent fading. A second calibration was performed using the $^{252}Cf$ source moderated with $D_2O$. For this calibration, the phantom and cards were placed at a distance of 0.5 m, which was chosen to minimize room-scattered radiation (ANSI, 1993). Once the exposures were completed, the materials were annealed and read using the previously described methods.

### 4.3 *Accelerator Exposures*

For the linear accelerator measurements, the field size was 10 x 10 cm, with a 100 cm SSD (source to skin) and/or TSD (target to water surface) distance. The absorbed dose was positioned at a water ($H_2O$) depth of 3.3 cm, which is the reference point on the central axis of the beam. With this size field, the monitor unit (MU) conversion to centigray is 1 (i.e., 1 MU = 1 cGy).

The Harshaw TLDs were taped to the outside of the Piesch Sphere, while one was inserted into a polyethylene case within the Sphere. The Sphere and detectors were placed on a 4 ft. aluminum stand, positioned at 5.22 meters within the accelerator maze. The accelerator delivered varying amounts of photon radiation. The process was repeated at the distances of 8.27, 10.10, 13.15, and 15.2 (door) meters within the accelerator maze. The same process was completed for the Panasonic detectors. However, these detectors were mounted on the PMMA phantom for irradiation. Twenty-four hours later, the TLDs were read and annealed at the Oak Ridge National Laboratory.

The Apfel bubble detectors were calibrated by the manufacturer prior to exposure in the radiation field produced by the 18 MeV linear accelerator. The bubble dosimeters were refrigerated prior to use at East Tennessee Baptist Hospital. The detectors were allowed to reach room temperature (22 °C) prior to exposure at the Hospital, as recommended by the supplier. The detectors were then suspended in the horizontal position from the ceiling with nylon cords at the same locations used in the TLD exposures. Again, the accelerator delivered varying amounts of electron radiation to the target, thus producing a mixed field.

Since bubble dosimeters provide a visual readout, the bubbles were counted after each irradiation to determine the dose.

### 4.4 *Correction Factors for Harshaw TLDs*

Once the calibrations are completed, the results obtained are used to develop correction factors: element correction factors and paired correction coefficients. For the Harshaw TLDs, element correction factors and paired correction factors are required before the dose to the unknown field can be determined from the TLD readings. Element correction coefficient (ECCs) can be described by the following equation:

$$ECC = \frac{DE(^{137}Cs)}{R_i} \tag{10}$$

where

ECC = element correction coefficient ($^{137}$Cs mrem equivalent $nC^{-1}$),

$DE(^{137}Cs)$ = 500 mrem,

and $R_i$ = response for the *i*th. chip (nC).

Once the ECCs were determined from the calibration exercise, each chip's response from the hospital exposure was multiplied by the corresponding ECC. The next step in determining the dose is the calculation of the dose produced by neutrons only.

Since the Harshaw TLD responds to both neutrons and gammas, the gamma component must be removed from the response. The chips positioned in locations 1 and 4 measure neutrons and gammas ($^{6}$LiF). The chips in positions 2 and 3 measure only gamma radiation ($^{7}$LiF). Therefore, the values for chip response due solely to neutrons can be determined by subtracting the response of chip 2 from chip 1 (1-2) and chip 3 from chip 4 (4-3). These neutron corrected values can then be used to determine the paired correction coefficient (PCC).

The PCC calculation is obtained by using Equation 11.

$$PCC_i = \frac{DE(^{252}Cf(D_2O))}{(R_{ij} - R_{ik})} \tag{11}$$

where

$PCC_i$ = paired correction coefficient for chip pair (1-2 or 4-3) (unitless),

$DE(^{252}Cf(D_2O)$ = 500 mrem,

R = ECC corrected response from $^{137}$Cs calibration (mrem),

j = chip 1 or 4, respectively,

and k = chip 2 or 3, respectively.

The accelerator exposure responses can be corrected using the following equations:

$$(X_1 - X_2)_j \times PCC_{(1-2)j} = W_j \quad (12)$$

$$(X_4 - X_3)_j \times PCC_{(4-3)j} = Y_j \quad (13)$$

where

$X_{1 \text{ through } 4}$ = ECF-corrected response from the accelerator exposure (mrem),

$PCC_j$ = paired correction coefficient for pairs (1-2 and 4-3) (unitless),

$W_j$ = dose for the cadmium covered pair (1-2) (mrem),

and $Y_j$ = dose for bare chip pair (4-3) (mrem).

For each location within the maze, the sphere has five responses (front, back, right side, left side, and center). The doses were obtained by averaging these five responses at each location.

### 4.5 *Correction Coefficients for Panasonic TLDs*

For Panasonic TLDs, the correction factors employed are the element correction factor and the neutron dose equivalent conversion factor. The element correction factor is determined by a three-step process described briefly:

1. Irradiate reference dosimeters to $^{137}Cs$ and read twenty-four hours after irradiation.
2. Divide the reference dose of $^{137}Cs$ by the response of each chip to obtain the ECF for each chip.
3. Calculate the mean ECF of the dosimeters.

The true $^{137}Cs$ millirem equivalent response of any Panasonic TLD chip can be determined with the set of ECFs produced in Step 3 (Panasonic, 1989). The reference dose was 500 mrem for each exposure used in determining the correction factor. The TLD cards were read after a twenty-four hour period to insure that all excited electrons within the phosphor could fall into a trap and to minimize fading, which decreases the light output response of the phosphor. The mean response was used to insure uniformity among all Panasonic TLD cards. Element correction factors (ECFs) can be determined by the following equation:

$$ECF = \frac{DE(^{137}Cs)}{R_i} \tag{14}$$

where

ECF = element correction factor ($^{137}Cs$ mrem equivalent mrem $mR^{*-1}$),

$DE(^{137}Cs)$ = 500 mrem,

and $R_i$ = response for the *i*th. chip ($mR^{*}$).

Another correction factor was used in determining the neutron dose is $k_n$, which corrects for neutron sensitivity. This correction factor represents the $D_2O$ moderated neutron dose in units of mrem $mR^{*-1}$. This correction factor can be determined using the procedure described above, with the exception of the reference source, which is a $^{252}Cf(D_2O)$ moderated source. Since the dose is expressed in mrem, the $k_n$ correction factor is multiplied by the ECF-corrected response instead of dividing by the response to obtain the dose. The Harshaw TLD PCC correction coefficient is the $k_n$ correction factor equivalent for Panasonic TLDs. The $k_n$ calculation is accomplished by using Equation 15.

$$k_n = \frac{DE(^{252}Cf(D_2O))}{R_i} \tag{15}$$

where

$k_n$ = neutron sensitivity correction factor for each chip (unitless),

$DE(^{252}Cf(D_2O)$ = 500 mrem,

and $R_i$ = ECF-corrected response from $^{137}Cs$ calibration (mrem).

## 5.0 *Results*

When estimating the radiation protection requirements for an installation that utilizes high energy accelerators, consideration must be given not only to x-rays produced by the machine, but also to the neutrons generated when high-energy photons or electrons are absorbed. Gamma shielding requirements are well known, but little precise information is available on a number of problems associated with neutron shielding. It is important, therefore, to be able to estimate the neutron-attenuating characteristics of entrance labyrinths for radiotherapy treatment rooms (Kersey, 1980.) Three methods, $Li_2B_4O_7$ TLDs, LiF TLDs, and bubble dosimeters, are presented for estimating the radiation dose to be expected at various locations within the treatment room maze, where neutrons are present.

### 5.1 *Equipment Setup*

Measurements were made at five separate locations within the labyrinth of the Baptist Hospital Radiation Oncology Department's linear accelerator treatment facility. The locations were 5.22, 8.27, 10.10, 13.15, and 15.2 meters away from the isocenter, the distance from the source to the axis of gantry rotation, of a water phantom at a depth of 1.7 cm, which is called the depth of maximum dose ($D_{max}$). $D_{max}$ is the depth at which the relative dose reaches its peak and begins to decline. The linear accelerator was operated under the standard calibration conditions for all simulations. The standard calibration conditions include a 10x10 cm rectangular field over the surface of the water phantom, with a source to skin distance (SSD) of 100 cm. The length of time the accelerator operates is described by the number of monitor units. Monitor units (MU) are essentially

the time that the accelerator is programmed to produce photons or electrons. Under the calibration conditions, 1 MU is equivalent to 1 cGy (centigray) at the isocenter in both x-ray and electron therapy modes. Electron therapy was not included in this research since neutron production is insignificant. Neutron production by electron therapy can be neglected since the electron beam current is only about 1% of that required for x-ray therapy (Kersey, 1980.)

### 5.2 *Detector Types*

The types of detectors utilized in this research include Harshaw TLDs, Panasonic TLDs, and Apfel bubble detectors. The Harshaw TLD chips are composed of $^{6}Li$ and $^{7}Li$ and placed within a polyacrylonitrylbutadienestylene resin (ABS plastic) card or holder. The cards were located on the front, back, right, left, and center of a polyethylene sphere known as the Piesch Sphere. The responses of each chip are summarized in Table A1 of the Appendix.

The Panasonic chips are composed of $^{6}Li_2{}^{10}B_4O_7$ and $^{7}Li_2{}^{11}B_4O_7$ and contained within a cadmium- and tin-filtered plastic card. The Panasonic chips were placed on the front of a polymethyl methacrylate (PMMA) phantom. The responses of the Panasonic TLDs are given in Table A2 of the Appendix.

The Apfel bubble detectors are composed of a superheated, viscous gel, which is located within a plastic vial. The vials of gel were suspended horizontally in air from the ceiling of

the treatment room with plastic thread. The responses of the bubble detectors are also provided in the Appendix (Table A3.).

### 5.3 *Calibration Factors*

Unlike the bubble detectors, both types of TLD used in this research are sensitive to gamma radiation. For this reason, the TLDs were calibrated against a known source of gamma radiation. $^{137}$Cesium was chosen to determine a correction factor for gamma rays because its radiation produces a good statistical response in all elements (Lee, 1994). The correction factor used for the Harshaw TLDs is an element correction coefficient (ECC), while the correction factor used for the Panasonic TLDs is an element correction factor (ECF). Both the ECC and the ECF are determined for each element by dividing the exposure dose in mrems by the chip response in nanocoulombs (nC) or mR*. For this research, the reference dose was 500 mrem. The mean ECC and ECF were determined and used to correct the original response of each chip or element. Once the response is corrected, its units are $^{137}$Cs equivalent mrem.

For the Harshaw TLDs, another correction factor, the paired correction coefficient (PCC), is required to determine the neutron sensitivity of the phosphors. The paired correction coefficient corrects each element's response for neutron sensitivity. A $^{252}$Californium heavy-water-moderated ($D_2O$) source chosen for this calibration. The $^{252}$Cf ($D_2O$) moderated source was selected due to the broad distribution of neutrons from thermal energies to above 5 MeV (Snapp, 1992). The PCC is determined by dividing the reference dose by the difference of the $^{137}$Cs equivalent responses of chips 1 and 2 or chips 3 and 4

(i.e. reference dose/[(R1 x ECC)-(R2 x ECC)] or [(R4 x ECC) - (R3 x ECC)]). The reference dose used to obtain the $^{252}Cf$ ($D_2O$) corrected response was also 500 mrem. The ECC and PCC values are shown in Tables A4 and A5, respectively in the Appendix. In addition to the ECC and the PCC, the Harshaw TLDs also require a calibration factor and two linear coefficients, $\alpha$ for chips 1 and 2 and $\beta$ for chips 3 and 4, when using the Piesch Sphere. The alpha and beta coefficients and the calibration factor were obtained from spectral experiments developed by Ernst Piesch (1984). The values for $\alpha$ and $\beta$ were $1.39 \times 10^{2}$ and $3.84 \times 10^{4}$, respectively. The calibration factor was $1.21 \times 10^{-4}$.

With any lithium phosphor, gamma rays are detected in addition to neutrons. In order to determine the dose produced by neutrons only, the gamma component must be subtracted from the total. Thus, the need for the subtraction response (R1-R2) and (R4-R3). In several instances during this research, the gamma response of chip 3 was greater than the combined response of chip 4 for neutrons and gammas, which resulted in negative values for the neutron dose for this chip pair. Since negative neutrons do not exist, the negative values were replaced by zero when determining the total neutron dose (Miller, 1996).

The Panasonic TLD also has an additional correction factor ($k_n$), which is equivalent to the Harshaw PCC. The correction factor $k_n$ is determined by dividing the $^{252}Cf(D_2O)$ moderated dose by the gamma corrected response of each element. In the Panasonic TLD, chip 1 is sensitive to only gamma radiation. The other three chips are sensitive to both gamma rays and neutrons. Therefore, to obtain the gamma corrected response, the response of chip 1 is subtracted from chips 2, 3, and 4. The response of chips 2, 3, and 4 are then individually divided into the reference dose to obtain the neutron dose for each

chip. These values can then be summed to determine the total neutron dose. The reference dose for the $^{252}Cf(D_2O)$ moderated source was 500 mrem. The chip responses and the ECF and $k_n$ correction factors are shown in Tables A6 and A7 of the Appendix.

The Apfel bubble detectors have only one correction factor, which is dependent on temperature. However, the temperature of the treatment room was 68° C (20° F), which does not require the temperature correction. The maximum dose per location and the maximum dose per monitor unit are displayed in Table A8 in the Appendix.

### *5.4 REDC Comparison*

The Piesch Sphere has been used by others to determine the dose equivalent above an open hot cell, in a counting room, and in the control room at ORNL's Radiochemical Engineering Development Center (REDC) (Snapp, 1992, and Casson, 1994). The correction coefficients (ECC and PCC) determined for these experiments were applied to the observed responses of the Harshaw TLD measurements conducted with the linear accelerator. The responses and neutron dose obtained by using the two different sets of correction coefficients are provided in Tables A9 and A10, respectively.

A comparison of the measured doses based on the three different sets of ECC and PCC values was made. The alpha, beta, and calibration factors were not varied. Table 4 in this section describes the results of this comparison in terms of percent difference, with Set 2 being arbitrarily chosen as the theoretical value. Chip responses from the linear accelerator exposure were multiplied by the corresponding ECC and PCC values for each set of REDC experiments and compared to the ECC and PCC corrected responses obtained from

Table 4. Harshaw TLD total dose comparison using different ECC and PCC values.

| TLD ID Number | Total Dose (Set 2) | Total Dose (Set 1) | Total Dose (Hospital) | % Difference (Set 2/ Set 1) | % Difference (Set 2/ Hospital) |
|---|---|---|---|---|---|
| unitless | mrem | mrem | mrem | % | % |
| | | | | | |
| 153300 | 344.01 | 663.00 | 276.34 | 93 | 20 |
| 153301 | 219.60 | 424.43 | 176.64 | 93 | 20 |
| 153302 | 95.76 | 185.88 | 77.18 | 94 | 19 |
| 153307 | 116.10 | 225.70 | 93.64 | 94 | 19 |
| 153309 | 12.62 | 26.15 | 10.49 | 107 | 17 |
| 153311 | 11.75 | 25.50 | 9.99 | 117 | 15 |
| 153313 | 22.15 | 45.57 | 18.35 | 106 | 17 |
| 153319 | 131.82 | 254.81 | 106.04 | 93 | 20 |
| 153327 | 86.16 | 167.17 | 69.43 | 94 | 19 |
| 153332 | 948.50 | 1823.36 | 761.03 | 92 | 20 |
| 153335 | 0.25 | 0.47 | 0.02 | 87 | 92 |
| 153341 | 1128.27 | 2187.60 | 908.91 | 94 | 19 |
| 153348 | 6.75 | 16.24 | 6.05 | 141 | 10 |
| 153349 | 488.04 | 940.15 | 391.96 | 93 | 20 |
| 153352 | 0.15 | 0.27 | 0.12 | 88 | 17 |
| 153365 | 540.33 | 1042.83 | 434.33 | 93 | 20 |
| 153368 | 804.03 | 1558.12 | 647.56 | 94 | 19 |
| 153373 | 374.57 | 731.60 | 302.80 | 95 | 19 |
| 153377 | 276.98 | 533.94 | 222.52 | 93 | 20 |
| 153382 | 198.77 | 383.98 | 159.84 | 93 | 20 |
| 153384 | 134.01 | 270.66 | 110.07 | 102 | 18 |
| 153387 | 1.00 | 1.86 | 0.81 | 186 | 19 |
| 153390 | 79.48 | 155.14 | 64.23 | 95 | 19 |
| 153392 | 0.46 | 0.85 | 0.37 | 85 | 19 |
| 153409 | 33.53 | 67.62 | 27.52 | 102 | 18 |

this study. The average ECC values for chips 1-4 determined by this research were 1.81, 1.60, 1.63, and 1.73, respectively. The average PCC value was 0.13 for chips 1 and 2 and 0.11 for chips 3 and 4. Average values were used so the response of any Harshaw TLD card could be used to describe the total neutron dose. If calibration equipment was not available, individual values for ECC and PCC correction factors could not be determined. Using each individual ECC and PCC is also impractical in personnel dosimetry since each TLD chip cannot be individually corrected prior to use in the field. The total neutron dose calculated from this research is within 10-20% of the neutron dose calculated using the ECC and PCC values from the second set of REDC experiments, with the exception of one TLD. This TLD contained chips (3 and 4) which produced a response greater to the gamma component than the combined gamma and neutron component. Since the response was greater to gammas only, the subtraction of the chips 3 and 4 resulted in a negative value, which was reported as a zero in subsequent calculations. Therefore, the total neutron dose for this TLD was based solely on chips 1 and 2, which measures the total neutron flux. The comparison between the two sets of ECC and PCC values determined during the REDC experiments produced differences between 85 and 141%, which indicates that the ECC and PCC are important factors in determining the total neutron dose with the Piesch Sphere.

### 5.5 *Detector Intercomparison*

A comparison of the three detector types was also conducted during this research. Table 5 describes the intercomparison of all three detectors. The bubble detector and the Panasonic neutron dose estimate per monitor unit varied by a factor of three for the initial point

Table 5. Comparison of the values for the total dose after exposure to the Varian Clinac® 2100C for the Panasonic, Harshaw, and Apfel detectors.

| Location | Panasonic | Harshaw | Apfel | Ratio of Apfel to Panasonic | Ratio of Apfel to Harshaw | Ratio of Panasonic to Harshaw |
|---|---|---|---|---|---|---|
| meters | mrem/MU (average) | mrem/MU (average) | mrem/MU (maximum) | unitless | unitless | unitless |
| | | | | | | |
| 5.22 | 7.99E-02 | 1.89E-01 | 2.56E-02 | 0.32 | 0.14 | 0.42 |
| 8.27 | 2.77E-02 | 5.54E-02 | 2.15E-03 | 0.08 | 0.04 | 0.50 |
| 10.10 | 1.51E-02 | 4.30E-02 | 1.27E-03 | 0.08 | 0.03 | 0.35 |
| 13.15 | 3.15E-03 | 3.63E-03 | 2.42E-05 | 0.01 | 0.01 | 0.87 |
| Door | 6.06E-04 | 1.51E-03 | 0.00E+00 | 0.00 | 0.00 | 0.40 |

(5.22 m) in the maze, but for the next two locations, 8.27 and 10.10 m, respectively, the values varied by a factor of 13. The Harshaw TLD and the bubble detector neutron dose responses were even more different than the Panasonic to Apfel ratios. The initial point in the maze had a correlation coefficient of 0.14, which is approximately a factor of 7 different for the Panasonic and Apfel detectors. The correlation worsens for locations closer to the door, with the largest difference occurring at 13.15 meters from the isocenter. Since the Apfel bubble detector did not detect any neutrons at the door, no comparison could be made at this location. The comparison between the two types of TLDs was much better. The total neutron dose per monitor unit was within a factor of 3 or less for all locations studied within the labyrinth. The responses were approximately equivalent at 13.15 meters from the isocenter.

### 5.6 *Kersey Method Comparison*

R.W. Kersey has proposed a method by which the neutron dose can be determined within an accelerator treatment room's maze. According to Kersey, this method has been found to empirically yield estimates of neutron levels at maze entrances which are correct to 50% of the measured value (Kersey, 1980). The assumptions made by Kersey include a workload of 50,000 rads per week at the isocenter, which is delivered in a 5 day period in the 16 MeV treatment mode. The workload represents the treatment of 25 patients per day in the 16 MeV treatment mode, with the a dose rate of 400 rads per minute at the isocenter. This representation is assumed to be realistic of the dose received by the hospital staff (Kersey, 1980). Since the dose rate employed at Baptist Hospital's linear accelerator is 320

rads per minute, a correction of 0.8 (320 rads $min^{-1}$/400 rads $min^{-1}$) was applied to all values used by Kersey to compensate for the difference in dose rates.

In Kersey's approximation, the inverse square law is used to determine the weekly neutron dose at the inner end of the maze. The point at the inner end of the maze is just visible from the isocenter. The point selected for this comparison was 5.22 meters. The assumed x-ray dose at 1 meter from the isocenter ($I_o$) was 50,000 rads per week, while the neutron dose at 1 meter from the isocenter ($I_n$) was 75 rems per week (Kersey, 1980). Correcting the values for $I_o$ and $I_n$ resulted in values of 40,000 rads per week and 60 rem per week, respectively. Thus, to find the weekly neutron dose at 5.22 meters, the neutron dose at 1 meter from the isocenter is divided by the square of the distance from the isocenter (5.22 m), which results in a neutron dose of 2202 mrem/week.

The dose at a point near the outer end of the maze can also be determined. The neutron dose at the outer end of the maze is dependent on the tenth value distance (TVD). The tenth value distance is defined as the distance along the centerline of the maze which attenuates the neutron dose in rem by a factor of 10. The TVD in air used by Kersey is approximately 5 meters, which agrees with experimental results (Kersey, 1980). The equation used in determining the neutron dose at the outer end of the maze is defined as

$$I_q = \frac{I_p}{10^{(\frac{d_2}{5})}} \tag{16}$$

where

$I_q$ = neutron dose at the outer end of the maze (mrem/week),

$I_p$ = weekly neutron dose at the inner end of the maze (mrem/week),

and $d_2$ = distance from the inner end of the maze to the outer end of the maze (m) (Kersey, 1980).

The resulting dose at the outer end of the maze was 58 mrem per week.

A comparison was made between the detectors placed at points 5.22 and 13.15 meters using this methodology. In all cases, the inner point neutron dose measurement was less than the dose predicted by Kersey. Both the TLD detectors over responded for the outer end of the maze, which is partially explained by the manner in which the TLDs were calibrated. The TLDs were calibrated with a known spectrum, but the spectrum was unknown at the hospital. The hospital spectrum should contain a larger thermal neutron component due to wall scatter. The larger thermal neutron component will cause the TLDs to over-respond. However, the Apfel detector again under responded. This can also be explained by the thermal neutron component. Since a certain amount of energy is required to nucleate a bubble, the bubble dosimeters would have under-responded at the door due to low energy neutrons. The Panasonic TLDs placed at both locations are within a factor of three to Kersey's estimate. Kersey's predicted response and that of the Harshaw TLD placed at the inner end of the maze were approximately equivalent. However, the response at the outer end of the maze was a factor of three different from Kersey's prediction. The Apfel detector did not respond as Kersey estimated. The bubble

detectors were a factor of 16 - 85 times less than the expected value. The comparison values are depicted in Table 6 of this section.

### 5.7 *McGinley Comparison*

McGinley and Butker evaluated Kersey's method and described the results obtained using this method and activation detector measurements at three linear accelerator facilities that utilized the Varian Clinac® 2100C. Kersey's estimates were 0.001 mrem/MU at 6.7 m from the isocenter, 0.006 mrem/MU at 6.1 m, and 0.02 mrem/MU at 5.3 m. The measured values were 0.001 mrem/MU, 0.004 mrem/MU, and 0.01 mrem/MU, respectively. A comparison was made with both sets of data at the 5.3 meter distance. The bubble detector provided approximately equivalent results (0.0256 mrem/MU at 5.22 m) for Kersey's approximation. The bubble detector response was a factor of 2 greater than the activation detector's measured value. The Harshaw TLD over-responded to the activation detector's measured value by a factor of 19, while it was less than a factor of 10 different than Kersey's approximation. The Panasonic TLD was a factor of 4 different than the predicted dose, but a factor of 8 greater than the measured value.

### 5.8 *Inverse Square Comparison*

The total neutron dose determined at each location was compared to the inverse square relationship. According to the inverse square relationship, the dose will decrease as the square of the distance from the source increases. For this research, the dose decreased as the distance from the isocenter increased, but not according to the inverse square

Table 6. Comparison of the values for the total dose after exposure to the Varian Clinac® 2100C for the Panasonic, Harshaw, and Apfel detectors using Kersey's methodology.

| Location | Panasonic | Harshaw | Apfel | Ratio of Kersey to Panasonic | Ratio of Kersey to Harshaw | Ratio of Kersey to Apfel |
|---|---|---|---|---|---|---|
| meters | mrem/week (average) | mrem/week (average) | mrem/week (maximum) | unitless | unitless | unitless |
| | | | | | | |
| 5.22 | 800.00 | 1870.00 | 128.00 | 0.36 | 0.85 | 0.01 |
| 13.15 | 158.00 | 165.00 | 3.65 | 0.37 | 0.35 | 0.06 |

relationship. The inverse square relationship was not followed because the accelerator is more representative of a line source than a point source. Since neutrons are produced when electrons strike the target and when the photons interact with the patient, a line source would better represent the accelerator. Room scatter also contributes to the number of neutrons in the room, which would also affect the inverse square relationship. At the inner end of the maze, the Panasonic and the Harshaw TLDs measured a higher dose than expected by the inverse square relationship, while the Apfel bubble detector measured a lower dose than expected. At a distance of 8.27 meters from the isocenter and in the center of the maze, both TLDs measured a greater dose, while the Apfel detector measured a lower dose. At the door, the bubble detector did not detect neutrons, but the TLD detectors both measured a dose lower than expected. Table 7 of this section describes the results and provides the percent difference for each detector. The percent difference allows a comparison of the theoretical value (provided by the inverse square relationship) and the measured values. A graphical description of the inverse square comparisons is also provided in Figure 18. From this information, the TLD dose response was more representative of the expected dose at the outer end of the maze than the inner end. The Apfel bubble detector responded in just the opposite manner: the dose response was more representative of the expected dose at the inner end of the maze than the outer end.

Table 7. Comparison of the values for the total dose after exposure to the Varian Clinac® 2100C for the Panasonic, Harshaw, and Apfel detectors using the inverse square relationship.

| Location | Inverse Square Estimate | Panasonic | Harshaw | Apfel | Ratio of Inverse Square to Panasonic | Ratio of Inverse Square to Harshaw | Ratio of Inverse Square to Apfel |
|---|---|---|---|---|---|---|---|
| meters | mrem | mrem (average) | mrem (average) | mrem (maximum) | unitless | unitless | unitless |
| | | | | | | | |
| 5.22 | 3.67E-02 | 7.99E-02 | 1.87E-01 | 2.56E-02 | 4.59E-01 | 1.96E-01 | 1.43 |
| 8.27 | 1.46E-02 | 2.77E-02 | 5.54E-02 | 2.15E-03 | 5.27E-01 | 2.64E-01 | 6.79 |
| 10.10 | 9.80E-03 | 1.51E-02 | 4.30E-02 | 1.27E-03 | 6.49E-01 | 2.28E-01 | 7.72 |
| 13.15 | 5.78E-03 | 3.15E-03 | 3.63E-03 | 2.42E-05 | 1.83 | 1.59 | 238.84 |
| Door | 4.44E-03 | 6.06E-04 | 1.51E-03 | 0.00E+00 | 7.33 | 2.94 | NA |

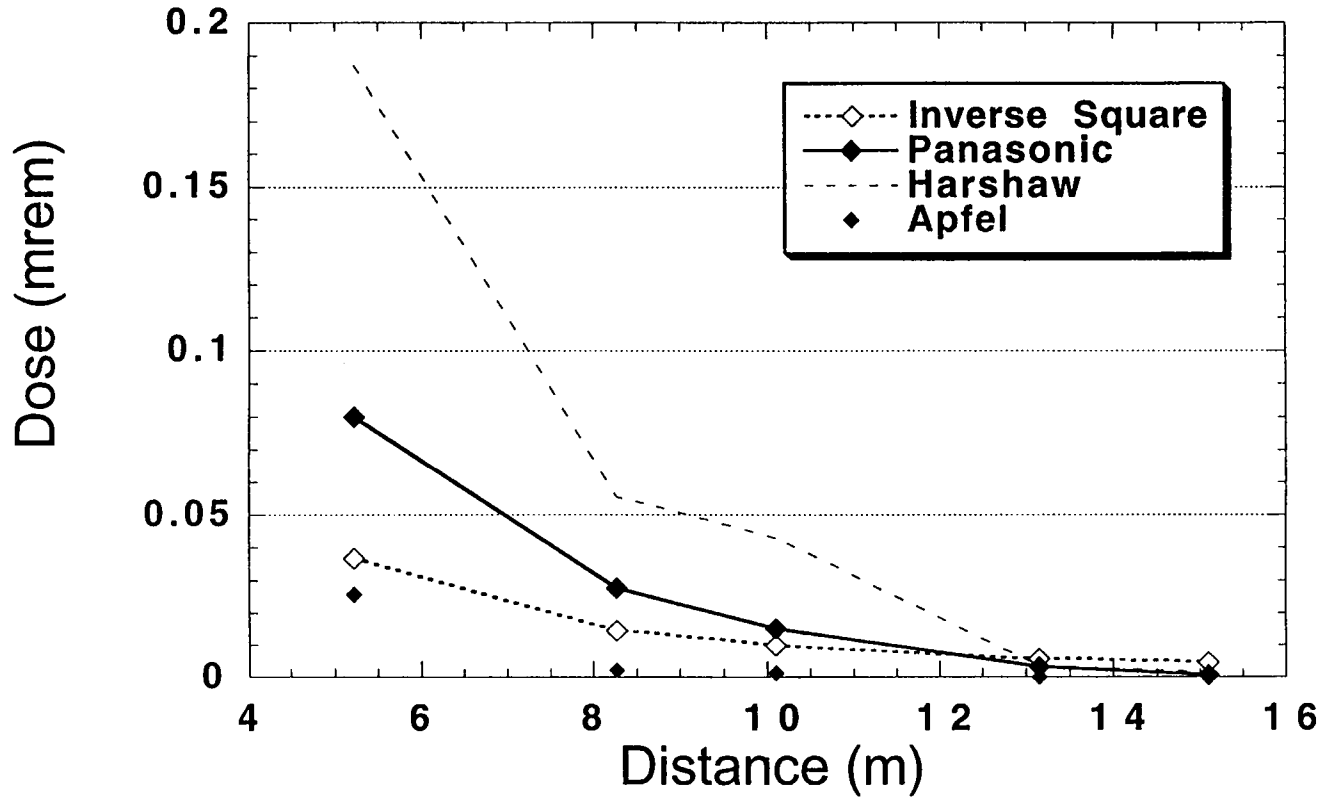


Figure 18. Diagram of the Inverse Square Relationship.

## 6.0 *Summary*

Neutron dosimetry is especially difficult due to spectral effects. However, the presence of gamma rays in neutron fields and the fact that most detectors respond to both particles compounds the problem . In the medical and biological sciences, a popular method used to determine the neutron and gamma ray component in mixed gamma/neutron radiation fields has been paired ionization chambers (Horowitz and Shachar, 1988). Thermoluminescent dosimetry is a convenient method with which to measure gamma exposures in medical facilities. However, in medical facilities, neutrons are also a component of the dose received by personnel and patients. Therefore, a study was undertaken to determine the neutron dose using thermoluminescent materials and a relatively new detector, the bubble detector.

Three types of detectors were used to determine the neutron dose expected in the maze of a linear accelerator: Panasonic TLDs, Harshaw TLDs, and Apfel bubble detectors. In all comparisons, the TLDs primarily responded in a similar manner. The bubble detectors' responses were not consistent with either of the TLDs used. However, when the responses were similar, in most instances, the dose response of the bubble detector was more similar to the response from the Panasonic TLD. The Harshaw and the Apfel detectors did not produce similar results.

The advantage of using the TLDs was that a dose estimate could be produced at the outer end of the maze, where the bubble detector did not respond. Using Kersey's method of estimating the dose at the inner and outer end of the maze, the Harshaw produced the best

comparison for the inner end of the maze, while none of the detectors gave an adequate response for the outer end of the maze. This may be partially explained by the configuration of the maze. Kersey's method involved a maze with two bends. The accelerator maze at Baptist Hospital has a sloping effect. As the beam leaves the accelerator head, the beam encounters the primary barrier to the front and the walls to the sides. The maze is located to the left of the primary barrier. The width of the maze gradually decreases until the initial bend, where the maze again begins to widen before reaching the door. This could explain the low response at the outer end of the maze for all three detectors.

The inverse square relationship was also studied. Again, none of the dosimeters studied responded exceptionally well, due to the production of neutrons in the target, patient, and walls. The Apfel bubble detector response was more representative of the inverse square relationship at the inner end of the maze. However, as the detectors were moved further away from the isocenter, the response deviated even more from the expected response. This may be explained by the fact that the energy of the neutrons reaching the door did not have sufficient energy to nucleate a bubble in the superheated gel. The TLDs on the other hand, performed just the opposite. These devices performed better at the outer end of the maze than at the inner end of the maze. This may be explained by the fact that once the beam leaves the treatment field (10 x 10 rectangular field in this case), the neutron dose drops significantly (Tosi et al., 1991). The neutrons emerging from the shield have an energy distribution different than the source distribution, owing to the multiple scattering suffered in the shield (Tosi et al., 1991). The inverse square relationship does not hold rigorously because the neutrons are not solely coming from the source directly, but also

from the shield, due to scattering events (Tosi et al., 1991). Neutrons coming from the shield, hit the concrete walls and mainly undergo elastic scattering due to the high hydrogen content of the concrete. While some neutrons are slowed down, thermalized, and captured inside the concrete walls, other neutrons are backscattered from the walls and can travel several times across the room before being thermalized and eventually captured (Tosi et al., 1991).

Although the TLDs responded at the door of the radiotherapy room while the bubble dosimeter did not, bubble detectors have several advantages over TLDs. Bubble dosimeters do not respond to gamma rays, whereas thermoluminescent dosimeters measure neutrons by the difference between the response of $^{6}Li$ and $^{7}Li$, both of which respond to gamma rays (Riel, 1993). Albedo dosimeter responses vary by orders of magnitude with neutron energy, but bubble dosimeter responses closely resemble the dose equivalent (Riel, 1993). Bubble detectors can provide a reliable indication of the presence of neutrons, they do not require a phantom to measure neutrons, and they respond to all energies of neutrons (Riel, 1993).

## 6.1 *Future Work*

Spectral measurements need to be made in accelerator facilities in order to characterize the beams and scattering effects. There are very few studies conducted in neutron spectral measurements, because, near a medical accelerator, photoneutrons are emitted as a pulsed beam mixed with the dominant numbers of primary x-rays (Uwamino et al., 1986).

Direct beam measurements also need to be conducted. This research focused on the occupational worker (technician) and the public (those individuals in the waiting room). Direct beam measurements would aid in the neutron dose determination to the patient undergoing radiation therapy. Bubble dosimeters could prove beneficial in this area of neutron dosimetry.

## 6.2 *Conclusions*

The Panasonic and the Harshaw thermoluminescent dosimeters and the Apfel bubble dosimeter are acceptable devices for measuring neutron doses in medical accelerator facilities. These devices respond differently at various locations; however, the types of neutrons encountered at each location are different. In the inner end of the maze, neutrons have a higher energy and are more likely to nucleate a bubble than to be thermalized and captured by a TL phosphor. At the outer end of the maze, the neutrons have traversed the maze several times and have lost energy due to wall scattering. These scattered neutrons are more likely to be detected in a TL phosphor due to the spectrum in which the TLDs were calibrated.

These devices could be used in combination to utilize each detector's strong qualities. The TLDs could be used to determine the dose at the outer end of the maze, with the bubble detectors being used at the inner end of the maze. Regardless of the detector type chosen, maze design and shielding will influence how the detectors respond to neutrons and to gammas if the detector is sensitive to these rays.

**Bibliography**

## *Bibliography*

Agosteo, S., A.F. Para, and B. Maggioni. 1993. *Neutron Fluxes in Radiotherapy Rooms.* Medical Physics, 20(2): 407-414.

Apfel Enterprises Incorporated. 1992. *Personal Neutron Dosimeter Instruction Manual.* New Haven, Connecticut.

Apfel, R.E. 1979. *The Superheated Drop Detector.* Nuclear Instruments and Methods 16: 603-608.

Apfel, R.E. and S.C. Roy. 1984. *Investigations on the Applicability of Superheated Drop Detectors in Neutron Dosimetry.* Nuclear Instruments and Methods in Physics Research, 219: 582-587.

Apfel, R.E., S.C. Roy, and Y.C. Lo. 1985. *Prediction of the Minimum Neutron Energy to Nucleate Vapor Bubbles in Superheated Liquids.* The American Physical Society, 31(5): 3194-3198.

Axton, E.J. and A.G. Bardell. 1972. *Neutron Production from Electron Accelerators Used for Medical Purposes.* Physics in Medical Biology, 17(2): 293-298.

Blackstock, A.W., J.R. Cortez, G.J. Littlejohn, and E. Storm. 1978. *Neutron Response of a New Albedo-Neutron Dosimeter.* Los Alamos Scientific Laboratory. Los Alamos, New Mexico. LA-UR-78-40.

Blake, S.W., J. Finch, D.E. Bonnett, and E. Shaw. 1988. *Patient Dosimetry and Staff Protection at the Clatterbridge High Energy Neutron Facility.* Radiation Protection Dosimetry, 23 (1): 369-372.

Buckner, M.A. 1991. *Improving Neutron Dosimetry Using Bubble Detector Technology.* Thesis. University of Tennessee, Knoxville, TN.

Buckner, M.A. 1994. *Empirical-Theoretical Determination of the Neutron Response Function for Teflon Encapsulated TLD-600 Using Harshaw Model 8800 Hot-Gas Reader.* Nuclear Instruments and Methods in Physics Research, 346: 266-272.

Buckner, M.A. C.S. Sims, and L.F. Miller. 1994. *Improving the Performance of the Combination Personal Neutron Dosemeter.* Radiation Protection Dosimetry, 51(1): 5-15.

Budzanowski, M., P. Bilski, P. Olko, T. Niewiadomski, B. Burgkhardt, and E. Piesch. *New TL Detectors for Personal Neutron Dosimetry.* Radiation Protection Dosimetry, 47(1): 419-423.

Burger, G. and H.G. Ebert. 1974. *Proceedings of the Second Symposium on Neutron Dosimetry in Biology and Medicine.* Commission of the European Communities. Luxembourg. EUR 5273 d-e-f.

Casson, W.H., G.T. Mei, and M.A. Buckner. 1991. *Test and Recommendations for the Application of the Centralized External Dosimetry System Dosimeter to Nuclear Accident Dosimetry.* Oak Ridge National Laboratory, Oak Ridge TN. ORNL-6667.

Casson, W.H. 1994. *Private Communication.*

Foster, A.R. and R.L. Wright, Jr. 1983. *Basic Nuclear Engineering.* Allyn and Bacon, Incorporated, Boston, Massachusetts.

Furuta, Y. and S. Tanaka. 1972. *Response of $^{6}LiF$ and $^{7}LiF$ Thermoluminescence Dosimeters to Fast Neutrons.* Nuclear Instrumentation and Methods, 104: 365-374.

G. & C. Merriam Company. 1973. *Webster's New Collegiate Dictionary.* G. & C. Merriam Company, Springfield, MA.

Glasser, D.A. 1952. *Some Effects of Ionizing Radiation on the Formation of Bubbles in Liquids.* Physics Review, 87: 665.

Griffith, R.V., J. Palfalvi, and U. Madhvanath. 1990. *Compendium of Neutron Spectra and Detector Responses for Radiation Protection Purposes.* International Atomic Energy Agency (IAEA), Vienna.

Harper, M.J. and M.E. Nelson. 1993. *Experimental Verification of a Superheated Liquid Droplet (Bubble) Neutron Detector Theoretical Model.* Radiation Protection Dosimetry, 47 (1): 535-542.

Harshaw Chemical Company. 1988. *TLD System 4400 Reader Instruction Manual.*

Health Physics Society. 1993. *Personnel Dosimetry Performance - Criteria for Testing.* American National Standards Institute, Incorporated. HPS N13.11-1993.

Horowitz, Y.S. and B.B. Shachar. 1988. *Thermoluminescent LiF:Cu, Mg, P for Gamma Ray Dosimetry in Mixed Fast Neutron-Gamma Radiation Fields.* Radiation Protection Dosimetry, 23(1): 401-404.

Hoy, J.E. 1972. *Personnel Albedo Neutron Dosimeter with Thermoluminescent $^{6}LiF$ and $^{7}LiF$.* Savannah River Laboratory, Aiken, South Carolina. DP-1277.

Ing, H. and E. Piesch. 1985. *Status of Neutron Dosimetry.* Radiation Protection Dosimetry, 10 (1): 5-15.

International Commission on Radiation Units and Measurements (ICRU). 1984. *Radiation Dosimetry: Electron Beams with Energies Between 1 and 50 MeV.* Bethesda, Maryland. ICRU Report 35.

International Commission on Radiation Units and Measurements (ICRU). 1989. *Clinical Neutron Dosimetry Part I: Determination of Absorbed Dose in a Patient Treated by External Beams of Fast Neutrons.* Bethesda, Maryland. ICRU Report 45.

Kersey, R.W. 1980. *The Estimation of Neutron and Gamma Radiation Doses in the Entrance Mazes of SL75-20 Treatment Rooms.* M.E.L., Crawley, England.

Khan, F.M. 1984. *The Physics of Radiation Therapy.* Williams & Wilkins, Baltimore, Maryland.

Kluge, H., K. Weise, and .B. Hunt. 1990. *Calibration of Neutron Sensitive Spherical Devices with Bare and $D_2O$-Moderated $^{252}Cf$ Sources in Rooms of Different Sizes.* Radiation Protection Dosimetry, 32(4): 233-244.

Lancaster, D.E. 1969. *Thermoluminescence: Theory & Applications.* Ziff-Davis Publishing Company.

LaRiviere, P.D. 1985. *Neutron Energies in Medical Electron Accelerator Rooms.* Medical Physics, 12 (6): 769-775.

Lee, E.B. 1994. *Accident Dosimetry Using Panasonic Dosimeters.* Thesis. University of Tennessee, Knoxville, Tennessee.

Manfredotti, C., U. Nastasi, E. Ornato, and A. Zinini. 1992. *Evaluation of the Undesired Neutron Dose Equivalent to Critical Organs in Patients Treated by Linear Accelerator Gamma Ray Therapy.* Radiation Protection Dosimetry, 44 (1): 457-462.

Manfredotti, C. and A. Zanini. 1993. *Calibration and Field Test of a Personal Albedo Neutron Dosimeter.* Radiation Protection Dosimetry, 47 (1): 381-385.

McCall, R.C. and C.M. Eisenhauer. 1987. *Effect of Air Scatter on Calibration Instruments for Detecting Neutrons.* Radiation Protection Dosimetry, 19: 77-84.

McGinley P.H. 1976. *Dose Levels Due to Neutrons in the Vicinity of High-Energy Medical Accelerators.* Medical Physics, 3 (6): 397-402.

McGinley, P.H. 1978. *Leakage Neutrons Produced by 10 MeV Medical Accelerators.* Health Physics, 36: 635-637.

McGinley, P.H. and E.K. Butker. 1991. *Evaluation of Neutron Dose Equivalent Levels at the Maze Entrance of Medical Accelerator Treatment Rooms.* Medical Physics, 18 (2): 279-281.

McGinley, P.H. 1992. *Photoneutron Fields in Medical Accelerator Rooms with Primary Barriers Constructed of Concrete and Metals.* Health Physics 63 (6): 698-701.

Miller, L.F. 1996. *Private Communication.*

Moscovitch, M. 1993. *Dose Algorithms for Personal Thermoluminescence Dosimetry.* Radiation Protection Dosimetry, 47 (1): 373-380.

Moscovitch, M., P.L. Taylor, J.E. Rodgers, and D.A. McRae. 1993. *An Algorithm for Supralinearity Correction Applied to Radiation Therapy Thermoluminescence Dosimetry.* Radiation Protection Dosimetry 47 (1): 505-508.

Nath, R., A.S. Meigooni, C.R. King, S. Smolen, and F. d'Errico. 1993. *Superheated Drop Detector for Determination of Neutron Dose Equivalent to Patients Undergoing High-Energy X-ray and Electron Radiotherapy.* Medical Physics, 20 (3): 781-787.

National Council on Radiation Protection and Measurements (NCRP). 1977. *Radiation Protection Design Guidelines for 0.1-100 MeV Particle Accelerator Facilities.* NCRP Report No. 51. Washington, DC.

National Council on Radiation Protection and Measurements (NCRP). 1981. *Dosimetry of X-ray and Gamma-Ray Beams for Radiation Therapy in the Energy Range 10 keV to 50 MeV.* NCRP Report No. 69. Bethesda, MD.

National Council on Radiation Protection and Measurement (NCRP). 1984. *Neutron Contamination from Medical Accelerators.* NCRP Report No. 79. Bethesda, MD.

National Council on Radiation Protection and Measurements (NCRP). 1993. *Limitation of Exposure to Ionizing Radiation.* NCRP Report No. 116. Bethesda, MD.

Nelson, M.E. and R. Gordon. 1993. *Comparison of Neutron Measurements at Linacs Using Bubble Dosemeters to Other Neutron Detectors.* Radiation Protection Dosimetry, 47 (1): 547-550.

Nuclear Regulatory Commission (NRC). 1995. *10 CFR Part 19 and 20.* Federal Register Rules and Regulations, Volume 60, No. 134.

Palta, J.R., K.R. Hogstrom, and C. Tannanonta. 1984. *Neutron Leakage Measurements from a Medical Linear Accelerator.* Medical Physics, 11 (4): 498-501.

Piesch, E., B. Burgkhardt, and W. Comper. 1985. *The Single Sphere Albedo System - A Useful Technique in Neutron Dosimetry.* Radiation Protection Dosimetry, 10 (1): 147-157.

Raver, R. 1994. *Presentation Handouts.*

Riel, G. 1993. *Role of Neutron Bubble Dosemeters.* Radiation Protection Dosimetry, 47 (1): 543-545.

Roy, S.C., R.E. Apfel, and Y.C. Lo. 1987. *Superheated Drop Detector: A Potential Tool in Neutron Research.* Nuclear Instruments and Methods in Physics Research, A255: 199-206.

Seitz, F. 1958. *On the Theory of the Bubble Chamber.* Physics of Fluids, 1: 2-13.

Sherwin, A.G., A.J. Pearson, D.J. Richards, and J.B. O'Hagan. 1988. *Measurement of Neutrons from High Energy Electron Linear Accelerators.* Radiation Protection Dosimetry, 23 (1): 337-340.

Snapp, J.P. 1992. *Development of a Neutron Area Monitor and Characterization System.* Thesis. University of Tennessee, Knoxville, Tennessee.

Sofield, J. 1993. *Presentation Handouts and Notes.*

Tanaka, S., and Y. Furuta. 1977. *Revised Energy Responses of $^{6}LiF$ and $^{7}LiF$ Thermoluminescence Dosimeters to Neutrons.* Nuclear Instruments and Methods, 140: 395-396.

Tosi, G., A.F. Para, V. Sangiust, L. Zeni, and M. Silari. 1991. *Neutron Measurements Around Medical Electron Accelerators by Active and Passive Detection Techniques.* Medical Physics, 18 (1): 54-60.

Turner, J.E. 1986. *Atoms, Radiation, and Radiation Protection.* Pergamon Press, New York, NY.

Uwamino. Y., T. Nakamura, T. Ohkubo, and A. Hara. 1986. *Measurement and Calculation of Neutron Leakage from a Medical Electron Accelerator.* Medical Physics, 13 (3): 374-384.

Valentin, J. 1995. *UNSCEAR Data Collections on Medical Radiation Exposures: Trends and Consequences.* Radiation Protection Dosimetry, 57 (1): 85-90.

Varian Associates, Incorporated. 1990. *Clinac 2100C Linear Accelerator Equipment Specifications Manual.* Varian Associates, Incorporated, Palo Alto, California.

Varian Associates, Incorporated. 1991. *2100C Clinac Systems Manual.* Varian Associates, Incorporated, Palo Alto, CA. Reference No. 283.

Zartman, J. 1996. *Private Communication.*

# Appendices

# Appendix A

Table A1. Response of each Harshaw TLD chip at each location within the labyrinth during the exposure to the Varian Clinac® 2100C.

| Location in Maze | Location on Piesch Sphere | TLD ID Number | Chip #1 Response | Chip #2 Reponse | Chip #3 Response | Chip #4 Response |
|---|---|---|---|---|---|---|
| Meters | unitless | unitless | nC | nC | nC | nC |
| | | | | | | |
| 5.22 | front | 153341 | 685.52 | 91.43 | 103.03 | 1133.09 |
| 5.22 | left | 153368 | 599.82 | 99.65 | 70.39 | 804.08 |
| 5.22 | right | 153373 | 306.29 | 70.82 | 54.67 | 396.46 |
| 5.22 | center | 153384 | 195.29 | 52.40 | 53.65 | 175.67 |
| 5.22 | back | 153387 | 233.11 | 31.28 | 27.68 | 0.00 |
| 8.27 | left | 153309 | 10.94 | 5.75 | 7.54 | 19.07 |
| 8.27 | front | 153332 | 456.22 | 5.27 | 26.67 | 892.83 |
| 8.27 | center | 153335 | 63.57 | 13.35 | 13.99 | 6.61 |
| 8.27 | right | 153349 | 224.58 | 21.36 | 21.17 | 466.97 |
| 8.27 | back | 153377 | 153.16 | 12.23 | 13.48 | 266.37 |
| 10.10 | left | 153300 | 169.70 | 16.90 | 16.14 | 330.33 |
| 10.10 | back | 153301 | 114.81 | 11.16 | 14.87 | 215.41 |
| 10.10 | front | 153365 | 261.57 | 22.31 | 30.94 | 524.44 |
| 10.10 | right | 153382 | 152.22 | 0.00 | 12.83 | 194.08 |
| 10.10 | center | 153409 | 42.11 | 13.36 | 13.05 | 43.61 |
| 13.15 | right | 153302 | 66.12 | 10.40 | 9.57 | 96.97 |
| 13.15 | left | 153307 | 59.39 | 10.27 | 12.84 | 118.89 |
| 13.15 | center | 153311 | 19.03 | 0.00 | 11.47 | 22.14 |
| 13.15 | back | 153352 | 43.50 | 14.30 | 11.65 | 0.00 |
| 13.15 | front | 153392 | 99.56 | 7.00 | 8.33 | 0.02 |
| Door | back | 153313 | 26.31 | 7.84 | 12.05 | 32.24 |
| Door | front | 153319 | 68.68 | 10.45 | 9.05 | 129.45 |
| Door | left | 153327 | 45.30 | 9.60 | 8.32 | 87.02 |
| Door | center | 153348 | 21.84 | 11.32 | 12.68 | 18.81 |
| Door | right | 153390 | 45.38 | 10.68 | 11.25 | 83.84 |

Table A2. Response of each Panasonic TLD element at each location within the labyrinth during the exposure to the Varian Clinac® 2100C.

| Location | ID No. | Element No. | Reading |
|---|---|---|---|
| meters | unitless | unitless | mR* |
| | | | |
| 5.22 | 25 | E1 | 93.10 |
| | | E2 | 316.00 |
| | | E3 | 199.00 |
| | | E4 | 259.00 |
| 5.22 | 35 | E1 | 79.00 |
| | | E2 | 310.00 |
| | | E3 | 192.00 |
| | | E4 | 316.00 |
| 5.22 | 20 | E1 | 71.70 |
| | | E2 | 295.00 |
| | | E3 | 180.00 |
| | | E4 | 302.00 |
| 8.27 | 1805 | E1 | 29.60 |
| | | E2 | 181.00 |
| | | E3 | 98.90 |
| | | E4 | 195.00 |
| 8.27 | 62 | E1 | 36.60 |
| | | E2 | 216.00 |
| | | E3 | 118.00 |
| | | E4 | 171.00 |
| 8.27 | 39 | E1 | 53.00 |
| | | E2 | 256.00 |
| | | E3 | 139.00 |
| | | E4 | 235.00 |
| 10.10 | 1807 | E1 | 20.50 |
| | | E2 | 113.00 |
| | | E3 | 55.60 |
| | | E4 | 110.00 |
| 10.10 | 29 | E1 | 22.00 |
| | | E2 | 128.00 |
| | | E3 | 63.90 |
| | | E4 | 102.00 |
| 10.10 | 1810 | E1 | 23.50 |
| | | E2 | 115.00 |
| | | E3 | 53.30 |
| | | E4 | 101.00 |

Table A2. Response of each Panasonic TLD element at each location within the labyrinth during the exposure to the Varian Clinac® 2100C (Continued).

| Location | ID No. | Element No. | Reading |
|---|---|---|---|
| meters | unitless | unitless | mR* |
| | | | |
| 13.15 | 47 | E1 | 20.50 |
| | | E2 | 63.10 |
| | | E3 | 32.10 |
| | | E4 | 49.30 |
| | 11 | E1 | 17.90 |
| 13.15 | | E2 | 58.00 |
| | | E3 | 34.00 |
| | | E4 | 44.50 |
| 13.15 | 64 | E1 | 17.40 |
| | | E2 | 65.00 |
| | | E3 | 46.90 |
| | | E4 | 62.70 |
| Door | 1812 | E1 | 15.20 |
| | | E2 | 39.40 |
| | | E3 | 25.30 |
| | | E4 | 32.80 |
| Door | 2800 | E1 | 16.00 |
| | | E2 | 35.90 |
| | | E3 | 26.60 |
| | | E4 | 36.80 |
| Door | 43 | E1 | 18.30 |
| | | E2 | 50.20 |
| | | E3 | 29.30 |
| | | E4 | 37.00 |

Table A3. Neutron dose response of the Apfel bubble dosimeter at each location within the labyrinth during the exposure to the Varian Clinac® 2100C.

| Location | Bubble ID No. | Total MonitorUnits | Reading |
|---|---|---|---|
| meters | unitless | MU | No. bubbles |
| | | | |
| 5.22 | 640 | 1000 | 141 |
| 8.27 | 641 | 1000 | 10 |
| 10.1 | 643 | 1000 | 10 |
| 13.15 | 642 | 1000 | 0 |
| Door | 639 | 1000 | 0 |
| | | | |
| 8.27 | 641 | 2000 | 26 |
| 10.1 | 643 | 2000 | 14 |
| 13.15 | 642 | 2000 | 0 |
| Door | 639 | 2000 | 0 |
| | | | |
| 8.27 | 641 | 3000 | 38 |
| 10.1 | 643 | 3000 | 21 |
| 13.15 | 642 | 3000 | 1 |
| Door | 639 | 3000 | 0 |
| | | | |
| 8.27 | 641 | 4000 | 53 |
| 10.1 | 643 | 4000 | 28 |
| 13.15 | 642 | 4000 | 1 |
| Door | 639 | 4000 | 0 |
| | | | |
| 8.27 | 641 | 5000 | 59 |
| 10.1 | 643 | 5000 | 35 |
| 13.15 | 642 | 5000 | 1 |
| Door | 639 | 5000 | 0 |
| | | | |
| 13.15 | 642 | 10000 | 1 |
| Door | 639 | 10000 | 0 |
| | | | |
| 13.15 | 642 | 20000 | 3 |
| Door | 639 | 20000 | 0 |
| | | | |
| 13.15 | 642 | 30000 | 4 |
| Door | 639 | 30000 | 0 |

Table A4. Resulting element correction coefficient (ECC) obtained for 30 Harshaw TLDs exposed to a 500 mrem $^{137}Cs$ source.

| TLD ID | Chip 1 Response | ECC | Chip 2 Response | ECC | Chip 3 Response | ECC | Chip 4 Response | ECC |
|---|---|---|---|---|---|---|---|---|
| unitless | nC | mrem/nC | nc | mrem/nC | nC | mrem/nC | nC | mrem/nC |
| | | | | | | | | |
| 153300 | 294.12 | 1.70 | 323.94 | 1.54 | 315.77 | 1.58 | 309.31 | 1.62 |
| 153301 | 276.81 | 1.81 | 301.33 | 1.66 | 319.76 | 1.56 | 292.87 | 1.71 |
| 153302 | 256.00 | 1.95 | 326.73 | 1.53 | 303.89 | 1.65 | 286.61 | 1.74 |
| 153307 | 266.65 | 1.88 | 325.55 | 1.54 | 310.77 | 1.61 | 265.94 | 1.88 |
| 153309 | 284.67 | 1.76 | 293.14 | 1.71 | 297.63 | 1.68 | 291.84 | 1.71 |
| 153311 | 258.25 | 1.94 | 304.50 | 1.64 | 321.42 | 1.56 | 281.30 | 1.78 |
| 153313 | 265.33 | 1.88 | 298.00 | 1.68 | 293.33 | 1.70 | 281.11 | 1.78 |
| 153319 | 273.01 | 1.83 | 308.14 | 1.62 | 279.47 | 1.79 | 287.05 | 1.74 |
| 153320 | 264.89 | 1.89 | 316.72 | 1.58 | 313.61 | 1.59 | 277.20 | 1.80 |
| 153327 | 287.74 | 1.74 | 279.19 | 1.79 | 311.05 | 1.61 | 268.27 | 1.86 |
| 153332 | 277.19 | 1.80 | 327.02 | 1.53 | 308.71 | 1.62 | 307.17 | 1.63 |
| 153333 | 301.74 | 1.66 | 319.04 | 1.57 | 291.42 | 1.72 | 311.81 | 1.60 |
| 153335 | 269.21 | 1.86 | 321.25 | 1.56 | 305.14 | 1.64 | 276.57 | 1.81 |
| 153341 | 270.92 | 1.85 | 267.02 | 1.87 | 297.28 | 1.68 | 297.01 | 1.68 |
| 153348 | 259.73 | 1.93 | 298.67 | 1.67 | 319.14 | 1.57 | 293.29 | 1.70 |
| 153349 | 267.10 | 1.87 | 371.44 | 1.35 | 315.57 | 1.58 | 280.02 | 1.79 |
| 153352 | 281.29 | 1.78 | 344.57 | 1.45 | 326.84 | 1.53 | 307.81 | 1.62 |
| 153355 | 272.37 | 1.84 | 312.94 | 1.60 | 277.15 | 1.80 | 296.48 | 1.69 |
| 153358 | 277.90 | 1.80 | 276.65 | 1.81 | 304.68 | 1.64 | 263.63 | 1.90 |
| 153365 | 268.62 | 1.86 | 308.71 | 1.62 | 305.69 | 1.64 | 296.80 | 1.68 |

Table A4. Resulting element correction coefficient (ECC) obtained for 30 Harshaw TLDs exposed to a 500 mrem $^{137}Cs$ source (Continued).

| TLD ID | Chip 1 Response | ECC | Chip 2 Response | ECC | Chip 3 Response | ECC | Chip 4 Response | ECC |
|---|---|---|---|---|---|---|---|---|
| unitless | nC | mrem/nC | nc | mrem/nC | nC | mrem/nC | nC | mrem/nC |
| | | | | | | | | |
| 153368 | 310.25 | 1.61 | 322.22 | 1.55 | 324.40 | 1.54 | 296.97 | 1.68 |
| 153369 | 271.43 | 1.84 | 319.25 | 1.57 | 295.95 | 1.69 | 278.81 | 1.79 |
| 153373 | 283.04 | 1.77 | 297.47 | 1.68 | 330.11 | 1.51 | 309.78 | 1.61 |
| 153377 | 276.02 | 1.81 | 289.90 | 1.72 | 307.61 | 1.63 | 296.90 | 1.68 |
| 153382 | 305.40 | 1.64 | 319.72 | 1.56 | 315.47 | 1.58 | 305.95 | 1.63 |
| 153384 | 292.89 | 1.71 | 351.20 | 1.42 | 341.99 | 1.46 | 277.07 | 1.80 |
| 153387 | 253.59 | 1.97 | 319.04 | 1.57 | 303.31 | 1.65 | 305.51 | 1.64 |
| 153390 | 288.60 | 1.73 | 331.20 | 1.51 | 276.44 | 1.81 | 300.31 | 1.66 |
| 153392 | 271.06 | 1.84 | 322.71 | 1.55 | 294.24 | 1.70 | 272.76 | 1.83 |
| 153409 | 282.53 | 1.77 | 330.14 | 1.51 | 312.21 | 1.60 | 298.56 | 1.67 |
| | **Averages** | **1.81** | | **1.60** | | **1.63** | | **1.73** |

Table A5. Resulting paired correction coefficient (PCC) obtained for 30 Harshaw TLDs exposed to a 500 mrem $^{252}Cf$ source.

| TLD ID | Chip 1 Response | ECC | R1 | Chip 2 Response | ECC | R2 | (R1-R2) | PCC |
|---|---|---|---|---|---|---|---|---|
| unitless | nC | mrem/nC | mrem | nc | mrem/nC | mrem | mrem | unitless |
| | | | | | | | | |
| 153300 | 1994.90 | 1.81 | 3610.77 | 86.52 | 1.60 | 138.43 | 3472.34 | 0.15 |
| 153301 | 1995.27 | 1.81 | 3611.44 | 80.67 | 1.60 | 129.07 | 3482.37 | 0.14 |
| 153302 | 1988.69 | 1.81 | 3599.53 | 85.60 | 1.60 | 136.96 | 3462.57 | 0.13 |
| 153307 | 1781.05 | 1.81 | 3223.70 | 81.49 | 1.60 | 130.38 | 3093.32 | 0.16 |
| 153309 | 2047.98 | 1.81 | 3706.84 | 75.18 | 1.60 | 120.29 | 3586.56 | 0.14 |
| 153311 | 1879.32 | 1.81 | 3401.57 | 83.60 | 1.60 | 133.76 | 3267.81 | 0.14 |
| 153313 | 1771.13 | 1.81 | 3205.75 | 74.16 | 1.60 | 118.66 | 3087.09 | 0.16 |
| 153319 | 1949.81 | 1.81 | 3529.16 | 79.27 | 1.60 | 126.83 | 3402.32 | 0.15 |
| 153320 | 2000.02 | 1.81 | 3620.04 | 80.08 | 1.60 | 128.13 | 3491.91 | 0.14 |
| 153327 | 2041.20 | 1.81 | 3694.57 | 70.62 | 1.60 | 112.99 | 3581.58 | 0.15 |
| 153332 | 1989.20 | 1.81 | 3600.45 | 82.74 | 1.60 | 132.38 | 3468.07 | 0.14 |
| 153333 | 2031.20 | 1.81 | 3676.47 | 99.42 | 1.60 | 159.07 | 3517.40 | 0.16 |
| 153335 | 1849.10 | 1.81 | 3346.87 | 76.56 | 1.60 | 122.50 | 3224.38 | 0.15 |
| 153341 | 1903.93 | 1.81 | 3446.11 | 69.68 | 1.60 | 111.49 | 3334.63 | 0.15 |
| 153348 | 2079.12 | 1.81 | 3763.21 | 80.52 | 1.60 | 128.83 | 3634.38 | 0.13 |
| 153349 | 1977.64 | 1.81 | 3579.53 | 93.48 | 1.60 | 149.57 | 3429.96 | 0.14 |
| 153352 | 2038.48 | 1.81 | 3689.65 | 90.96 | 1.60 | 145.54 | 3544.11 | 0.14 |
| 153355 | 2066.37 | 1.81 | 3740.13 | 82.72 | 1.60 | 132.35 | 3607.78 | 0.14 |
| 153358 | 2036.48 | 1.81 | 3686.03 | 83.58 | 1.60 | 133.73 | 3552.30 | 0.14 |
| 153365 | 1846.99 | 1.81 | 3343.05 | 78.47 | 1.60 | 125.55 | 3217.50 | 0.15 |

Table A5 . Resulting paired correction coefficient (PCC) obtained for 30 Harshaw TLDs exposed to a 500 mrem $^{252}Cf$ source (Continued).

| TLD ID | Chip 1 Response | ECC | R1 | Chip 2 Response | ECC | R2 | (R1-R2) | PCC |
|---|---|---|---|---|---|---|---|---|
| unitless | nC | mrem/nC | mrem | nc | mrem/nC | mrem | mrem | unitless |
| | | | | | | | | |
| 153368 | 2263.72 | 1.81 | 4097.33 | 89.93 | 1.60 | 143.89 | 3953.45 | 0.14 |
| 153369 | 2008.15 | 1.81 | 3634.75 | 85.26 | 1.60 | 136.42 | 3498.34 | 0.14 |
| 153384 | 2182.82 | 1.81 | 3950.90 | 95.60 | 1.60 | 152.96 | 3797.94 | 0.14 |
| 153387 | 1954.21 | 1.81 | 3537.12 | 87.46 | 1.60 | 139.94 | 3397.18 | 0.13 |
| 153390 | 2141.29 | 1.81 | 3875.73 | 90.26 | 1.60 | 144.42 | 3731.32 | 0.14 |
| 153392 | 1903.83 | 1.81 | 3445.93 | 79.13 | 1.60 | 126.61 | 3319.32 | 0.15 |
| 153409 | 2120.77 | 1.81 | 3838.59 | 88.01 | 1.60 | 140.82 | 3697.78 | 0.14 |
| | | | | | | | **Average** | **0.13** |

Table A5 . Resulting paired correction coefficient (PCC) obtained for 30 Harshaw TLDs exposed to a 500 mrem $^{252}Cf$ source (Continued).

| TLD ID | Chip 3 Response | ECC | R3 | Chip 4 Response | ECC | R4 | (R4-R3) | PCC |
|---|---|---|---|---|---|---|---|---|
| unitless | nC | mrem/nC | mrem | nC | mrem/nC | mrem | mrem | unitless |
| | | | | | | | | |
| 153300 | 71.22 | 1.63 | 116.09 | 2649.64 | 1.73 | 4583.88 | 4467.79 | 0.12 |
| 153301 | 70.29 | 1.63 | 114.57 | 2413.71 | 1.73 | 4175.72 | 4061.15 | 0.12 |
| 153302 | 69.38 | 1.63 | 113.09 | 2816.95 | 1.73 | 4873.32 | 4760.23 | 0.10 |
| 153307 | 68.09 | 1.63 | 110.99 | 2366.07 | 1.73 | 4093.30 | 3982.31 | 0.12 |
| 153309 | 70.94 | 1.63 | 115.63 | 2662.94 | 1.73 | 4606.89 | 4491.25 | 0.11 |
| 153311 | 69.40 | 1.63 | 113.12 | 2499.13 | 1.73 | 4323.49 | 4210.37 | 0.12 |
| 153313 | 62.23 | 1.63 | 101.43 | 2487.47 | 1.73 | 4303.32 | 4201.89 | 0.12 |
| 153319 | 63.27 | 1.63 | 103.13 | 2546.05 | 1.73 | 4404.67 | 4301.54 | 0.12 |
| 153320 | 65.27 | 1.63 | 106.39 | 2585.80 | 1.73 | 4473.43 | 4367.04 | 0.11 |
| 153327 | 65.35 | 1.63 | 106.52 | 2355.24 | 1.73 | 4074.57 | 3968.04 | 0.12 |
| 153332 | 67.63 | 1.63 | 110.24 | 2800.40 | 1.73 | 4844.69 | 4734.46 | 0.11 |
| 153333 | 63.36 | 1.63 | 103.28 | 2760.15 | 1.73 | 4775.06 | 4671.78 | 0.12 |
| 153335 | 63.01 | 1.63 | 102.71 | 2498.44 | 1.73 | 4322.30 | 4219.59 | 0.11 |
| 153341 | 65.16 | 1.63 | 106.21 | 2544.41 | 1.73 | 4401.83 | 4295.62 | 0.12 |
| 153348 | 72.90 | 1.63 | 118.83 | 2814.06 | 1.73 | 4868.32 | 4749.50 | 0.11 |
| 153349 | 67.32 | 1.63 | 109.73 | 2530.49 | 1.73 | 4377.75 | 4268.02 | 0.11 |
| 153352 | 70.79 | 1.63 | 115.39 | 2847.23 | 1.73 | 4925.71 | 4810.32 | 0.11 |
| 153355 | 59.88 | 1.63 | 97.60 | 2721.29 | 1.73 | 4707.83 | 4610.23 | 0.11 |
| 153358 | 66.76 | 1.63 | 108.82 | 2412.71 | 1.73 | 4173.99 | 4065.17 | 0.11 |

Table A5 . Resulting paired correction coefficient (PCC) obtained for 30 Harshaw TLDs exposed to a 500 mrem $^{252}Cf$ source (Continued).

| TLD ID | Chip 3 Response | ECC | R3 | Chip 4 Response | ECC | R4 | (R4-R3) | PCC |
|---|---|---|---|---|---|---|---|---|
| unitless | nC | mrem/nC | mrem | nC | mrem/nC | mrem | mrem | unitless |
| | | | | | | | | |
| 153365 | 71.17 | 1.63 | 116.01 | 2598.18 | 1.73 | 4494.85 | 4378.84 | 0.12 |
| 153368 | 81.16 | 1.63 | 132.29 | 2753.87 | 1.73 | 4764.20 | 4631.90 | 0.11 |
| 153369 | 65.32 | 1.63 | 106.47 | 2572.85 | 1.73 | 4451.03 | 4344.56 | 0.11 |
| 153373 | 87.84 | 1.63 | 143.18 | 2777.17 | 1.73 | 4804.50 | 4661.32 | 0.11 |
| 153377 | 66.41 | 1.63 | 108.25 | 2608.59 | 1.73 | 4512.86 | 4404.61 | 0.12 |
| 153382 | 68.41 | 1.63 | 111.51 | 2640.81 | 1.73 | 4568.60 | 4457.09 | 0.12 |
| 153384 | 78.40 | 1.63 | 127.79 | 2557.90 | 1.73 | 4425.17 | 4297.38 | 0.11 |
| 153387 | 68.87 | 1.63 | 112.26 | 2743.83 | 1.73 | 4746.83 | 4634.57 | 0.11 |
| 153390 | 62.72 | 1.63 | 102.23 | 2668.20 | 1.73 | 4615.99 | 4513.75 | 0.12 |
| 153392 | 64.88 | 1.63 | 105.75 | 2589.90 | 1.73 | 4480.53 | 4374.77 | 0.11 |
| 153409 | 68.55 | 1.63 | 111.74 | 2670.90 | 1.73 | 4620.66 | 4508.92 | 0.11 |
| | | | | | | | **Average** | **0.11** |

Table A6. Elemental responses and element correction factor (ECF) calculated responses for the Panasonic TLDs at each location within the labyrinth during the exposure to the Varian Clinac® 2100C.

| ID No. | Element No. | Reading | ECF | ECF Corrected Response |
|---|---|---|---|---|
| unitless | unitless | mR* | unitless | mR* |
| | | | | |
| 25 | E1 | 93.10 | 0.56 | 166.85 |
| | E2 | 316.00 | 0.74 | 429.93 |
| | E3 | 199.00 | 0.79 | 253.50 |
| | E4 | 259.00 | 0.63 | 411.11 |
| 35 | E1 | 79.00 | 0.55 | 143.12 |
| | E2 | 310.00 | 0.75 | 415.55 |
| | E3 | 192.00 | 0.82 | 234.15 |
| | E4 | 316.00 | 0.72 | 438.28 |
| 20 | E1 | 71.70 | 0.56 | 127.58 |
| | E2 | 295.00 | 0.78 | 377.24 |
| | E3 | 180.00 | 0.79 | 226.70 |
| | E4 | 302.00 | 0.79 | 382.28 |
| 1805 | E1 | 29.60 | 0.61 | 48.84 |
| | E2 | 181.00 | 0.65 | 280.62 |
| | E3 | 98.90 | 0.68 | 144.80 |
| | E4 | 195.00 | 0.61 | 318.11 |
| 62 | E1 | 36.60 | 0.53 | 69.71 |
| | E2 | 216.00 | 0.69 | 311.24 |
| | E3 | 118.00 | 0.84 | 140.14 |
| | E4 | 171.00 | 0.67 | 256.37 |

Table A6. Elemental responses and element correction factor (ECF) calculated responses for the Panasonic TLDs at each location within the labyrinth during the exposure to the Varian Clinac® 2100C (Continued).

| ID No. | Element No. | Reading | ECF | ECF Corrected Response |
|---|---|---|---|---|
| unitless | unitless | mR* | unitless | mR* |
| | | | | |
| 39 | E1 | 53.00 | 0.66 | 80.18 |
| | E2 | 256.00 | 0.83 | 309.18 |
| | E3 | 139.00 | 0.95 | 146.78 |
| | E4 | 235.00 | 0.83 | 282.79 |
| 1807 | E1 | 20.50 | 0.52 | 39.20 |
| | E2 | 113.00 | 0.68 | 166.18 |
| | E3 | 55.60 | 0.59 | 94.24 |
| | E4 | 110.00 | 0.61 | 180.33 |
| 29 | E1 | 22.00 | 0.55 | 40.29 |
| | E2 | 128.00 | 0.75 | 171.12 |
| | E3 | 63.90 | 0.78 | 81.92 |
| | E4 | 102.00 | 0.66 | 155.02 |
| 1810 | E1 | 23.50 | 0.61 | 38.52 |
| | E2 | 115.00 | 0.65 | 176.38 |
| | E3 | 53.30 | 0.53 | 101.14 |
| | E4 | 101.00 | 0.54 | 186.35 |

Table A6. Elemental responses and element correction factor (ECF) calculated responses for the Panasonic TLDs at each location within the labyrinth during the exposure to the Varian Clinac® 2100C (Continued).

| ID No. | Element No. | Reading | ECF | ECF Corrected Response |
|---|---|---|---|---|
| unitless | unitless | mR* | unitless | mR* |
| | | | | |
| 47 | E1 | 20.50 | 0.63 | 32.44 |
| | E2 | 63.10 | 0.69 | 91.58 |
| | E3 | 32.10 | 0.72 | 44.52 |
| | E4 | 49.30 | 0.65 | 75.73 |
| 11 | E1 | 17.90 | 0.50 | 35.94 |
| | E2 | 58.00 | 0.68 | 85.80 |
| | E3 | 34.00 | 0.74 | 45.82 |
| | E4 | 44.50 | 0.66 | 67.42 |
| 64 | E1 | 17.40 | 0.62 | 27.88 |
| | E2 | 65.00 | 0.76 | 85.87 |
| | E3 | 46.90 | 0.79 | 59.75 |
| | E4 | 62.70 | 0.74 | 84.50 |
| 1812 | E1 | 15.20 | 0.59 | 25.63 |
| | E2 | 39.40 | 0.64 | 61.28 |
| | E3 | 25.30 | 0.59 | 42.88 |
| | E4 | 32.80 | 0.54 | 60.97 |
| 2800 | E1 | 16.00 | 0.56 | 28.83 |
| | E2 | 35.90 | 0.62 | 57.72 |
| | E3 | 26.60 | 0.65 | 41.18 |
| | E4 | 36.80 | 0.57 | 64.90 |

Table A6. Elemental responses and element correction factor (ECF) calculated responses for the Panasonic TLDs at each location within the labyrinth during the exposure to the Varian Clinac® 2100C (Continued).

| ID No. | Element No. | Reading | ECF | ECF Corrected Response |
|---|---|---|---|---|
| unitless | unitless | mR* | unitless | mR* |
| | | | | |
| 43 | E1 | 18.30 | 0.58 | 31.72 |
| | E2 | 50.20 | 0.67 | 75.38 |
| | E3 | 29.30 | 0.72 | 40.53 |
| | E4 | 37.00 | 0.69 | 53.31 |

Table A7. Neutron dose per element and the average dose per TLD for the Panasonic TLDs at each location within the labyrinth during the exposure to the Varian Clinac® 2100C.

| Location | Monitor Units | ID No. | Kn (avg.)$_2$ | Neutron Dose | Kn (avg.)$_3$ | Neutron Dose | Kn (avg.)$_4$ | Neutron Dose | Average Dose per TLD |
|---|---|---|---|---|---|---|---|---|---|
| meters | MU | unitless | mrem/ mR* | Element 2 | mrem/ mR* | Element 3 | mrem/ mR* | Element 4 | mrem |
| | | | | mrem | | mrem | | mrem | |
| | | | | | | | | | |
| 5.22 | 2000 | 25 | 1.01 | 265.93 | 1.02 | 88.07 | 0.46 | 111.94 | 155.31 |
| 5.22 | 2000 | 35 | 1.01 | 275.38 | 1.02 | 92.52 | 0.46 | 135.27 | 167.72 |
| 5.22 | 2000 | 20 | 1.01 | 252.35 | 1.02 | 100.74 | 0.46 | 116.72 | 156.61 |
| 8.27 | 5000 | 1805 | 1.01 | 234.28 | 1.02 | 97.53 | 0.46 | 123.40 | 151.73 |
| 8.27 | 5000 | 62 | 1.01 | 244.13 | 1.02 | 71.58 | 0.46 | 85.54 | 133.75 |
| 8.27 | 5000 | 39 | 1.01 | 231.47 | 1.02 | 67.69 | 0.46 | 92.85 | 130.67 |
| 10.10 | 5000 | 1807 | 1.01 | 128.25 | 1.02 | 56.14 | 0.46 | 64.92 | 83.10 |
| 10.10 | 5000 | 29 | 1.01 | 132.24 | 1.02 | 42.31 | 0.46 | 52.58 | 75.71 |
| 10.10 | 5000 | 1810 | 1.01 | 139.34 | 1.02 | 63.64 | 0.46 | 67.74 | 67.66 |
| 13.15 | 10000 | 47 | 1.01 | 59.78 | 1.02 | 12.28 | 0.46 | 19.84 | 30.64 |
| 13.15 | 10000 | 11 | 1.01 | 50.39 | 1.02 | 10.04 | 0.46 | 14.43 | 24.95 |
| 13.15 | 10000 | 64 | 1.01 | 58.61 | 1.02 | 32.38 | 0.46 | 25.95 | 38.98 |
| Door | 35000 | 1812 | 1.01 | 36.03 | 1.02 | 17.53 | 0.46 | 16.19 | 23.25 |
| Door | 35000 | 2800 | 1.01 | 29.20 | 1.02 | 12.55 | 0.46 | 16.53 | 19.43 |
| Door | 35000 | 43 | 1.01 | 44.13 | 1.02 | 8.95 | 0.46 | 9.90 | 20.99 |

Table A8. Maximum dose measured by the Apfel bubble detector after exposure to the Varian Clinac® 2100C.

| Location | ID No. | Monitor Units Exposed | Maximum No. of Bubbles | Maximum Dose | Dose/MU (max) |
|---|---|---|---|---|---|
| Meters | Unitless | MU | No. | mrem | mrem/MU |
| | | | | | |
| 5.22 | 640 | 1000 | 141 | 25.64 | 2.56E-02 |
| 8.27 | 641 | 5000 | 59 | 10.73 | 2.15E-03 |
| 10.1 | 643 | 5000 | 35 | 6.36 | 1.27E-03 |
| 13.15 | 642 | 30000 | 4 | 0.73 | 2.42E-05 |
| Door | 639 | 30000 | 0 | 0.00 | 0.00E+00 |

Table A9. Harshaw TLD response and total dose after exposure to the Varian Clinac® 2100C, using Set 1 ECC and PCC values .

| TLD ID Number | Chip #1 Response | Average ECC | R1 | Chip #2 Reponse | Average ECC | R2 | (R1-R2) |
|---|---|---|---|---|---|---|---|
| unitless | nC | mrem/nC | mrem | nC | mrem/nC | mrem | mrem |
| | | | | | | | |
| 153300 | 169.70 | 1.85 | 313.95 | 16.90 | 1.78 | 30.08 | 283.86 |
| 153301 | 114.81 | 1.85 | 212.40 | 11.16 | 1.78 | 19.86 | 192.53 |
| 153302 | 66.12 | 1.85 | 122.32 | 10.40 | 1.78 | 18.51 | 103.81 |
| 153307 | 59.39 | 1.85 | 109.87 | 10.27 | 1.78 | 18.28 | 91.59 |
| 153309 | 10.94 | 1.85 | 20.24 | 5.75 | 1.78 | 10.24 | 10.00 |
| 153311 | 19.03 | 1.85 | 35.21 | 0.00 | 1.78 | 0.00 | 35.21 |
| 153313 | 26.31 | 1.85 | 48.67 | 7.84 | 1.78 | 13.96 | 34.72 |
| 153319 | 68.68 | 1.85 | 127.06 | 10.45 | 1.78 | 18.60 | 108.46 |
| 153320 | 18.12 | 1.85 | 33.52 | 6.99 | 1.78 | 12.44 | 21.08 |
| 153327 | 45.30 | 1.85 | 83.81 | 9.60 | 1.78 | 17.09 | 66.72 |
| 153332 | 456.22 | 1.85 | 844.01 | 5.27 | 1.78 | 9.38 | 834.63 |
| 153333 | 19.42 | 1.85 | 35.93 | 12.51 | 1.78 | 22.27 | 13.66 |
| 153335 | 63.57 | 1.85 | 117.60 | 13.35 | 1.78 | 23.76 | 93.84 |
| 153341 | 685.52 | 1.85 | 1268.21 | 91.43 | 1.78 | 162.75 | 1105.47 |
| 153348 | 21.84 | 1.85 | 40.40 | 11.32 | 1.78 | 20.15 | 20.25 |
| 153349 | 224.58 | 1.85 | 415.47 | 21.36 | 1.78 | 38.02 | 377.45 |
| 153352 | 43.50 | 1.85 | 80.48 | 14.30 | 1.78 | 25.45 | 55.02 |
| 153355 | 15.62 | 1.85 | 28.90 | 8.42 | 1.78 | 14.99 | 13.91 |
| 153358 | 19.30 | 1.85 | 35.71 | 10.01 | 1.78 | 17.82 | 17.89 |
| 153365 | 261.57 | 1.85 | 483.90 | 22.31 | 1.78 | 39.71 | 444.19 |

Table A9. Harshaw TLD response and total dose after exposure to the Varian Clinac® 2100C, using Set 1 ECC and PCC values (Continued).

| TLD ID Number | Chip #1 Response | Average ECC | R1 | Chip #2 Reponse | Average ECC | R2 | (R1-R2) |
|---|---|---|---|---|---|---|---|
| unitless | nC | mrem/nC | mrem | nC | mrem/nC | mrem | mrem |
| | | | | | | | |
| 153368 | 599.82 | 1.85 | 1109.67 | 99.65 | 1.78 | 177.38 | 932.29 |
| 153369 | 18.99 | 1.85 | 35.13 | 19.00 | 1.78 | 33.82 | 1.31 |
| 153373 | 306.29 | 1.85 | 566.64 | 70.82 | 1.78 | 126.06 | 440.58 |
| 153377 | 153.16 | 1.85 | 283.35 | 12.23 | 1.78 | 21.77 | 261.58 |
| 153382 | 152.22 | 1.85 | 281.61 | 0.00 | 1.78 | 0.00 | 281.61 |
| 153384 | 195.29 | 1.85 | 361.29 | 52.40 | 1.78 | 93.27 | 268.01 |
| 153387 | 233.11 | 1.85 | 431.25 | 31.28 | 1.78 | 55.68 | 375.58 |
| 153390 | 45.38 | 1.85 | 83.95 | 10.68 | 1.78 | 19.01 | 64.94 |
| 153392 | 99.56 | 1.85 | 184.19 | 7.00 | 1.78 | 12.46 | 171.73 |
| 153409 | 42.11 | 1.85 | 77.90 | 13.36 | 1.78 | 23.78 | 54.12 |

Table A9. Harshaw TLD response and total dose after exposure to the Varian Clinac® 2100C, using Set 1 ECC and PCC values (Continued).

| TLD ID Number | Chip #3 Response | Average ECC | R3 | Chip #4 Response | Average ECC |
|---|---|---|---|---|---|
| unitless | nC | mrem/nC | mrem | nC | mrem/nC |
| | | | | | |
| 153300 | 16.14 | 1.68 | 27.12 | 330.33 | 1.92 |
| 153301 | 14.87 | 1.68 | 24.98 | 215.41 | 1.92 |
| 153302 | 9.57 | 1.68 | 16.08 | 96.97 | 1.92 |
| 153307 | 12.84 | 1.68 | 21.57 | 118.89 | 1.92 |
| 153309 | 7.54 | 1.68 | 12.67 | 19.07 | 1.92 |
| 153311 | 11.47 | 1.68 | 19.27 | 22.14 | 1.92 |
| 153313 | 12.05 | 1.68 | 20.24 | 32.24 | 1.92 |
| 153319 | 9.05 | 1.68 | 15.20 | 129.45 | 1.92 |
| 153320 | 7.62 | 1.68 | 12.80 | 17.54 | 1.92 |
| 153327 | 8.32 | 1.68 | 13.98 | 87.02 | 1.92 |
| 153332 | 26.67 | 1.68 | 44.81 | 892.83 | 1.92 |
| 153333 | 7.87 | 1.68 | 13.22 | 6.26 | 1.92 |
| 153335 | 13.99 | 1.68 | 23.50 | 6.61 | 1.92 |
| 153341 | 103.03 | 1.68 | 173.09 | 1133.09 | 1.92 |
| 153348 | 12.68 | 1.68 | 21.30 | 18.81 | 1.92 |
| 153349 | 21.17 | 1.68 | 35.57 | 466.97 | 1.92 |
| 153352 | 11.65 | 1.68 | 19.57 | 0.00 | 1.92 |
| 153355 | 6.43 | 1.68 | 10.80 | 17.29 | 1.92 |
| 153358 | 9.76 | 1.68 | 16.40 | 15.60 | 1.92 |
| 153365 | 30.94 | 1.68 | 51.98 | 524.44 | 1.92 |

Table A9. Harshaw TLD response and total dose after exposure to the Varian Clinac® 2100C, using Set 1 ECC and PCC values (Continued).

| TLD ID Number | Chip #3 Response | Average ECC | R3 | Chip #4 Response | Average ECC |
|---|---|---|---|---|---|
| unitless | nC | mrem/nC | mrem | nC | mrem/nC |
| | | | | | |
| 153368 | 70.39 | 1.68 | 118.26 | 804.08 | 1.92 |
| 153369 | 9.12 | 1.68 | 15.32 | 0.00 | 1.92 |
| 153373 | 54.67 | 1.68 | 91.85 | 396.46 | 1.92 |
| 153377 | 13.48 | 1.68 | 22.65 | 266.37 | 1.92 |
| 153382 | 12.83 | 1.68 | 21.55 | 194.08 | 1.92 |
| 153384 | 53.65 | 1.68 | 90.13 | 175.67 | 1.92 |
| 153387 | 27.68 | 1.68 | 46.50 | 0.00 | 1.92 |
| 153390 | 11.25 | 1.68 | 18.90 | 83.84 | 1.92 |
| 153392 | 8.33 | 1.68 | 13.99 | 0.02 | 1.92 |
| 153409 | 13.05 | 1.68 | 21.92 | 43.61 | 1.92 |

Table A9. Harshaw TLD response and total dose after exposure to the Varian Clinac® 2100C, using Set 1 ECC and PCC values (Continued).

| R4 | (R4-R3) |
|---|---|
| mrem | mrem |
| | |
| 634.23 | 607.12 |
| 413.59 | 388.61 |
| 186.18 | 170.10 |
| 228.27 | 206.70 |
| 36.61 | 23.95 |
| 42.51 | 23.24 |
| 61.90 | 41.66 |
| 248.54 | 233.34 |
| 33.68 | 20.88 |
| 167.08 | 153.10 |
| 1714.23 | 1669.43 |
| 12.02 | 0.00 |
| 12.69 | 0.00 |
| 2175.53 | 2002.44 |
| 36.12 | 14.81 |
| 896.58 | 861.02 |
| 0.00 | 0.00 |
| 33.20 | 22.39 |
| 29.95 | 13.56 |
| 1006.92 | 954.95 |

Table A9. Harshaw TLD response and total dose after exposure to the Varian Clinac® 2100C, using Set 1 ECC and PCC values (Continued).

| R4 | (R4-R3) |
|---|---|
| mrem | mrem |
| | |
| 1543.83 | 1425.58 |
| 0.00 | 0.00 |
| 761.20 | 669.36 |
| 511.43 | 488.78 |
| 372.63 | 351.08 |
| 337.29 | 247.15 |
| 0.00 | 0.00 |
| 160.97 | 142.07 |
| 0.04 | 0.00 |
| 83.73 | 61.81 |

Table A10. Harshaw TLD response and total dose after exposure to the Varian Clinac® 2100C, using Set 2 ECC and PCC values .

| TLD ID Number | Chip #1 Response | R1 | Chip #2 Reponse | R2 | (R1-R2) |
|---|---|---|---|---|---|
| unitless | nC | mrem | nC | mrem | mrem |
| | | | | | |
| 153300 | 169.70 | 307.16 | 16.90 | 30.59 | 276.57 |
| 153301 | 114.81 | 207.81 | 11.16 | 20.20 | 187.61 |
| 153302 | 66.12 | 119.68 | 10.40 | 18.82 | 100.85 |
| 153307 | 59.39 | 107.50 | 10.27 | 18.59 | 88.91 |
| 153309 | 10.94 | 19.80 | 5.75 | 10.41 | 9.39 |
| 153311 | 19.03 | 34.44 | 0.00 | 0.00 | 34.44 |
| 153313 | 26.31 | 47.62 | 7.84 | 14.19 | 33.43 |
| 153319 | 68.68 | 124.31 | 10.45 | 18.91 | 105.40 |
| 153320 | 18.12 | 32.80 | 6.99 | 12.65 | 20.15 |
| 153327 | 45.30 | 81.99 | 9.60 | 17.38 | 64.62 |
| 153332 | 456.22 | 825.76 | 5.27 | 9.54 | 816.22 |
| 153333 | 19.42 | 35.15 | 12.51 | 22.64 | 12.51 |
| 153335 | 63.57 | 115.06 | 13.35 | 24.16 | 90.90 |
| 153341 | 685.52 | 1240.79 | 91.43 | 165.49 | 1075.30 |
| 153348 | 21.84 | 39.53 | 11.32 | 20.49 | 19.04 |
| 153349 | 224.58 | 406.49 | 21.36 | 38.66 | 367.83 |
| 153352 | 43.50 | 78.74 | 14.30 | 25.88 | 52.85 |
| 153355 | 15.62 | 28.27 | 8.42 | 15.24 | 13.03 |

Table A10. Harshaw TLD response and total dose after exposure to the Varian Clinac® 2100C, using Set 2 ECC and PCC values (Continued).

| TLD ID Number | Chip #1 Response | R1 | Chip #2 Reponse | R2 | (R1-R2) |
|---|---|---|---|---|---|
| unitless | nC | mrem | nC | mrem | mrem |
| | | | | | |
| 153358 | 19.30 | 34.93 | 10.01 | 18.12 | 16.81 |
| 153365 | 261.57 | 473.44 | 22.31 | 40.38 | 433.06 |
| 153368 | 599.82 | 1085.67 | 99.65 | 180.37 | 905.31 |
| 153369 | 18.99 | 34.37 | 19.00 | 34.39 | 0.00 |
| 153373 | 306.29 | 554.38 | 70.82 | 128.18 | 426.20 |
| 153377 | 153.16 | 277.22 | 12.23 | 22.14 | 255.08 |
| 153382 | 152.22 | 275.52 | 0.00 | 0.00 | 275.52 |
| 153384 | 195.29 | 353.47 | 52.40 | 94.84 | 258.63 |
| 153387 | 233.11 | 421.93 | 31.28 | 56.62 | 365.31 |
| 153390 | 45.38 | 82.14 | 10.68 | 19.33 | 62.81 |
| 153392 | 99.56 | 180.20 | 7.00 | 12.67 | 167.53 |
| 153409 | 42.11 | 76.22 | 13.36 | 24.18 | 52.04 |

Table A10. Harshaw TLD response and total dose after exposure to the Varian Clinac® 2100C, using Set 2 ECC and PCC values (Continued).

| TLD ID Number | Chip #3 Response | R3 | Chip #4 Response | R4 | (R4-R3) |
|---|---|---|---|---|---|
| unitless | nC | mrem | nC | mrem | mrem |
| | | | | | |
| 153300 | 16.14 | 29.05 | 330.33 | 594.59 | 565.54 |
| 153301 | 14.87 | 26.77 | 215.41 | 387.74 | 360.97 |
| 153302 | 9.57 | 17.23 | 96.97 | 174.55 | 157.32 |
| 153307 | 12.84 | 23.11 | 118.89 | 214.00 | 190.89 |
| 153309 | 7.54 | 13.57 | 19.07 | 34.33 | 20.75 |
| 153311 | 11.47 | 20.65 | 22.14 | 39.85 | 19.21 |
| 153313 | 12.05 | 21.69 | 32.24 | 58.03 | 36.34 |
| 153319 | 9.05 | 16.29 | 129.45 | 233.01 | 216.72 |
| 153320 | 7.62 | 13.72 | 17.54 | 31.57 | 17.86 |
| 153327 | 8.32 | 14.98 | 87.02 | 156.64 | 141.66 |
| 153332 | 26.67 | 48.01 | 892.83 | 1607.09 | 1559.09 |
| 153333 | 7.87 | 14.17 | 6.26 | 11.27 | 0.00 |
| 153335 | 13.99 | 25.18 | 6.61 | 11.90 | 0.00 |
| 153341 | 103.03 | 185.45 | 1133.09 | 2039.56 | 1854.11 |
| 153348 | 12.68 | 22.82 | 18.81 | 33.86 | 11.03 |
| 153349 | 21.17 | 38.11 | 466.97 | 840.55 | 802.44 |
| 153352 | 11.65 | 20.97 | 0.00 | 0.00 | 0.00 |
| 153355 | 6.43 | 11.57 | 17.29 | 31.12 | 19.55 |

Table A10. Harshaw TLD response and total dose after exposure to the Varian Clinac® 2100C, using Set 2 ECC and PCC values (Continued).

| TLD ID Number | Chip #3 Response | R3 | Chip #4 Response | R4 | (R4-R3) |
|---|---|---|---|---|---|
| unitless | nC | mrem | nC | mrem | mrem |
| | | | | | |
| 153358 | 9.76 | 17.57 | 15.60 | 28.08 | 10.51 |
| 153365 | 30.94 | 55.69 | 524.44 | 943.99 | 888.30 |
| 153368 | 70.39 | 126.70 | 804.08 | 1447.34 | 1320.64 |
| 153369 | 9.12 | 16.42 | 0.00 | 0.00 | 0.00 |
| 153373 | 54.67 | 98.41 | 396.46 | 713.63 | 615.22 |
| 153377 | 13.48 | 24.26 | 266.37 | 479.47 | 455.20 |
| 153382 | 12.83 | 23.09 | 194.08 | 349.34 | 326.25 |
| 153384 | 53.65 | 96.57 | 175.67 | 316.21 | 219.64 |
| 153387 | 27.68 | 49.82 | 0.00 | 0.00 | 0.00 |
| 153390 | 11.25 | 20.25 | 83.84 | 150.91 | 130.66 |
| 153392 | 8.33 | 14.99 | 0.02 | 0.04 | 0.00 |
| 153409 | 13.05 | 23.49 | 43.61 | 78.50 | 55.01 |

Table A10. Harshaw TLD response and total dose after exposure to the Varian Clinac® 2100C, using Set 2 ECC and PCC values (Continued).

| TLD ID Number | (R1-R2) * PCC | (R4-R3) * PCC | (R1-R2) * PCC * a | (R4-R3) * PCC * b | [(R1-R2)+ (R4-R3)] * calibra. | Total Neutron Dose |
|---|---|---|---|---|---|---|
| unitless | mrem | mrem | mrem | mrem | mrem | mrem |
| | | | | | | |
| 153300 | 83.74 | 143.89 | 11639.80 | 5467708.31 | 5479348.11 | 663.00 |
| 153301 | 56.80 | 92.10 | 7894.84 | 3499782.03 | 3507676.88 | 424.43 |
| 153302 | 30.62 | 40.31 | 4256.73 | 1531963.83 | 1536220.56 | 185.88 |
| 153307 | 27.02 | 48.99 | 3755.68 | 1861518.59 | 1865274.27 | 225.70 |
| 153309 | 2.95 | 5.68 | 410.21 | 215668.48 | 216078.70 | 26.15 |
| 153311 | 10.39 | 5.51 | 1443.60 | 209292.24 | 210735.84 | 25.50 |
| 153313 | 10.24 | 9.87 | 1423.62 | 375161.14 | 376584.76 | 45.57 |
| 153319 | 31.99 | 55.30 | 4447.28 | 2101460.04 | 2105907.32 | 254.81 |
| 153320 | 6.22 | 4.95 | 864.38 | 188002.05 | 188866.43 | 22.85 |
| 153327 | 19.68 | 36.28 | 2735.73 | 1378825.80 | 1381561.54 | 167.17 |
| 153332 | 246.21 | 395.65 | 34223.86 | 15034868.57 | 15069092.42 | 1823.36 |
| 153333 | 4.03 | 0.00 | 560.10 | 0.00 | 56.10 | 6.79E-03 |
| 153335 | 27.68 | 0.00 | 3847.97 | 0.00 | 3847.97 | 4.66E-01 |
| 153341 | 326.11 | 474.58 | 45329.66 | 18033996.25 | 18079325.91 | 2187.60 |
| 153348 | 5.98 | 3.51 | 830.53 | 133404.08 | 134234.61 | 16.24 |
| 153349 | 111.35 | 204.06 | 15477.43 | 7754317.30 | 7769794.73 | 940.15 |
| 153352 | 16.23 | 0.00 | 2256.14 | 0.00 | 2256.14 | 2.73E-01 |
| 153355 | 4.10 | 5.31 | 570.35 | 201683.97 | 202254.32 | 24.47 |
| 153358 | 5.28 | 3.21 | 733.46 | 122078.13 | 122811.60 | 14.86 |
| 153365 | 131.04 | 226.32 | 18214.12 | 8600240.07 | 8618454.20 | 1042.83 |

Table A10. Harshaw TLD response and total dose after exposure to the Varian Clinac® 2100C, using Set 2 ECC and PCC values (Continued).

| TLD ID Number | (R1-R2) * PCC | (R4-R3) * PCC | (R1-R2) * PCC * a | (R4-R3) * PCC * b | [(R1-R2)+ (R4-R3)] * calibra. | Total Neutron Dose |
|---|---|---|---|---|---|---|
| unitless | mrem | mrem | mrem | mrem | mrem | mrem |
| | | | | | | |
| 153368 | 275.03 | 337.86 | 38228.55 | 12838759.07 | 12876987.62 | 1558.12 |
| 153369 | 0.39 | 0.00 | 53.78 | 0.00 | 53.78 | 6.51E-03 |
| 153373 | 129.97 | 158.64 | 18065.86 | 6028234.55 | 6046300.40 | 731.60 |
| 153377 | 77.17 | 115.84 | 10725.95 | 4401988.70 | 4412714.65 | 533.94 |
| 153382 | 83.07 | 83.21 | 11547.30 | 3161819.28 | 3173366.57 | 383.98 |
| 153384 | 79.06 | 58.58 | 10989.93 | 2225872.53 | 2236862.46 | 270.66 |
| 153387 | 110.79 | 0.00 | 15400.46 | 0.00 | 15400.46 | 1.86 |
| 153390 | 19.16 | 33.67 | 2662.97 | 1279507.64 | 1282170.61 | 155.14 |
| 153392 | 50.66 | 0.00 | 7041.62 | 0.00 | 7041.62 | 0.85 |
| 153409 | 15.97 | 14.65 | 2219.30 | 556635.64 | 558854.94 | 67.62 |

**Appendix B**

Equations for obtaining the average dose of the LiF TLDs at each location within the labyrinth after exposure to the Varian Clinac® 2100C.

$$[(R_1 \times ECC_1) - (R_2 \times ECC_2) \times PCC_{1\text{-}2} \times \alpha] = \text{Neutron Dose}_{1\text{-}2}$$

$$[(685.52 \times 1.81) - (91.43 \times 1.60) \times 0.13 \times 139] = 19777.67 \text{ mrem}$$

$$[(R_4 \times ECC_4) - (R_3 \times ECC_3) \times PCC_{4\text{-}3} \times \beta] = \text{Neutron Dose}_{4\text{-}3}$$

$$[(1133.09 \times 1.73) - (103.03 \times 1.63) \times 0.11 \times 3.84\text{x}10^{4}) = 7570703.92 \text{ mrem}$$

$$(\text{Neutron Dose}_{1\text{-}2} + \text{Neutron Dose}_{4\text{-}3}) \times \text{Calibration Factor} = \text{Total Neutron Dose}$$

$$(19777.67 + 7570703.92) \times 1.21\text{x}10^{-4} = \underline{918.45 \text{ mrem}}$$

Equations for obtaining the average dose of the $Li_2B_4O_7$ TLDs at each location within the labyrinth after exposure to the Varian Clinac® 2100C.

$$(R_1/ECF_1) = \gamma$$

$$(93.10/0.56) = 166.25 \text{ mrem}$$

$$[((R_2/ECF_2) - \gamma) \times k_{n2}] = \text{Neutron Dose}_2$$

$$[((316.00/0.74) - 166.25) \times 1.01] = 263.38 \text{ mrem}$$

$$[((R_3/ECF_3) - \gamma) \times k_{n3}] = \text{Neutron Dose}_3$$

$$[((199.00/0.79) - 166.25) \times 1.02 = 87.36 \text{ mrem}$$

$$[((R_4/ECF_4) - \gamma) \times k_{n4}] = \text{Neutron Dose}_4$$

$$[((259.00/0.63) - 166.25) \times 0.46] = 112.64 \text{ mrem}$$

$$(\text{Neutron Dose}_2 + \text{Neutron Dose}_3 + \text{Neutron Dose}_4)\ 3 = \text{Average Total Neutron Dose}$$

$$(263.38 + 87.36 + 112.64) / 3 = \underline{154.46 \text{ mrem}}$$

*Vita*

Cathy J. Lewis was born in South Charleston, West Virginia on December 25, 1968 to Mr. Robert F. and Mrs. Wilma J. Lewis. Ms. Lewis attended public schools in the Saint Albans, West Virginia area. In June 1987, she graduated Salutatorian from Saint Albans High School. The following August, Cathy entered the University of Tennessee at Knoxville to pursue a Bachelor of Science degree in Nuclear Engineering. During the next four years, Ms. Lewis was active in the Pi Beta Phi Sorority, the American Nuclear Society, and intramural sports. In August 1991, she received her Bachelor of Science degree and re-entered the University in September for a second degree. A Master of Science in Nuclear Engineering with a concentration in Health Physics was conferred in May 1996. Currently, Ms. Lewis is a Research Associate at *SENES* Oak Ridge, Incorporated.